OM

Ocean Models

Ocean Models

1 Introduction

We have embarked upon this exposition of ocean models with three goals: (a) to outline the hydrodynamic and numerical foundations upon which the current ocean models rest; (b) to provide the initial tools for beginners (and even for more advanced modelers) to simulate and forecast the oceanic environment; and (c) to provide a general overview for technical people in all fields on the current approaches in modeling the circulation and thermodynamic state of the ocean. In general, most of the methods that we will consider have been proven to be successful in depicting at least some part of the ocean, and to be consistent with available hydrographic and remotely sensed observations. We will reference some of the papers containing model-data verification at the proper stages in the presentation, so that the reader can follow up and be able to form a more complete understanding of the overall success of these models with an insight into the current prospects for simulating and forecasting the oceanic environment.

Clearly, changes in the world ocean are going to be important factors in any global change processes. Even on shorter time scales, such as the 4–7 year El Nino[1] cycle, the ocean has been shown to have a profound effect on our weather and climate. The global ice–ocean system is also a vast storehouse of "stored" water, heat and carbon dioxide, and thus becomes one of the main controllers of global warming. Some semi-enclosed seas, for example the Mediterranean and the Arctic with limited flushing capabilities, have been the site of dumping of non-radioactive and radioactive wastes with serious environmental consequences.

As is known from previous modeling efforts and our knowledge of the physical processes of the ocean, it is difficult to build a "universal" ocean model that can treat accurately phe-

---

[1] El Nino is an oceanographic phenomenon first observed in the eastern Pacific near Peru. It occurs periodically with an irregular period of about 4–7 years, and consists of anomalous warming of the waters near Peru and cooling near the Philippines. It involves major changes in both the atmospheric and oceanic circulation over the Equatorial Pacific, and is a clear example of large-scale air–sea coupling and short term climatic variation. The first observations noted an unusual warming of the waters off Peru (which came usually around Christmas, hence the name, which means "Christ child"). The warming diminishes the usual upwelling of cold and nutrient-rich waters to the surface, so it leads to a disastrous decrease in anchovies and other fish production with large economic consequences.

nomena on all spatial and temporal scales in the various ocean basins of the world. This is due both to finite computer size and CPU speed, and to an imperfect description of the physical processes, such as turbulence. Thus ocean modeling efforts have diversified into different classes, some concerned only with the turbulent surface boundary layers, some with continental shelves, and many with the meso-scale eddy-resolving circulation in a given part of, or a whole, ocean basin. World ocean models of such high resolution are just on the threshold of being built and tested. Similarly, models that aim to give real-time nowcasts/forecasts using objectively analyzed initial density fields and model-predicted atmospheric forcing, have only recently begun to be tested extensively with real-time observations. In the past, these models have been confined to a limited domain with some open boundaries present, and in the predictive mode could profess to make successful predictions only for a few days without additional information provided at the boundaries and/or from observations made within the domain. Lately, the arrival of new supercomputers and more extensive ocean surveillance (i.e. satellite altimetry and IR sensing) have extended the area and period of prediction, e.g. with the whole global ocean 25-level model being initialized and modeled at a resolution of 1/6 degree (16 km) or better on a 256 processor CM-5.

We can therefore finally afford to start building an eddy-resolving world ocean model that will treat both the thermodynamic and hydrodynamic aspects. The fine resolution versions of such models can be used to do real-time forecasts for periods of several weeks. These forecasts will be quite useful to the fishing industry, ship routing, long range weather prediction and search and rescue operations. The more coarse resolution versions will be used to do long term climate simulation.

1.1 Classification of Ocean Models

In the last two decades several criteria have emerged by which oceanographers classify their models (see Figure 1). Geography is clearly one criterion, with models being designed for the world ocean, the Atlantic and Pacific Basins, the Mediterranean, the Gulf of Mexico, etc. A second criterion utilizes the physical processes described: models can be hydrodynamic, thermodynamic or both. The surface mixed layer models mentioned above fit into the thermodynamic class, and some of the simple layered models (see below) are of the hydrodynamic type. A third criterion is concerned with the condition one puts on the surface of the ocean. A fourth is concerned with the way the vertical degree of freedom is handled (including modal decomposition in the vertical), and a fifth with the presence of density variations.

1.1.1 Free Surface and Rigid Lid Models

In reality, the ocean surface is free to deform under the influence of wind, heating and tidal forces. We find wind-driven waves and surges up to several meters high on its surface. These are typically short-lived, have short spatial scales and fast wave speeds. The surface elevations due to the large, quasi-permanent ocean currents, on the other hand, such as those associated with the Gulf Stream and its eddies, and mid-ocean gyres, are only fractions of

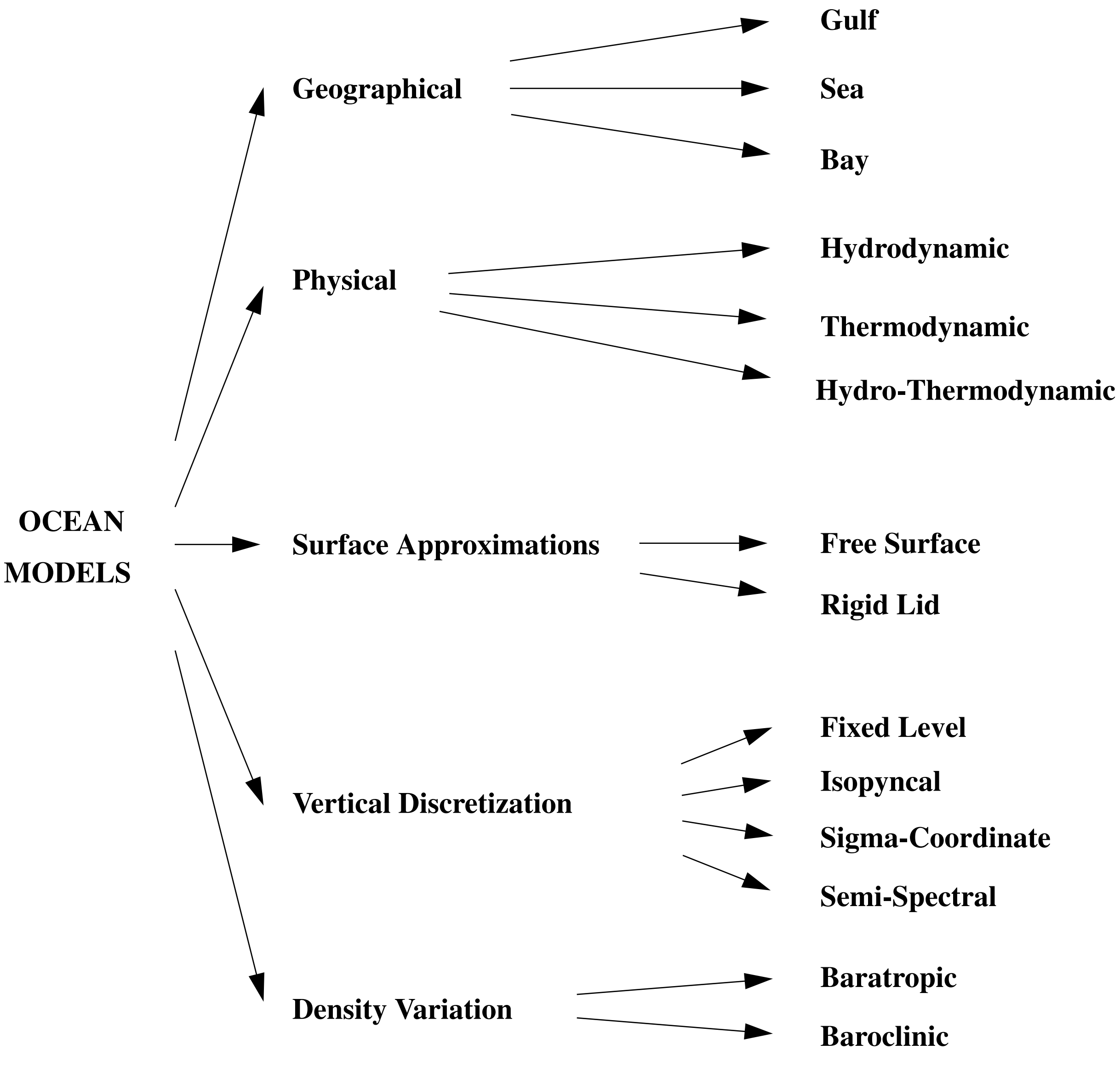

Figure 1: Ocean Models

a meter or so, and move very slowly. In order to avoid the severe limitation on the time step due to the fast gravity waves (to be discussed below), one puts a rigid lid on the ocean as this affects the large-scale motions only slightly. The first such model was formulated by Bryan [4]. This model has been recently reformulated by Killworth et al. [36] to retain the free surface by treating the fast modes separately. Models that treat the fast waves implicitly have been developed by Hurlburt et al. [31] in connection with "layered" models, by Madala and Piacsek [39] in connection with "level" models, and by Blumberg and Mellor [3] in connection with "sigma-coordinate" models [for definitions of "layered", "level" and "sigma" see the next section].

1.1.2 Fixed Level, Isopycnal, Sigma-Coordinate and Semi-Spectral Models

The models of Bryan [4], Madala and Piacsek [37] and Killworth et al. [36] have all used fixed levels in the vertical z-direction, with a variable spacing of the depth levels to resolve the rapid changes in the surface layers. On the other hand, Blumberg and Mellor [3] and Haidvogel et al. [25] have introduced a stretched coordinate usually referred to as sigma (for its previous usage in meteorology), defined as $\sigma = z/D$ where D is the fluid depth. This leads to boundary surfaces that can be put at $\sigma = 0, -1$ and an automatic accommodation of the depth contours. In addition Haidvogel et al. [25] have introduced a semi-spectral representation of the vertical dimension (sigma layout) in terms of Chebyshev polynomials (collocation method). Both of these have employed the free-surface formulation. See Figure 2 and Figure 3.

About the same time that the z-level models were developed, several investigators have proceeded to exploit the fact that the ocean is shallow and hydrostatic, and that its vertical structure has a semi-permanent tendency. A modal decomposition by empirical orthogonal functions or by linear dynamic modes has shown that the first three or four modes can usually capture 95 percent of the energy. Thus by vertically integrating the equations of motion in z between isopycnal (i.e. equal density) surfaces (employing the hydrostatic relation (1)) they have derived a system where the layer-averaged velocities and layer-thicknesses are the dependent variables. Since the isopycnal surfaces move with the fluid, this representation is in fact quasi-Lagrangian. The first model using this approach in the free surface formulation was built by O'Brien [51], and in the rigid-lid formulation by Holland and Lin [30]. More recent formulations that allow the layers to surface have been done by Bleck and Boudra [2] and Oberhuber [49].

1.1.3 Barotropic vs. Baroclinic Models

In general, ocean models describe the response of a variable density ocean to atmospheric momentum and heat forcing. This response can very simply be represented in terms of eigenmodes of a linearized system of equations. We will attempt now to give a simplified physical description of these modes (at this point the student should also read Chapter 6 of Gill [22]). The zeroth mode is equivalent to the vertically-averaged component of the motion, also known as the *barotropic* mode. The higher modes are called *baroclinic* modes

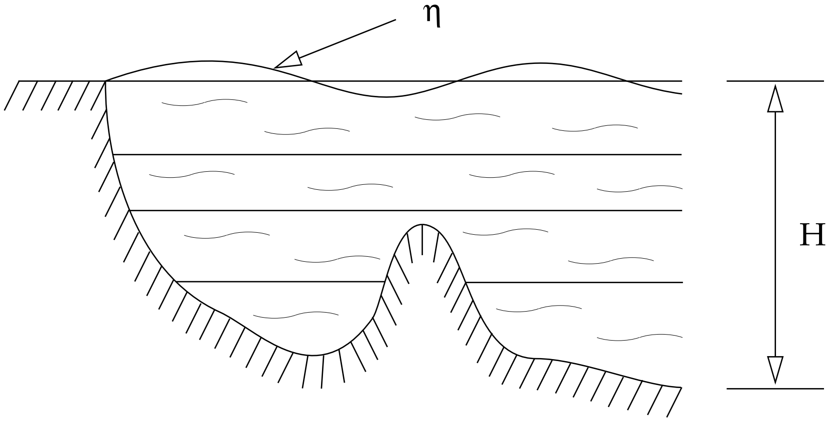

z-Coordinate Model

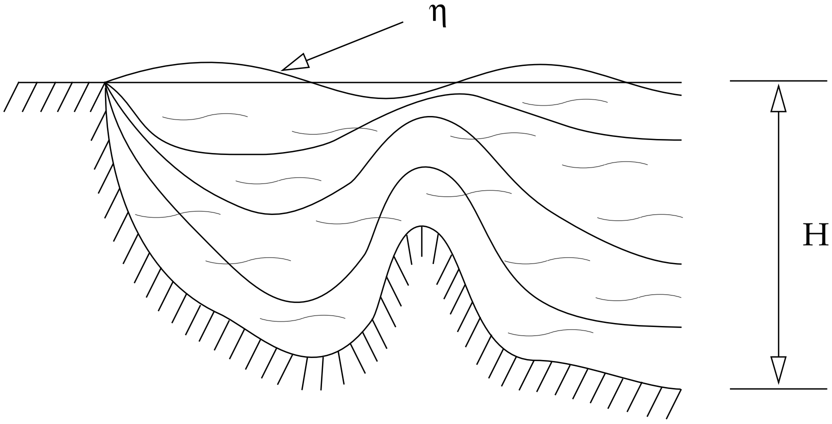

σ-Coordinate Model

Figure 2: Vertical discretization in ocean models; H is the bottom depth and η the sea surface deflection.

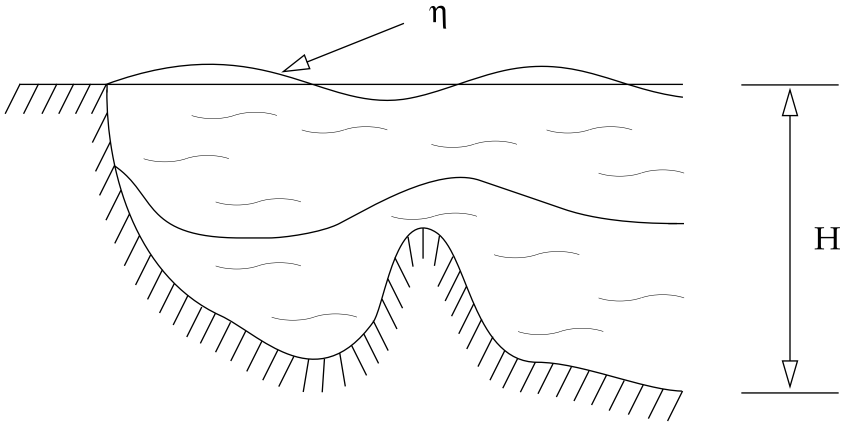

Layered/Isopycnal-Coordinate Model

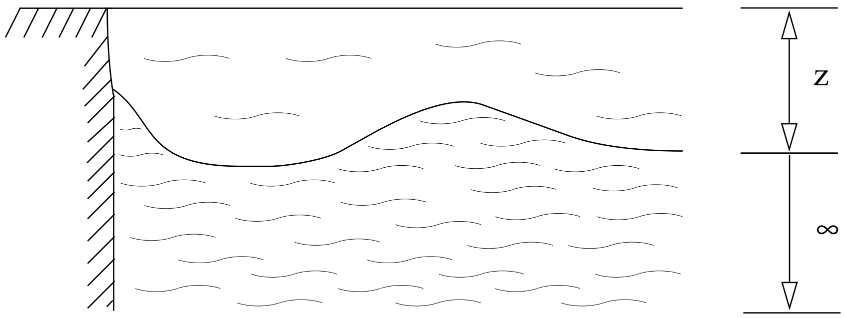

Reduced Gravity-Coordinate Model

Figure 3: Vertical discretization in ocean models; H is the bottom depth, h is the thickness of the upper layer and η is the free surface deflection.

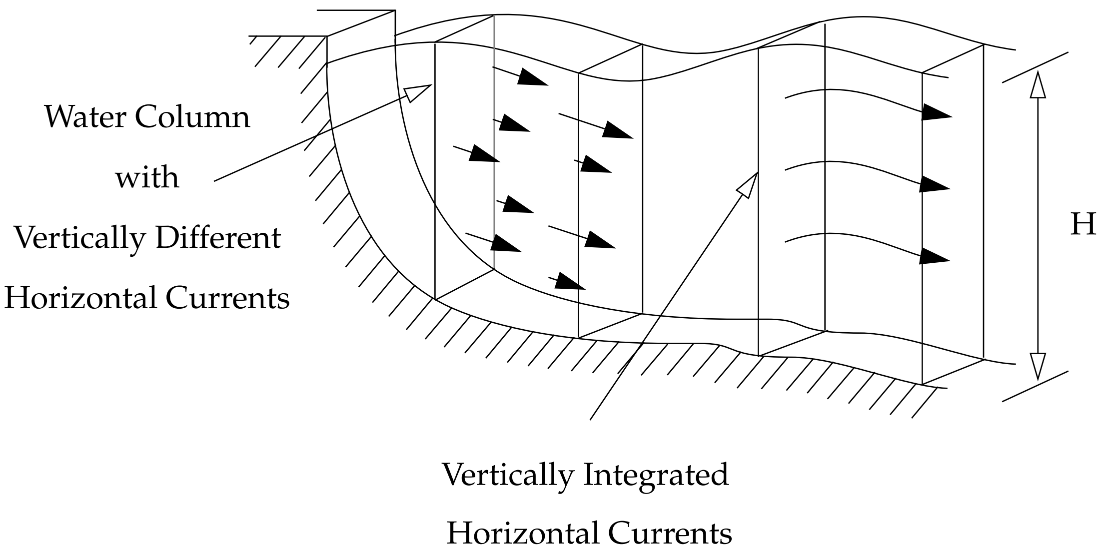

Figure 4: Barotropic Model where a region of the ocean's water column is vertically integrated to obtain one value for the vertically different horizontal currents.

and are associated with higher order components of the vertical density profile. All ocean models described in this chapter will make the *hydrostatic* shallow water approximation, in which the pressure p depends only on the depth z, i.e. it's given by the classic hydrostatic relation

$$\frac{dp}{dz} = \rho g. \tag{1}$$

This relation holds if the horizontal dimensions of the ocean volume under consideration are much larger than the vertical dimension, hence the *shallow water* designation.

As we will see in section 2.1, the pressure gradients associated with the free surface elevation are constant with depth. Thus they form part of the zeroth mode or the vertically-averaged mode, and appear only in the barotropic mode equations. Consequently, the baroclinic system representing the higher-order modes has no surface elevation associated with it, and the corresponding surface boundary condition is that of a rigid lid.

A particular form of the baroclinic models are the so-called *reduced gravity* models. These are essentially isopycnal models of several deformable layers where the lowest layer has infinite depth and zero velocity. Clearly no barotropic mode is associated with such models, and although the motions are driven by the density differences between layers, there are restrictions on the motions and interface deformations. For example, in a two-layer reduced gravity (RG) model the deviations of the interface between the two layers (representing excursions of the pycnocline) are multiples of the free surface elevation, by a factor which is proportional to the ratio $\rho/\Delta\rho$, ρ being the density and $\Delta\rho$ the density difference between the two layers (the lower one being heavier, of course).

We will discuss the barotropic models in the next section and the reduced gravity models in section 3.

2 Barotropic Models

There are several reasons why a barotropic model is interesting and important *per se*. The first, and most important, has been discussed above, i.e. that the free surface elevation couples directly to the barotropic mode. Satellite altimeter measurements[2] of the free surface elevation are one of the important data fields used as part of the initialization and updating procedures for real-time ocean prediction. Thus information from altimeters may first enter the ocean model through the barotropic mode, where it represents a direct forcing (see a similar *data forcing* with tide gauge information in section 6.)

A second feature of barotropic models is the presence of the fast free surface gravity waves.[3] The simple explicit finite-difference schemes treating such waves are subject to severe time step limitations, so that solution of the barotropic mode may lead to large CPU requirements. Thus it is important to study the solution of this system with efficient numerical schemes, before incorporating it into the general 3-D baroclinic–barotropic ocean model. For a discussion of explicit and implicit methods, as well as limitations on the time step, the student should consult section 2.4.

2.1 Model Equations for a Barotropic Ocean

The derivation of model equations for the barotropic and baroclinic components of a hydrostatic ocean, from the Navier–Stokes equations for incompressible flow on a rotating Earth, will be given in an appendix in the next release of this chapter. Here we will only present them in Cartesian coordinates and with constant friction coefficients to simplify the arithmetical text.

$$\frac{dU}{dt} = +fV - gH\left(\frac{d\eta}{dx}\right) + (\tau_{\mathrm{w}} - \tau_{\mathrm{b}})_x + A\nabla^2 U - \frac{d}{dx}(UU/H) - \frac{d}{dy}(UV/H), \tag{2}$$

$$\frac{dV}{dt} = -fU - gH\left(\frac{d\eta}{dy}\right) + (\tau_{\mathrm{w}} - \tau_{\mathrm{b}})_y + A\nabla^2 V - \frac{d}{dx}(UV/H) - \frac{d}{dy}(VV/H), \tag{3}$$

---

[2] A radar altimeter measures the distance from the satellite to the surface of the ocean, and if the position of the satellite in space is known, this measurement allows the ocean surface deviations from the level corresponding to no motion to be inferred on time scales of a few days to years. The time scale of significant large scale variation of wind forcing is a few days and is called synoptic time scale.

[3] Gravity waves are waves that propagate at the air–sea interface under the action of gravity. Note that the displacement of the heavy fluid represents available potential energy and the resulting equations are somewhat similar to those governing waves on a string.

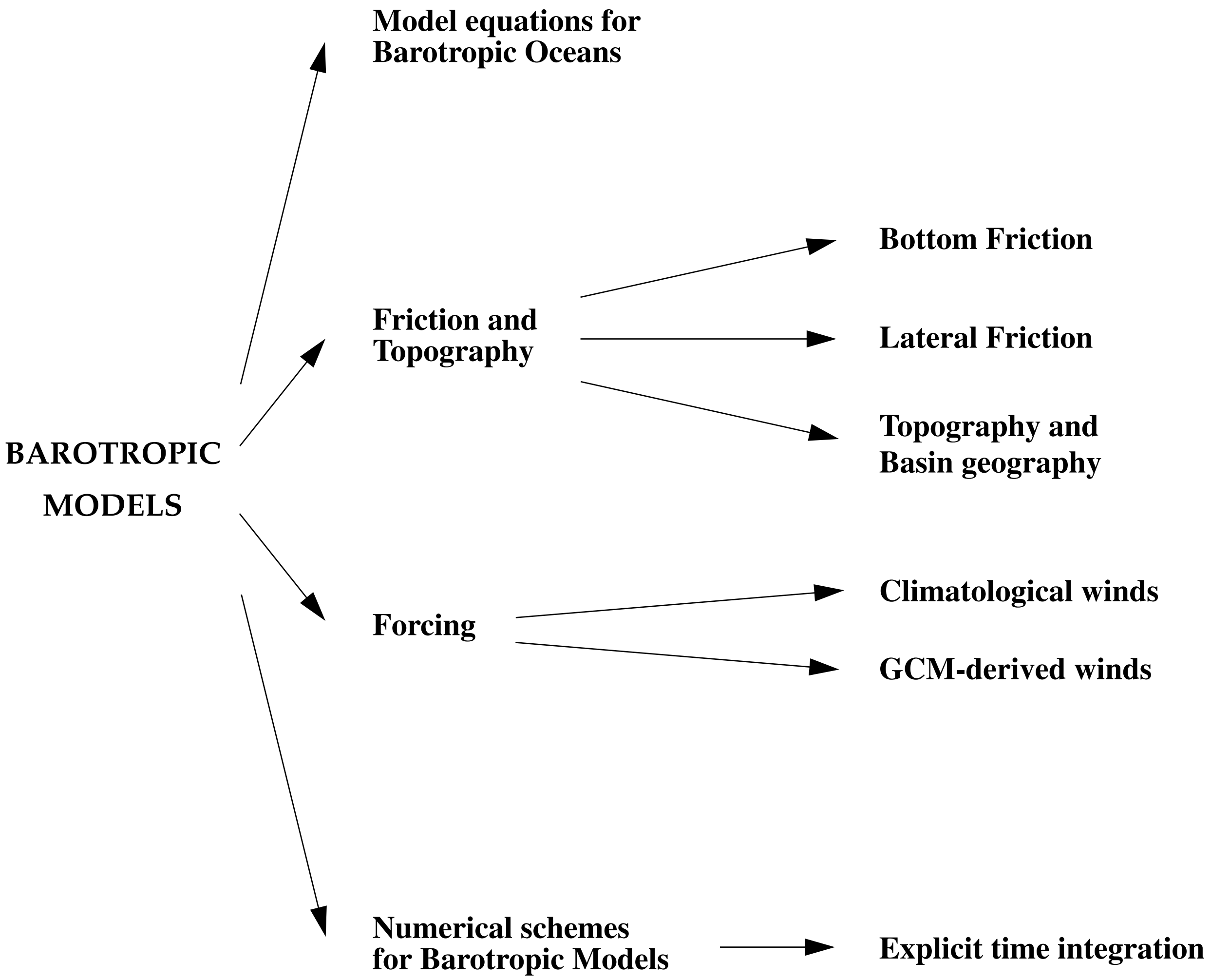

Figure 5: Breakdown of Barotropic Models

$$\frac{d\eta}{dt} = -\left(\frac{dU}{dx} + \frac{dV}{dy}\right), \tag{4}$$

where

$\vec{U} = (U, V)$ —mass transports in the x- and y-directions, respectively
$\vec{\tau}_{\mathrm{w}} = [(\tau_{\mathrm{w}})_x, (\tau_{\mathrm{w}})_y]$ —wind stress components
$\vec{\tau}_{\mathrm{b}} = [(\tau_{\mathrm{b}})_x, (\tau_{\mathrm{b}})_y]$ —bottom stress components
η —free surface elevation
$f = 2\Omega \sin \phi$ —Coriolis parameter for latitude ϕ;
Ω is the angular rotation rate of the Earth ($7 \times 10^{-5}\mathrm{s}^{-1}$)
$H(x, y)$ —topography (bottom depth)
g —acceleration due to gravity
∇^2 —Laplacian operator in horizontal coordinates x, y
A —coefficient of lateral friction
Δx —grid spacing in the longitudinal direction
Δy —grid spacing in the latitudinal direction
Δt —time step

The bottom stress τ_{b} can be related in a linear or nonlinear way to the bottom velocity, which in this case has to be replaced by the depth-mean averaged velocity. For a formulation of these terms and a discussion of the typical values used in previous modeling efforts see the next section.

We come now to a discussion of the boundary conditions. The main criterion here is whether a boundary is closed (like at a shore) or open (like at a strait where waves and currents can enter and exit the model region). As our first exercise we choose closed boundaries in a rectangular geometry $[0 < x < L_x,\ 0 < y < L_y]$, for which the relevant conditions imposed on U, V, and η are as follows:

$$\begin{aligned} U &= V = 0 && \text{on all boundaries} \\ \frac{d\eta}{dx} &= \frac{1}{gH}\left[(\tau_{\mathrm{w}} - \tau_{\mathrm{b}})_x \left(\frac{d^2U}{dx^2}\right)\right] && \text{at } x = 0, L_x \\ \frac{d\eta}{dy} &= \frac{1}{gH}\left[(\tau_{\mathrm{w}} - \tau_{\mathrm{b}})_y \left(\frac{d^2V}{dy^2}\right)\right] && \text{at } y = 0, L_y. \end{aligned} \tag{5}$$

The vanishing of the tangential velocity implies the existence of frictional boundary layers, because the velocity is brought to zero from the free stream value across a thin boundary layer, and in this layer, friction is important.

Before we discuss the numerical procedure for solving the above equations (2)–(5) we must discuss the formulation and magnitudes of the lateral and bottom friction terms, and the nature and source of the wind stresses used to force or drive the ocean model.

2.2 Friction and Topography

2.2.1 The Bottom Friction

Even in multi-level ocean models where there is an attempt to model in great detail the vertical structure, the effort to resolve boundary layers is usually confined to the surface mixed layers (see section 4 "Mixed-Layer Models"), paying little attention to the so-called "benthic" or bottom boundary layer (i.e. the turbulent frictional layer along the ocean bottom). Generally, most ocean models resort to the application of some sort of drag law in the lowest layer to represent the turbulent frictional processes there. The use of lateral (i.e. horizontal) friction, on the other hand, is an almost universal constraint imposed on all hydrodynamic numerical models by their inability to follow the nonlinear cascade of energy below scales of the mesh size. This friction effectively prevents the pileup of energy in a numerical simulation in the wavelength range corresponding to the mesh size (the nonlinear terms in 3-D turbulence cause an *energy cascade* down toward high wave numbers or short length scales). The form of the bottom friction term can take either a linear or nonlinear form; both formulations have been used in the past in ocean models of various types.

a. The linear approach: This has been used by several modelers utilizing layered-type ocean models. Nowlin [48], during an investigation of the energy transfers in a two layer model, has also derived some magnitudes for the value of σ' from spindown considerations, where the wind is turned off suddenly and the flow decelerates due to bottom friction (with minimum lateral friction) in this case. His recommended value of σ' is in the range 1–5×10^{-7}/sec. Creegan [6] has utilized the linear drag law in a study of the wind-driven circulation in the GIN[4] Sea and used a value of $\sigma' = 10^{-7}$/sec.

b. The non-linear approach: Many of the modeling efforts in the North Sea have employed a nonlinear bottom stress of the form

$$\begin{aligned} \tau_{\mathrm{b}_x} &= C_{\mathrm{d}}\left|\vec{U}\right|U \\ \tau_{\mathrm{b}_y} &= C_{\mathrm{d}}\left|\vec{U}\right|V, \end{aligned} \tag{6}$$

with the value of the drag coefficient C_{d} taken to be either .0025 or .0050, depending on the author. Many studies [62], [1], [12], [13], and [9] have used $C_{\mathrm{d}} = .0025$, whereas [8] and [17] have used a value of $C_{\mathrm{d}} = .0050$. These values were generally determined during computation of tides, from their transient behavior. In considering an application of these values for the barotropic experiments carried out here, we must consider whether the nature of the benthic boundary layer processes in the North Sea are really very different from the ones at the bottom of the GIN Sea. To really answer this question one would need to know the typical benthic boundary layer thicknesses, interior flow speeds and the size of the turbulent eddies. On first approximation it doesn't appear that these processes would be very different at a depth of 500m from those at, say 2500m, and hence the use of drag coefficients with the same magnitude appears to be warranted.

---

[4] GIN Sea: Greenland–Iceland–Norwegian Sea.

2.2.2 The Lateral (Horizontal) Friction

As discussed above, the use of a lateral friction coefficient is a general requirement for modeling all hydrodynamic processes that have strong nonlinearities, and as such it becomes a necessary part of ocean models as well. As mentioned above, such friction is necessary both for physical and numerical reasons. The size of such a coefficient can be estimated from various arguments, as we present below.

It has been found during the long history of numerical simulation of nonlinear flows that the size of this friction coefficient A is determined by a constraint laid on the so-called mesh-box Reynolds number, defined as $R_c = (\Delta x U)/A$, where Δx is the mesh size and U is the magnitude of the velocity in that mesh box. This number is constrained generally to take on values ≤ 4 in nonlinear flow simulations, as discussed by Roache [56]. Though the barotropic flow modeled here has actually an almost linear behavior, the presence of a sharp topography can be shown to cause effects similar to those of nonlinearity. From Equations (1), (2), and (3) we can derive a wave equation of the form

$$\frac{d^2\eta}{dt^2} = gH\nabla^2\eta + g\Delta H \cdot \nabla\eta. \tag{7}$$

We note that the second term has the form of an advection term, and in particular that $\sqrt{g\Delta H}$ represents a "velocity" by dimension, namely the speed of fast surface gravity waves in an ocean of depth ΔH. Inserting this "velocity" into the formula for the critical sub-mesh Reynolds number gives $R_c = \Delta x(\sqrt{g(\Delta H)})/A$. Thus $R_c \sim \sqrt{\Delta H}$; for a bottom-slope rise of 100 m in 25 km, a value of $R_c = 4$ implies a lateral friction value of 2×10^5 m^2/s, and for a rise of $\Delta H = 1000$ m a value of 6×10^4 m^2/s.

2.2.3 Forcing for Barotropic Models

The circulation in a barotropic ocean is generally the result of two kinds of "forcings": the wind stress at the ocean's surface, and the source–sink mass flows at the basin boundaries. The source flows could be ocean currents that enter the basin due to wind forcing in an adjacent basin, or enter simply to replace mass driven out by the wind or baroclinic pressure gradients in the model basin. Sink flows have similar origins. However, in this first paper on the barotropic circulation we will only consider closed boundaries and confine ourselves to consideration of the wind forcing.

During the model testing stage, we will utilize only steady winds. With a steady wind forcing, the ocean will generally arrive at a steady circulation via a "spin-up" process. Steady winds are also customarily used in theoretical studies when one studies the balance of forces and energy conversions, and when one tries to obtain the mean or climatological circulation.

2.3 Sample Databases

Ocean models require certain data for initialization and forcing. There are a variety of sources for these data. Those that are in the public domain, we present here a few examples to

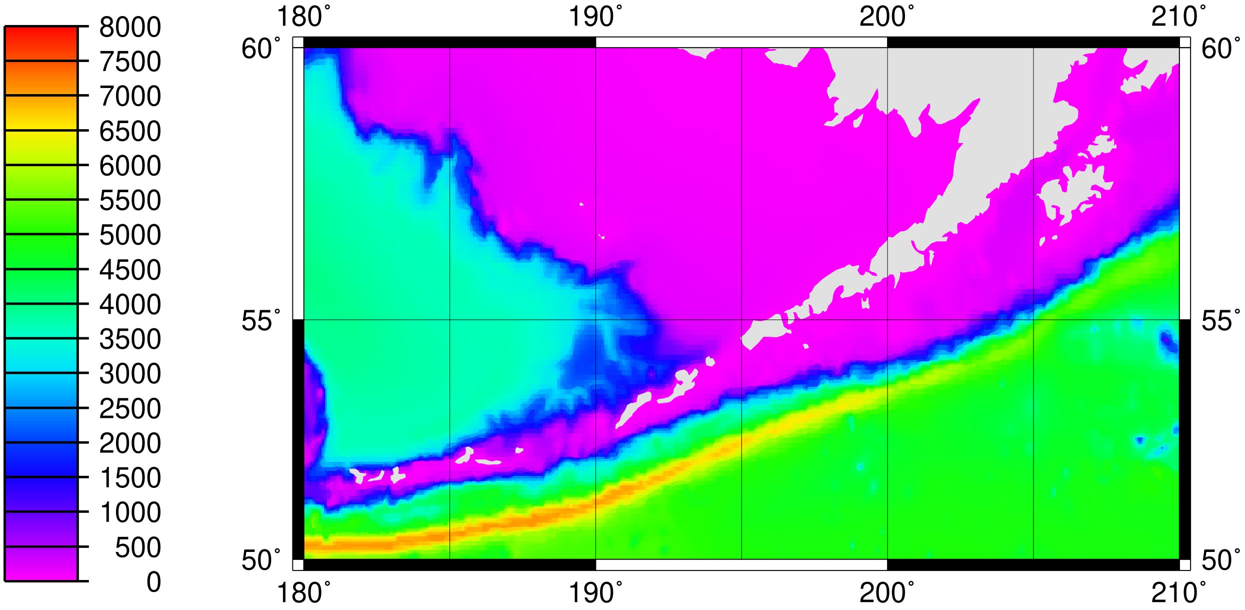

Figure 6: Ocean Depth Surrounding the Aleutian Islands (in meters)

illustrate the nature of processing needed to access the data base and extract the information desired.

2.3.1 Bottom Topography

Bottom depth is one of the most important parameters for a realistic ocean model. Bottom depth is derived from acoustic soundings from a ship. Naturally, all ocean basins are not covered equally well. Regions near coasts of well-developed countries such as the U.S. and regions well-traversed by ships are covered reasonably well, while vast areas of the southern hemisphere are not explored very well. Very high resolution (approaching 1 km) bottom topography is generally not available in the public domain. The best resolution public domain topography thus far is the gridded ETOP05 data base at the National Center for Atmospheric Research (NCAR), which contains 5 min (roughly 9 km) resolution of Earth's topography (including land). This data base is generally adequate for deeper parts of the ocean, but is less reliable over continental shelves (< 200 m deep). Nevertheless, for most ocean models it suffices. Provided is a program to derive topography for any region delineated by the latitude–longitude limits and at any desired grid resolution. The program averages the depths available from the data base in each model grid. Another topographic data set is the DBDB-5 (Digital Bathymetry Data Base at 5 min intervals), developed by the U.S. Naval Oceanographic Office in about 1982. Below are figures illustrating some topographically interesting oceanic areas from around the world. These figures were created using data sets like the ones mentioned above.

Basin geometry, another important factor in ocean modeling, is derived from the topographic data sets, which usually have default values of, for example, $(0, -10, -11)$ for the

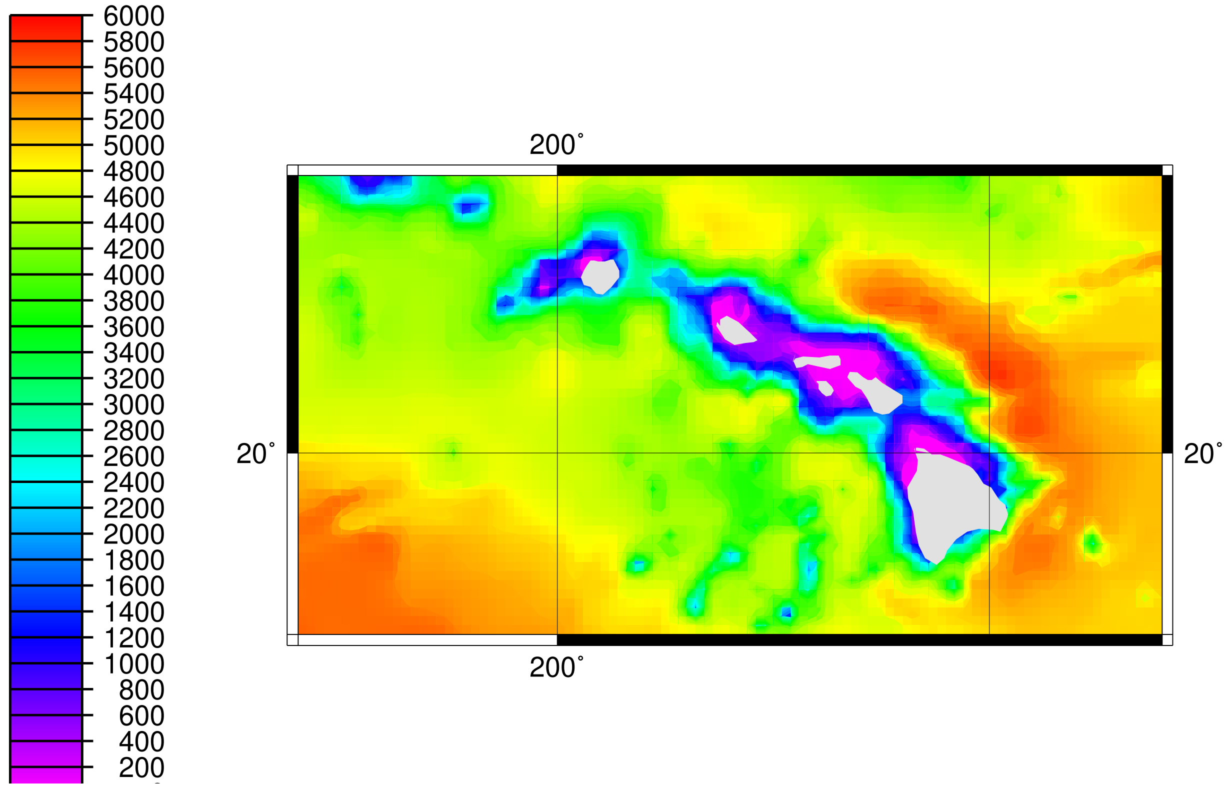

Figure 7: Ocean Depth Surrounding the Hawaiian Islands (in meters)

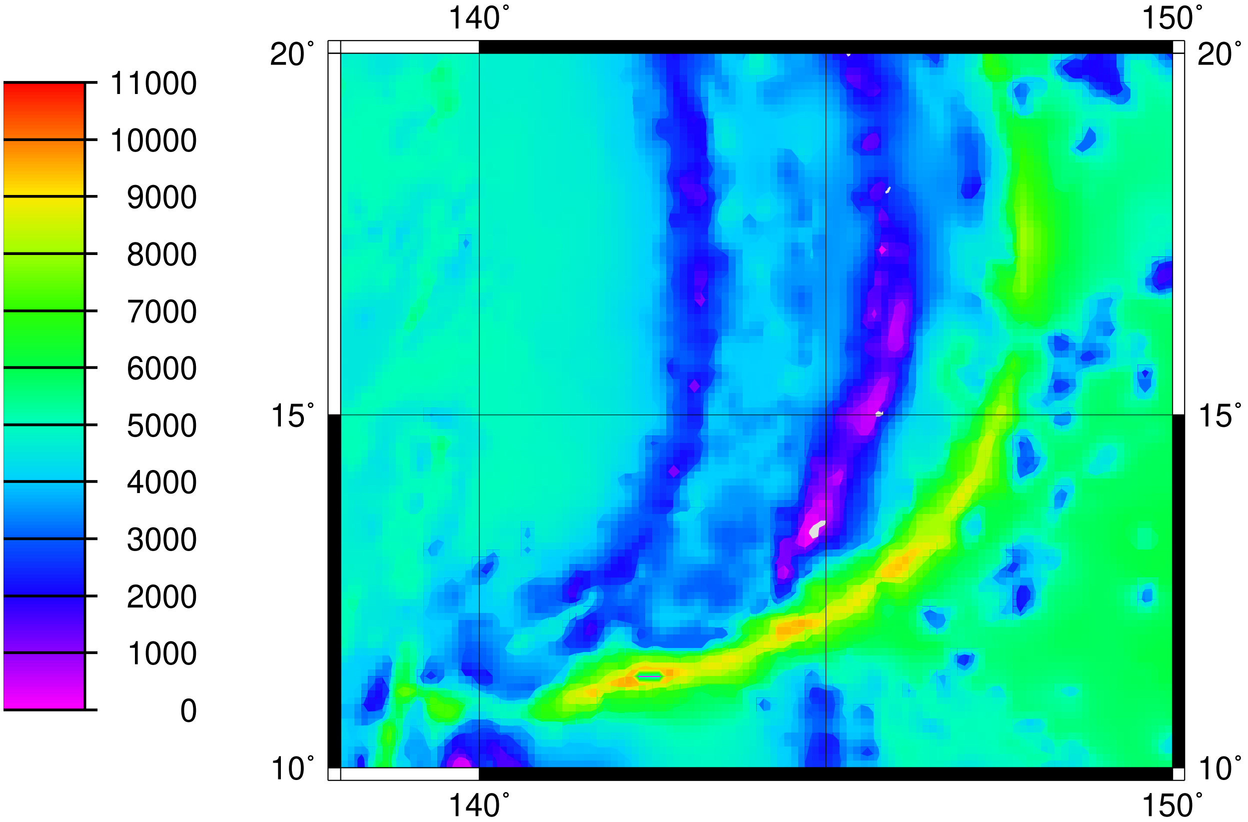

Figure 8: Ocean Depth Surrounding the Mariana Islands (in meters)

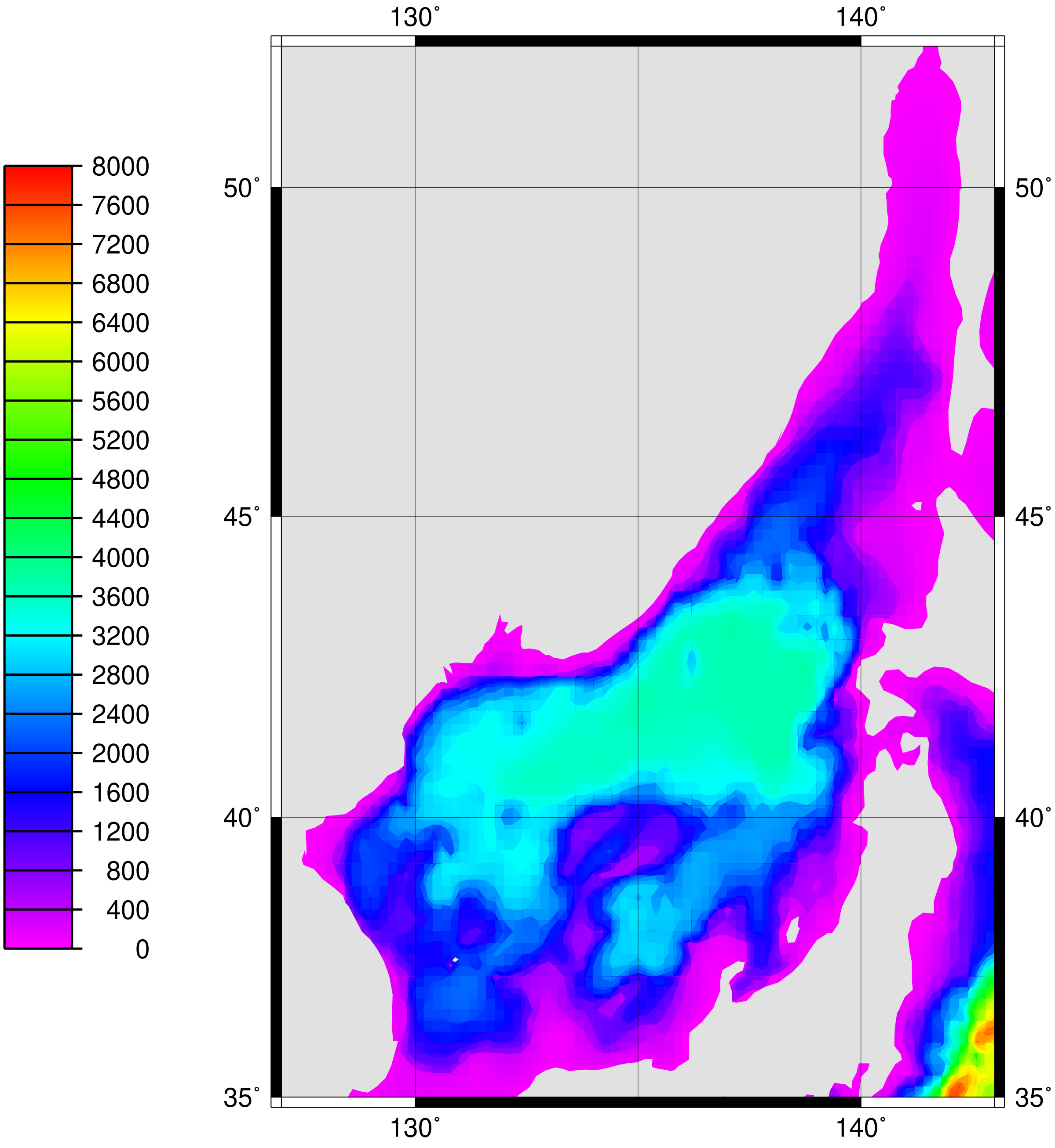

Figure 9: Sea of Japan Topography (in meters)

land points.

See exercises 1 and 2.

2.3.2 Wind Stress

Winds blowing at the surface constitute a very important driving force for ocean currents. Wind stress at the surface is therefore a necessary forcing parameter for an ocean model. Winds are routinely observed at many coastal locations around the world, but these are little help in deducing the winds over the open ocean. Historically, observations from ships constitute a major portion of our knowledge of winds over the oceans, although remote sensing using microwave scatterometers and radar altimeters (instruments that essentially measure the wind-induced roughness of the sea surface and thereby infer the wind stress acting at the sea surface) might become an important future source. Since winds vary over a variety of time scales including hourly to annual, it is difficult to obtain complete wind information at all temporal and spatial scales over the oceans. Numerical weather prediction models are one source of "synoptic" winds, however imperfect.

For longer time scales, marine surface observations from ships are an important source. These observations have been collected and archived, and long-term averages over many decades incorporated into a historical data base. Hellerman and Rosenstein [29] derived monthly average wind stresses from such a data base over global oceans at a resolution of 2 degrees (roughly 200 km). This data base is often adequate for simulating seasonal evolution of currents in an ocean model. Most ocean model results to date have been obtained with such climatological wind fields. Provided is a program to access the Hellerman–Rosenstein data base and extract monthly wind stresses for any region with prescribed latitudinal–longitudinal extent. These fields can be displayed using GMT and can also be animated to look at the seasonal evolution of wind stress/wind over the region. Below are figures depicting the monthly averaged winds for the Sea of Japan during the four seasons.

Another dataset that has just been released is the Comprehensive Oceanographic Data Set (COADS), that is the latest (to 1992) archive of marine surface observations. Thus not only winds but also surface heat fluxes are available as an average over each month of the year until 1992 at 2 degrees × 2 degrees resolution.

Climatological wind fields in the past have usually been computed from many years of ship observations, but they can also be obtained from a series of analyzed pressure or wind field outputs of weather prediction models.

To assist synoptic (i.e. at the same time or real-time) type ocean model simulations several of the weather prediction centers around the world have started to archive their analyzed and predicted pressure fields, winds and surface heat fluxes. Among these are the British Meteorological Office in Bracknell, England and the European Centre for Medium Range

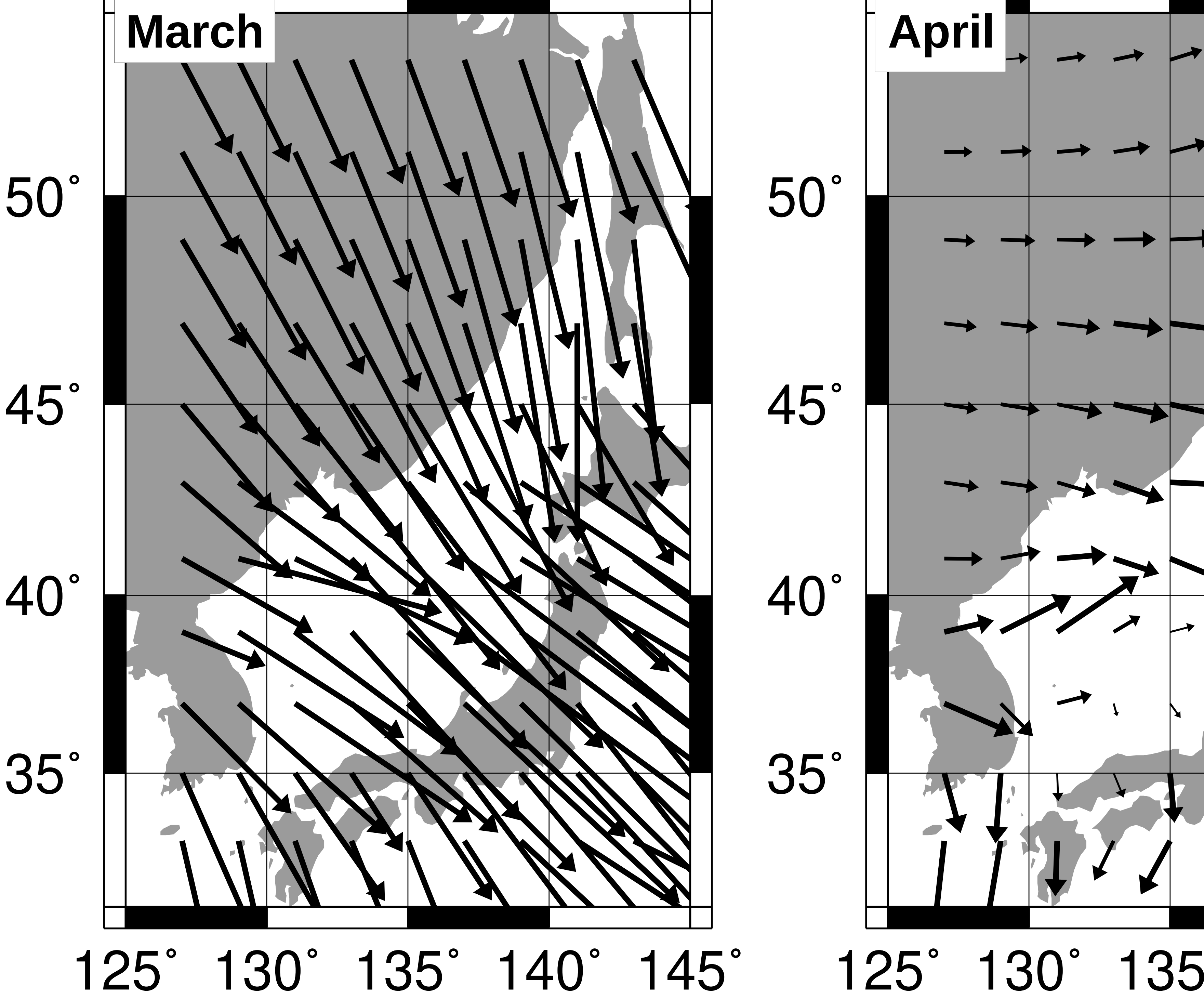
March
April
50°
45°
40°
35°
125°
130°
135°
140°
145°
50°
45°
40°
35°
125°
130°
135

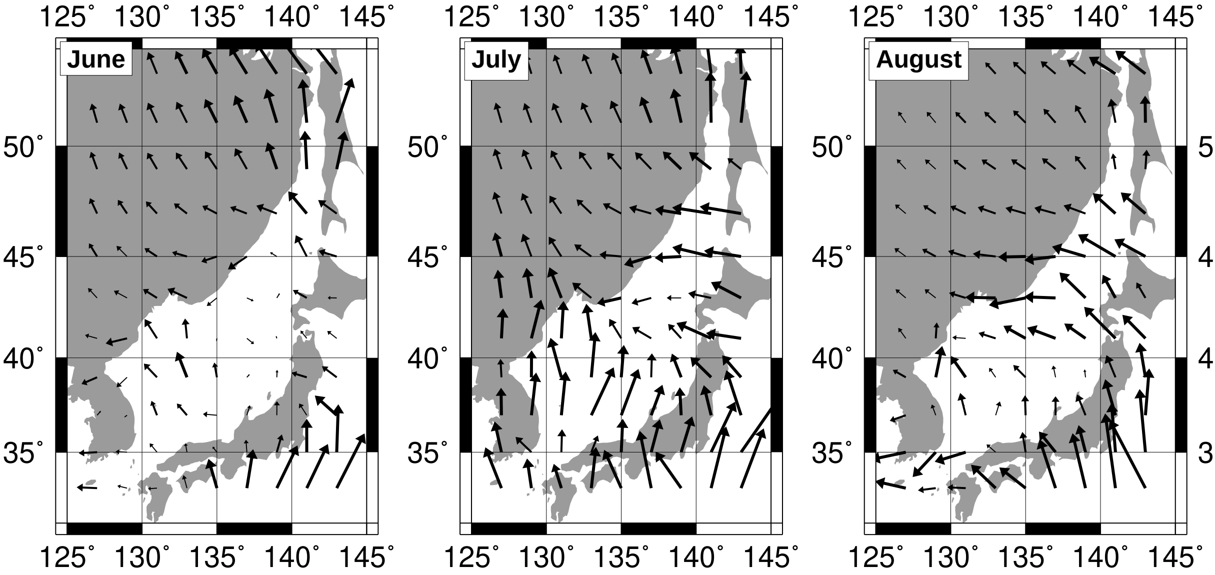

Figure 11: Summer Monthly Wind Averages in the Sea of Japan

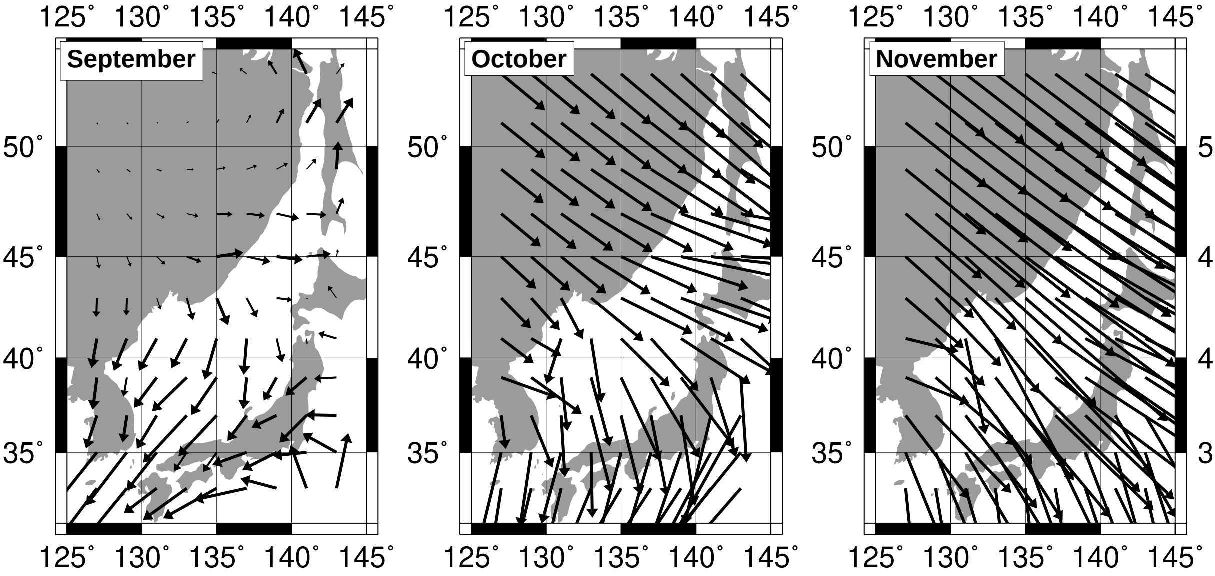

Figure 12: Autumn Monthly Wind Averages in the Sea of Japan

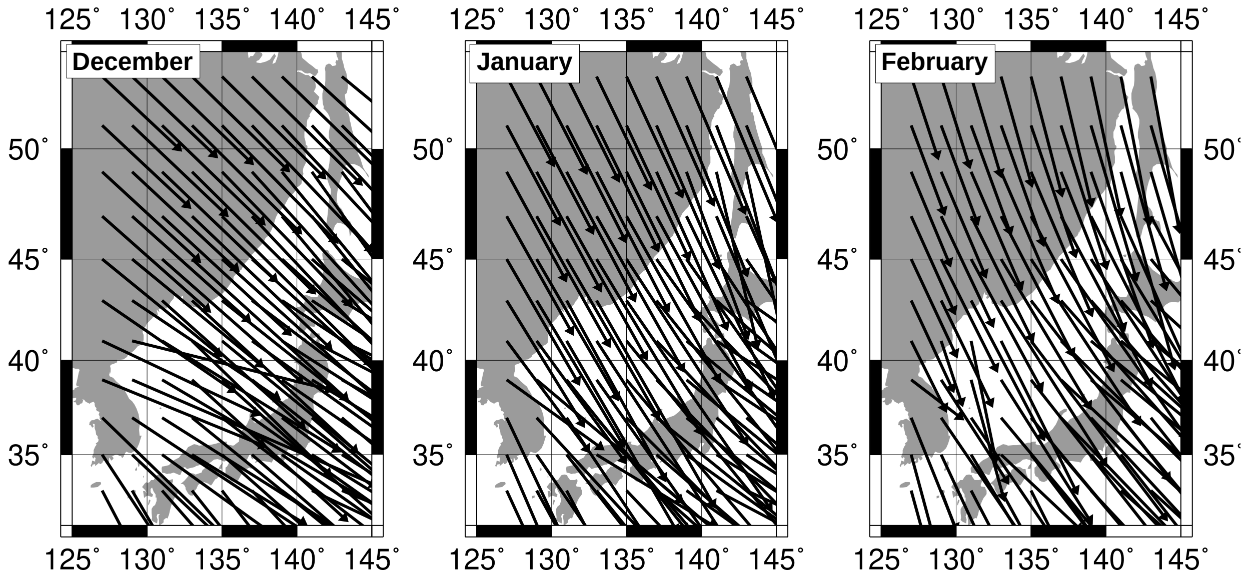

Figure 13: Winter Monthly Wind Averages in the Sea of Japan

Weather Forecasting (ECMWF) in Reading, England. The ECMWF fluxes are available from July 1, 1985.

The US Navy at Fleet Numerical Ocean Central (FNOC) at Monterey, CA also runs an operational GCM on a daily basis covering the whole globe, the output of which is available every 6 hours in near-real time. One can obtain two sets of winds, computed by different models at two different height levels. One, at the 10m level above the surface, is computed by the (Global) Planetary Boundary Layer (PBL) model, using output fields of the global weather prediction model. The other set, winds at the 50m level, are direct outputs from the global prediction model. The surface heat flux components are all outputs of the PBL model. An example of the winds over the North Pacific for May 1993 will be shown in the next release of this chapter.

The vast majority of results to date have been obtained from models with climatological wind fields. Examples of recent global model results with these winds can be found in Semtner and Cherwin [58] and Hurlburt et al. [31].

See exercise 3.

2.3.3 Water Masses (Temperature and Salinity)

Water masses govern to a large extent the circulation in an ocean basin away from the immediate vicinity of the surface. It is essential to initialize any ocean model with the temperature T and salinity S prevalent during the time of the model run. Unfortunately, it is very expensive to collect data on water masses in the ocean because of the large ship times needed to probe the deep parts of the ocean basin. However, the deep water masses do change very slowly, over time scales of hundreds of years and therefore it is possible to regard them as quasi-steady. Thus, appeal can be made to T and S data archived at national archives such as the National Oceanographic Data Center (NODC) and FNOC. These historical data can then be analyzed to derive gridded T and S fields for model initialization. Levitus [37] has done so at 1 degree resolution over the global oceans at 33 depths ranging from the surface to about 5000 m depth. There are enough data in the archives to derive meaningful temperatures over the upper 1000 m on a seasonal time scale and in the upper 200 m or so at monthly time scales. Data on salinity are more sparse. There are other T & S data bases, but none of these are so readily available for the general public. Provided is a program to access a Levitus gridded data base and extract any given region delineated by longitude and latitude and plot the results using GMT. These fields can also be animated.

See exercise 4.

2.4 Numerical Schemes for Barotropic Models

We note that the system of equations (2)–(4) has both parabolic and hyperbolic properties, the former associated with the diffusion terms and the latter with the pressure gradients and nonlinear terms. Diffusion of momentum will lead (by itself) to a parabolic partial differential equation. The coupling of the time derivatives (in all three equations) to the pressure gradients and the Coriolis terms (in equations (2) and (3)) will lead to a system that describes inertia-gravity waves and has hyperbolic characteristics. (Note: inertia-gravity waves here refer to gravity waves where the restoring buoyancy force is modified by the rotation of the Earth by the Coriolis force).

The basic techniques for the numerical solutions to these various classes of partial differential equations are given in the PDE chapter of this book. For geophysical fluid dynamic problems, an extensive survey of more specific finite-difference schemes has been given by Grammeltvedt [24] and Arakawa and Mesinger [45]. Another collection of numerical methods in oceanography can be found in O'Brien [51]. As the reader will see from both the outside literature and the various chapters of this book, the numerical schemes for solving time-dependent partial differential equations fall generally into two classes: explicit or implicit. To explain this terminology, let us assume that all variables are evaluated at discrete time and space intervals such that $(U^n)_{ij}$ represents $U(n\,dt, i\,dx, j\,dy)$ and dU/dt is approximated as $(U^{n+1} - U^n)/dt$. Then the term "explicit" denotes a scheme where all terms on the right hand sides (r.h.s.) of system (2)–(4) are evaluated at time steps n, $n-1$, etc., i.e. at any given time t^n the r.h.s. is known from previous time steps. On the other hand, "implicit" denotes a scheme where some of the terms on the r.h.s. are evaluated at time step t^{n+1} and thus are not known at time t^n. In order to proceed then, one needs to transfer these terms to the left hand sides (l.h.s) of the equations and invert the corresponding coefficient matrix for the unknown variables at t^{n+1}.

The implicit treatment (to be defined below) of the barotropic equations invokes the inversion of matrices via direct or iterative solvers. It is precisely in this area that most of the recent advances in the numerical solution of partial differential equations have taken place. Some of these advances have changed our concepts as to which iterative or direct matrix solvers are "fastest", because "fastness" depends nowadays on compatibility with computer hardware as well as on numerical convergence rates! This has become very obvious since the introduction of vector pipeline computers, and even more so with the appearance of massively parallel ones.

At the same time, the different nature of new computer architectures and the increasing size of computer memories are leading to renewed consideration of the explicit treatment of the barotropic mode. After all, as the number of vertical levels or layers increases (exceeds 20, 30 or even 60), or as we add additional transport equations for the various biochemical species, the fraction of computer time spent in solving the 2-D barotropic equations per level tends to decrease. At the same time, we notice that most explicit techniques are usually fully vectorizable and "parallelizable", thus giving strong competition to the implicit techniques on computers of this and the next decade.

2.4.1 Explicit Time Integration

We commence with explicit time marching schemes because they do not involve matrix inversion or iterative solvers. Before we write down the complete finite difference analog of equations (2)–(4), we must give finite difference expressions to the first and second spatial derivatives in the x- and y-directions. We will use only centered differences unless otherwise stated. Denoting $f(x,y) = f(i\,dx, j\,dy) = f_{i,j}$, we have

$$\frac{dU}{dx} = (U_{i+1,j} - U_{i-1,j})/\Delta x, \tag{8}$$

$$\frac{dV}{dy} = (V_{i,j+1} - V_{i,j-1})/\Delta y, \tag{9}$$

$$\frac{d^2U}{dx^2} = (U_{i+1,j} + U_{i-1,j} - 2U_{i,j})/\Delta x^2, \tag{10}$$

$$\frac{d^2V}{dy^2} = (V_{i,j+1} + V_{i,j-1} - 2V_{i,j})/\Delta y^2. \tag{11}$$

Though we avoid having to use a matrix inverter to solve for the values at t^{n+1}, we pay the price by being restricted in the time step we can take. The size of a time step one can take in solving time-marching differential equations by explicit methods is governed by the famous Courant–Friedrichs–Levy (CFL) stability condition. For wave equations the time step is limited by the wave speed, in this case the speed of the surface gravity waves c_{w}, and is given by

$$\Delta t < \Delta x / c_{\mathrm{w}}. \tag{12}$$

Typically, $c_{\mathrm{w}} = \sqrt{gH}$ exceeds 200 m/sec in basins of depth > 4000 m, so Δt is of order 100 sec for a spatial resolution of 20 km normally associated with eddy-resolving basin-scale ocean models. This is wasteful for baroclinic calculations, because the interior of the ocean adjusts very slowly to changes in forcing.

Expressions for the bottom stress τ_{b} in terms of the velocity components have already been given in section 2.2.1,

$$\begin{aligned} \tau_{\mathrm{b}_x} &= C_{\mathrm{d}} \left|\vec{U}\right| U \\ \tau_{\mathrm{b}_y} &= C_{\mathrm{d}} \left|\vec{U}\right| V \end{aligned} . \tag{13}$$

In the linear formulation τ_{b} takes the form

$$\begin{aligned} \tau_{\mathrm{b}_x} &= \sigma' U \\ \tau_{\mathrm{b}_y} &= \sigma' V, \end{aligned} \tag{14}$$

where σ' has values typically between 10^{-6} or 10^{-7} sec^{-1}, depending on the application.

The value of A has to be deduced by considering the topography gradients as well as the strength of the nonlinear terms; however, the latter are quite small except in very shallow waters. For a discussion of the mesh-box Reynolds number criterion, see section 2.2.2.

We will now write out the finite-difference analogs of equations (2), (3) and (4). In the first exercise we will omit the nonlinear terms, since these are shown not to be important in barotropic flows of the deep ocean. Furthermore, we will use the linear bottom friction formulation (14), and locate the variables on a staggered mesh, called the *C-grid* by Arakawa and Mesinger [45] (see Figure 14).

In this arrangement the pressure p and height h variables are located at the center of the mesh boxes, and the mass transports U and V at the center of the box boundaries facing the x and y directions, respectively.

A C-grid is a composite grid whereby three variables are solved for. It is composed of three subgrids. The first subgrid shows a mesh for the variable η (free surface height), the second shows a mesh for the variable U (West–East transport), and the third shows a mesh for the variable V (North–South transport). The overlay with the respective shifts (see Figure 16, Figure 17 and Figure 18) comprises the composite grid.

$$\begin{aligned} \frac{U_{i,j}^{n+1} - U_{i,j}^{n-1}}{\Delta t} &= fV_{i,j}^{n} - \frac{gH}{\Delta x}(\eta_{i,j}^{n} - \eta_{i-1,j}^{n}) \\ &+ \frac{A}{\Delta x^2}(U_{i+1,j}^{n-1} + U_{i-1,j}^{n-1} + U_{i,j+1}^{n-1} + U_{i,j-1}^{n-1} - 4U_{i,j}^{n-1}), \\ &+ (\tau_x)_{i,j}^{n} - C_{\mathrm{d}} U_{i,j}^{n-1} \end{aligned} \tag{15}$$

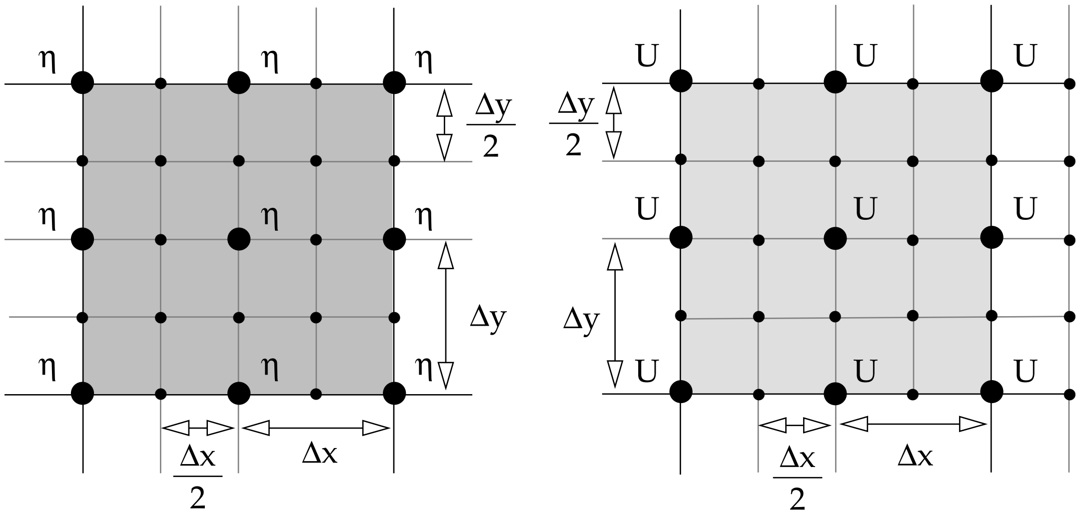

η–Grid

U-Grid (Shifted West by dx/2)

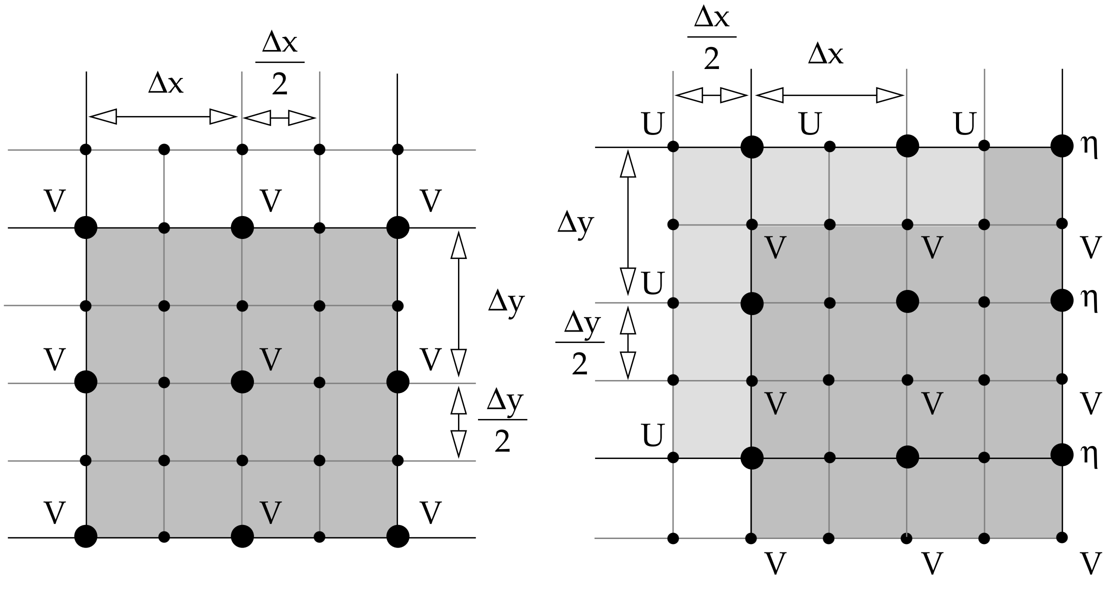

V-Grid (Shifted South by dy/2)

Composite Grid

Figure 14: The Sigma Coordinate Grid Representation composed of the η subgrid, the V subgrid, and the U subgrid.

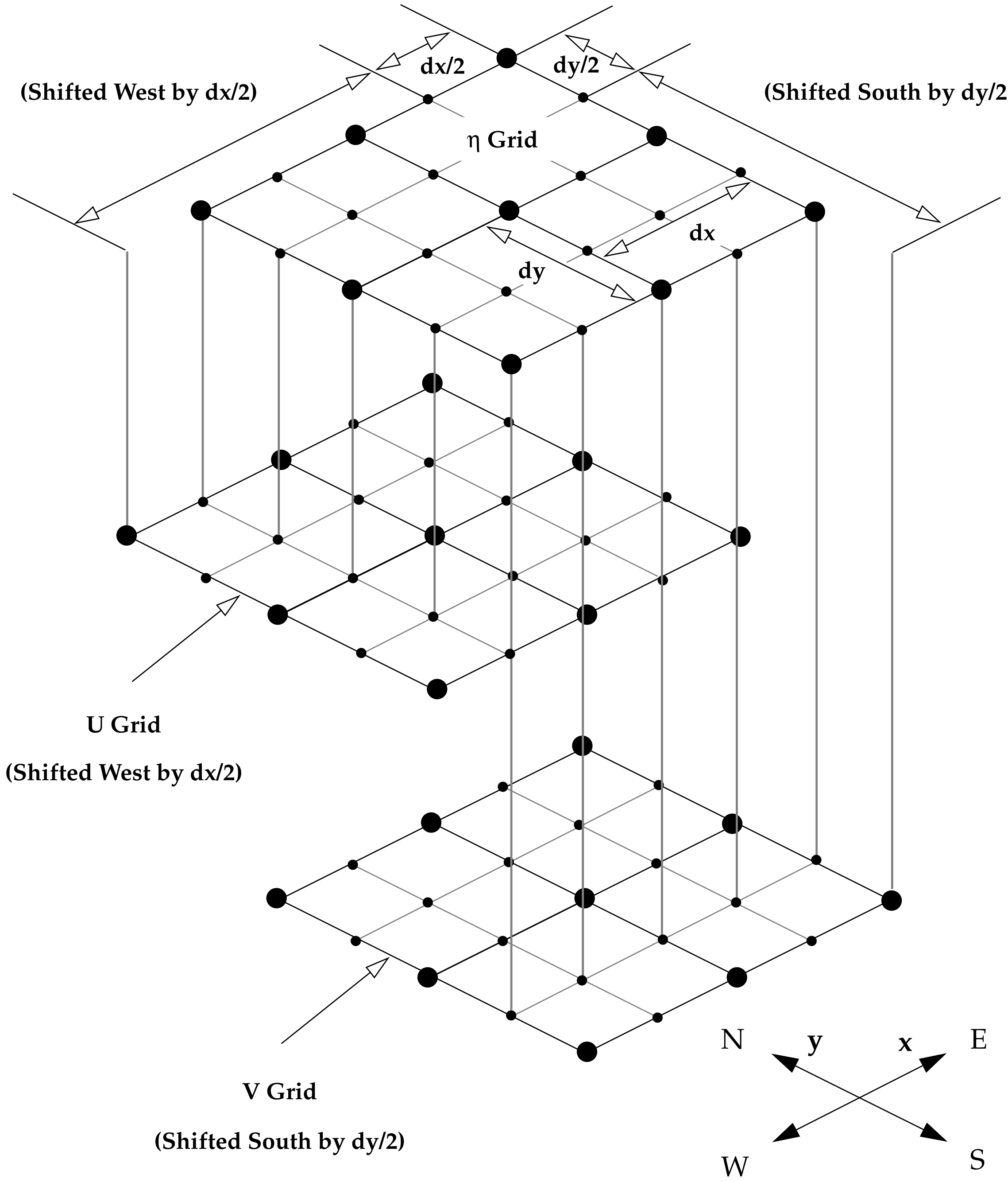

Figure 15: Exploded View of the Sigma Coordinate Grid Representation

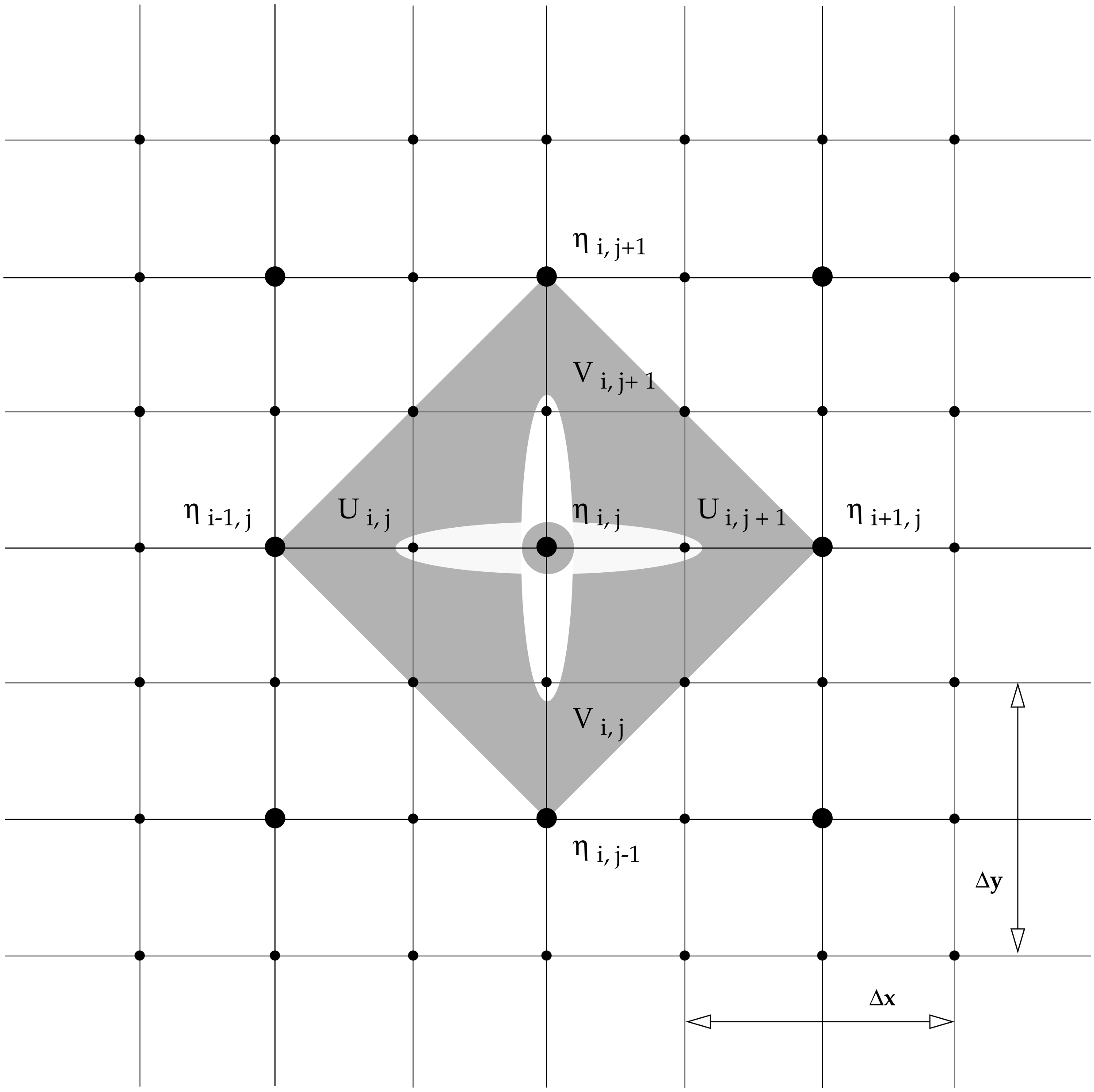

Figure 16: Expanded View of the Sigma Coordinate Grid Representation and the Variables needed to solve for $\eta_{i,j}$.

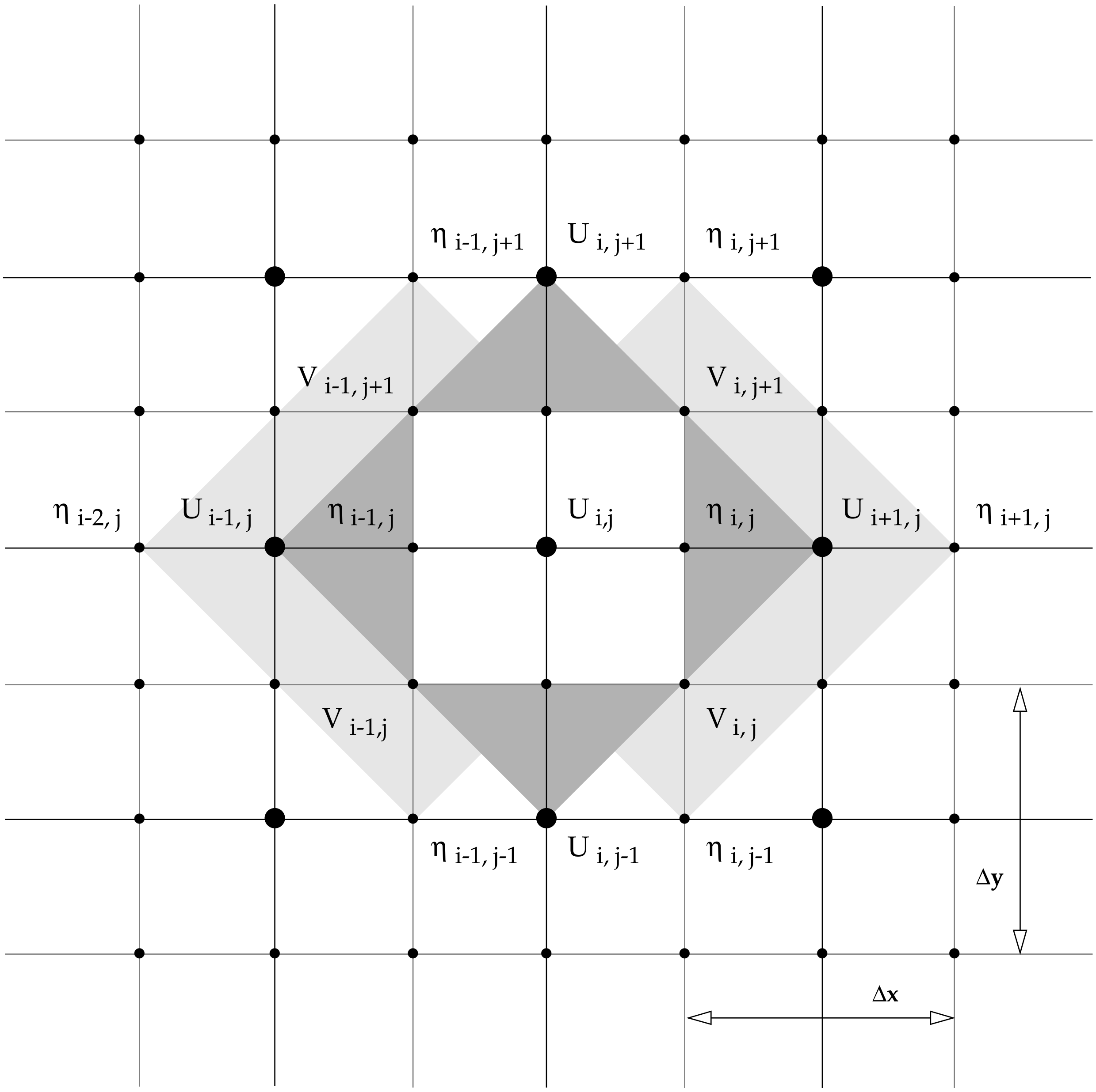

Figure 17: Expanded View of the Sigma Coordinate Grid Representation and the Variables needed to solve for $U_{i,j}$.

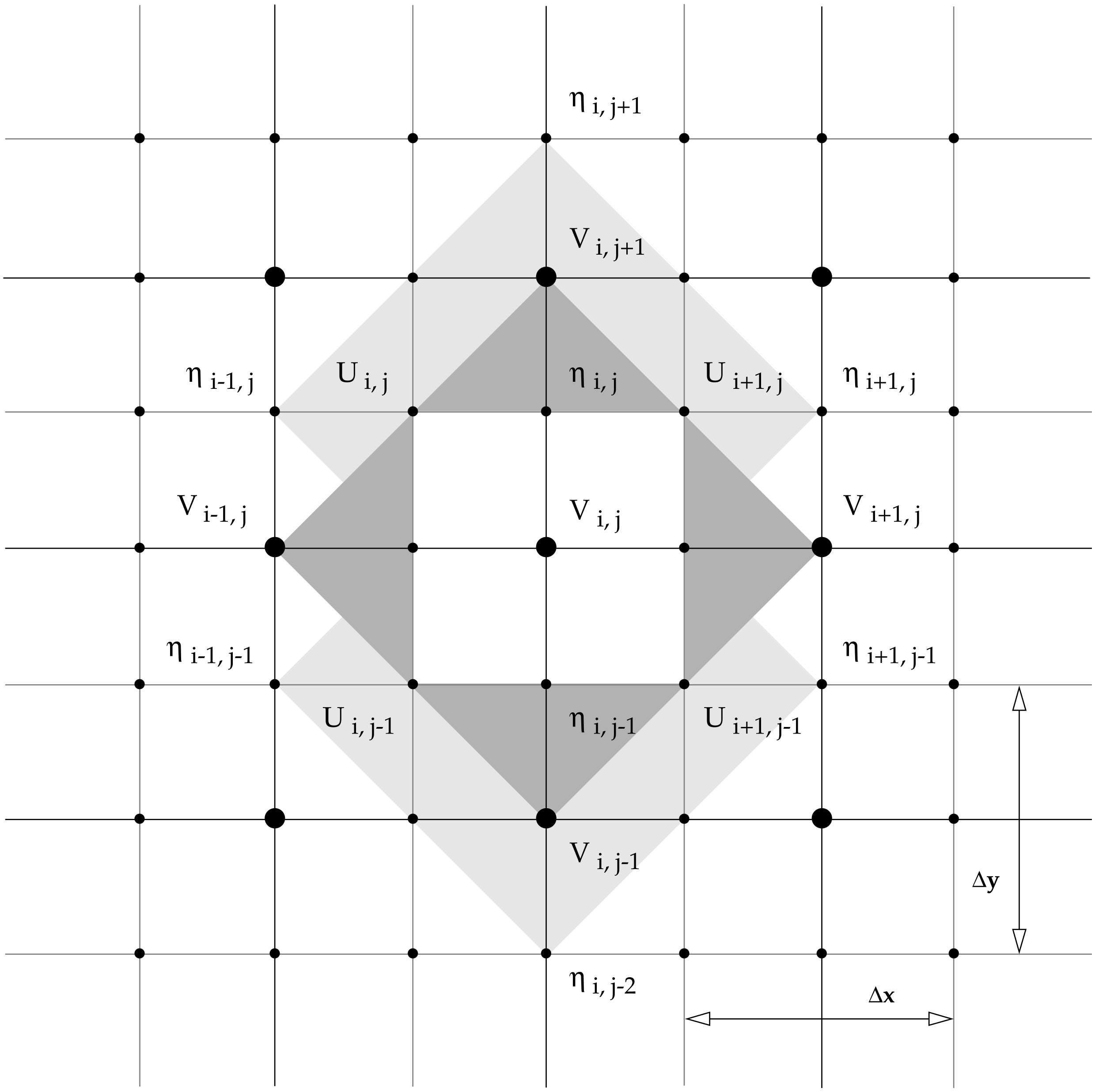

Figure 18: Expanded View of the Sigma Coordinate Grid Representation and the Variables needed to solve for $V_{i,j}$.

$$
\begin{aligned}
\frac{V_{i,j}^{n+1} - V_{i,j}^{n-1}}{\Delta t} \quad &= fU_{i,j}^{n} - \frac{gH}{\Delta y}(\eta_{i,j}^{n} - \eta_{i,j-1}^{n}) \\
&+ \quad \frac{A}{\Delta y^2}(V_{i+1,j}^{n-1} + V_{i-1,j}^{n-1} + V_{i,j+1}^{n-1} + V_{i,j-1}^{n-1} - 4V_{i,j}^{n-1}), \qquad (16) \\
&+ \quad (\tau_y)_{i,j}^{n} - C_{\mathrm{d}} V_{i,j}^{n-1}
\end{aligned}
$$

$$
\frac{\eta_{i,j}^{n+1} - \eta_{i,j}^{n-1}}{\Delta t} = \frac{(U_{i+1,j}^{n} - U_{i,j}^{n})}{\Delta x} - \frac{(V_{i,j+1}^{n} - V_{i,j}^{n})}{\Delta y}. \qquad (17)
$$

We will execute the above model now on three classes of computers:

(a) ordinary serial computers such as the SPARC2 or Silicon Graphics Iri;

(b) vector pipeline computers such as the Cray YMP, with one processor or multitasked for several processors.

(c) massively parallel computers such as the CM-200 or CM-5 of Thinking Machines Corporation.

The respective codes can be found in the directory of this Chapter. We note that for this simple explicit code the only impediments to either vectorization or "parallelization" are contained in the friction terms. There is recursion when sweeping a grid incrementing the `I` index, for then `T(I-1)` will have a new value when the computation commences at point `I` for `T(I)`, but neither in a vector pipeline, nor in a message-passing parallel computer, can this value be accessed when needed. The solution is to introduce an auxiliary storage vector, say `TR`, into which the values T^{n-1} are loaded at the beginning of the timestep, so that the right hand sides of the expression for T^{n+1} are computed using `TR`, and hence use the correct T^{n-1} values.

See exercises 5 and 6.

---

3 Reduced Gravity Models

As discussed in section 1.1.3, reduced gravity models are a simple form of isopycnal models. The simplest case, to be discussed here, is the "one-active layer" (also referred to as 1.5 layer) reduced gravity model, in which a top layer of a given initial thickness (say 300–500m) overlays a layer of infinite depth in which there are no motions. A peculiarity of these models is the fact that deviations of the interface between the two layers (representing excursions of the pycnocline) are multiples of the free surface elevation, by a factor which is proportional to the ratio $\rho/\Delta\rho$, ρ being the density and $\Delta\rho$ the density jump between the two layers (the lower one being heavier, of course). The derivation of the appropriate equations, from the 3-D Navier–Stokes equations for incompressible flow on a rotating Earth, will be given in connection with isopycnal models in a later release of this case study. Only the equations for the one-active layer model are given below.

3.1 Model Equations for a Reduced Gravity Ocean

Here we will present them for Cartesian coordinates and for constant friction coefficients only; the extension to spherical coordinates and non-constant friction will be left to the student. These equations are given in detail in Hurlburt and Thompson [31] and Preller and Hurlburt [55].

$$\begin{gathered}
\frac{\partial U}{\partial t} = +fV - g'h\left(\frac{\partial h}{\partial x}\right) + (\tau_{\mathrm{w}} - \tau_{\mathrm{i}})_x + A\nabla^2 U - \frac{\partial}{\partial x}\left(\frac{UU}{h}\right) - \frac{\partial}{\partial y}\left(\frac{VU}{h}\right) \\
\frac{\partial V}{\partial t} = -fV - g'h\left(\frac{\partial h}{\partial y}\right) + (\tau_{\mathrm{w}} - \tau_{\mathrm{i}})_y + A\nabla^2 V - \frac{\partial}{\partial x}\left(\frac{UV}{h}\right) - \frac{\partial}{\partial y}\left(\frac{VV}{h}\right) \\
\frac{\partial h}{\partial t} = -\left(\frac{\partial U}{\partial x} + \frac{\partial V}{\partial y}\right)
\end{gathered} \tag{18}$$

where,

$\vec{\tau_{\mathrm{i}}} = [(\tau_{\mathrm{i}})_x, \tau_{\mathrm{i}})_y]$ —interfacial stress components
h —total upper layer thickness (mean + pycnocline + surface deviations)
g' —reduced gravity is $g\Delta\rho/\rho$

Other quantities are as in the barotropic model.

The interfacial stress τ_{i} can be related in a linear or a nonlinear way to the velocity jump across the layers. For the formulation of these terms and a discussion of the typical values used in modeling efforts see section 2.2.1. The boundary conditions at the lateral walls (coastlines) are essentially the same as were used for the barotropic velocities discussed at the end of section 2.1. We have defined h to be the total upper layer thickness, and it is equal to

$$h = h_0 + \eta + P, \tag{19}$$

where h_0 is the mean (initial undisturbed) layer thickness, η is the free surface elevation, and P is the pycnocline deviation. As noted before,

$$P = (\frac{\rho}{\Delta\rho})\eta, \tag{20}$$

where $\Delta\rho$ is the density jump between the upper and lower layers, (with the lower being heavier).

The student should note that the two deformations η and P constitute only one dependent variable, because of the relation (20). Also, equations (18) are very similar to equations (2)–(4) for the barotropic ocean, with the total upper layer thickness h replacing the free surface elevation η in the continuity equation (2) and g' replacing g in the pressure gradient terms in (2) and (3). However, also note that the variable upper layer thickness h has also replaced the topography H in the momentum equations, so that now the pressure terms have become nonlinear.

4 Mixed-Layer Models

4.1 The Turbulent Surface Layer

The surface layers of the ocean form a part of the ocean–atmosphere boundary layer system, and as such are dominated by turbulent mixing processes and the air–sea heat and momentum fluxes. These layers are referred to collectively as the "mixed-layer" because there is almost always present at least one homogeneous layer near the surface in which the temperature and salinity profiles are constant with depth (the result of mixing), and the sound velocity increases with depth due to pressure effects. The bottom of the mixed-layer then most often represents the surface maximum of the sound velocity profile.

Many times, however, the situation is more complicated, in that the "mixed-layer" is actually composed of a sandwich of several homogeneous layers, each the result of different mixing, cooling and heating epochs on the diurnal, synoptic (i.e. weather) and seasonal scales, or any combination of these. Due to the limited scope of this chapter we will present only three of four of these configurations, selected on the basis of frequency of occurrence and their effect on acoustic propagation.

The boundary layer nature of the near-surface layers has strong implications for the models designed to simulate them. The principal requirement for these models is the correct specification of the fluxes of momentum and heat across the air–sea interface, and the correct simulation of the turbulent mixing due to surface wave breaking and shear of the wind-driven currents.

Due to the large discrepancy in spatial scales between the horizontal extent of atmospheric cyclones and the depth of the mixed layer, mixed-layer models have been generally constructed as 1-D models, with pressure gradients and all horizontal gradients neglected (see Kantha and Clayson [34], Martin [40]). These assumptions are very similar to the usual boundary layer approximations in hydrodynamics.

4.2 The Mixed Layer Equations

The principal balance in the equations of motion comes from a balance of momentum acceleration, vertical momentum diffusion and the Coriolis force due to the Earth's rotation:

$$\frac{\partial U}{\partial t} = \frac{\partial}{\partial z}\left(K_{\mathrm{m}}\frac{\partial U}{\partial z}\right) + fV, \tag{21}$$

$$\frac{\partial V}{\partial t} = \frac{\partial}{\partial z}\left(K_{\mathrm{m}}\frac{\partial V}{\partial z}\right) - fU, \tag{22}$$

where U and V are the E–W and N–S components of the velocity, f is the Coriolis parameter and K_{m} is the coefficient of turbulent momentum diffusion. The transport equation for heat balances vertical diffusion of heat and incident solar radiation Q_{s} in 1-D models, and also advection of heat in 3-D models (1-D meaning that the spatial gradients in only one direction, in this case z, are retained. In other words, fluid flow is regarded as horizontally homogeneous). Thus,

$$\frac{\partial T}{\partial t} = \frac{\partial}{\partial z}\left(K_{\mathrm{h}}\frac{\partial T}{\partial z}\right) + Q_{\mathrm{s}} \tag{23}$$

where T is the temperature. There is similarly a transport equation for salt,

$$\frac{\partial S}{\partial t} = \frac{\partial}{\partial z}\left(K_{\mathrm{s}}\frac{\partial S}{\partial z}\right), \tag{24}$$

where K_{h} and K_{s} are turbulent diffusion coefficients for heat and salt, respectively, and S is salinity.

More recently, these 1-D models have been extended to 3-D to take into account divergences in the various fluxes resulting from the horizontal inhomogeneity of the winds, and the effect of the dynamic ocean currents that advect momentum, heat and salt on even smaller scales.

In the above transport equations, we have used an approximation in the turbulent diffusion terms for the generalized vertical turbulent fluxes of momentum and heat, $\overline{wu}$, $\overline{wv}$, and $\overline{wt}$. These approximations are obtained via so-called *closure* procedures, as is usually done in the simulation of turbulent flows. A review of these methods for geophysical flows is given in a survey by Mellor and Yamada [44] and Kantha and Clayson [34]. An application of first and second order closure procedures to the oceanic mixed layer was performed in [66]. For brevity, we shall outline below only the so-called *first-order* closure or *eddy diffusion* models, where the vertical turbulent fluxes $\overline{wu}$, etc. are approximated as follows

$$-\overline{wu} = K_{\mathrm{m}}\frac{\partial U}{\partial z}, \tag{25}$$

$$-\overline{wt} = K_{\mathrm{h}}\frac{\partial T}{\partial z}, \tag{26}$$

where the K's are computed from relations of the type

$$(K_{\mathrm{m}}, K_{\mathrm{h}}) = lq(S_{\mathrm{m}}, S_{\mathrm{h}}), \tag{27}$$

with $\frac{1}{2}q^2$ being the turbulence kinetic energy $\overline{\frac{1}{2}u_i u_i}$, l is the so-called "integral length scale" of turbulence, defined as

$$l = \frac{\displaystyle\int_z^0 qz\,dz}{\displaystyle\int_z^0 q\,dz}, \tag{28}$$

and S_m, S_h are *stability* factors that have a functional dependence on the Richardson number (the ratio of the vertical density variation to the vertical velocity shear squared). In its simplest form, this factor is approximated as $(1 - Ri/Ri_c)^\gamma$, with γ commonly having a value of .5 and Ri_c, the so-called critical Richardson number (above which turbulence cuts off), having a value of .25. The turbulence quantity q is obtained from an equation which balances diffusion, shear production and buoyancy production due to stratification against self-decay of turbulence, but it will not be reproduced here. For a more detailed description of these models, we refer the reader to the papers of Mellor and Yamada [44], Kantha and Clayson [34], and Martin [40].

4.3 Bulk vs. Profile Models

At this point we must introduce the concept of *bulk* or *profile* models (the latter are also called *diffusive* or *differential*), depending on whether the above equations are vertically integrated through the layer, or left in their differential form (as above). Bulk models always presuppose the existence of a mixed layer and consider the changes of its momentum and heat content due to entrainment of heat and momentum at the surface and at the bottom of the mixed-layer. Examples of bulk models are the Niiler Model [47, 7], and the Garwood model [21]. The profile-type model considered here is the Mellor–Yamada model [43] with various degrees of turbulence closure, known as the "Level 2, 2.5, etc." model. For a thorough examination and comparison of several models of each type the reader is referred to the work of Martin [40] and Kantha and Clayson [34], who used meteorological data and hydrography at several locations around the globe to assess the performance of each model.

5 Sigma-Coordinate Model

The very first 3-D ocean models were multi-level, z-coordinate models applied to highly idealized oceans rectangular in shape and uniform in depth (Figure 2(a)). The real oceans have complicated geometry and large changes in bottom depth, ranging from a very few meters near the coast to a few kilometers in the deep basins. It is generally difficult to resolve the water column equally well and equally efficiently in both shallow and deep regions of a basin simultaneously. Since the number of vertical levels in an ocean model is constrained principally by economic considerations, either the deep or the near-surface regions have to be sacrificed. Thus for strong topographic variations, z-coordinate models are inherently disadvantageous. That is why, while rigid lid three-dimensional z-coordinate models have enjoyed wide-spread application to deep ocean basins, applications to shallow coastal regions or basins where shallow regions are not excluded are quite rare. Since turbulent mixing plays an important role in the circulation in the entire water column in shallow water, a better simulation of both the upper and bottom mixed layers is possible with a topographically conformal vertical coordinate system, the so-called sigma coordinate system (Figure 2(b)).

In a sigma-coordinate system, the number of vertical levels in the water column is the same everywhere in the domain irrespective of the depth of the water column. This is achieved by transformation of the governing equations from z-coordinate to sigma-coordinate in the vertical:

$$\sigma = \frac{z}{D}, \tag{29}$$

where $D = H + \eta$, is the depth of the water column. Notice that unlike the z-coordinate system, where the *layer* thicknesses are uniform in the horizontal, it is the normalized thicknesses that are uniform in the sigma-coordinate system, while the *layer* thicknesses vary widely from grid point to grid point. Also no grid point is wasted in the vertical, unlike the z-coordinate model, where high resolution in deeper regions of an ocean basin means inevitable loss of those grid points in shallower regions. Besides, the sigma coordinate enables the bottom (benthic) boundary layer to be better resolved everywhere in the domain. It is easy to see that adequate resolution of the benthic layer everywhere in the domain can be achieved in z-coordinates only with the use of a prohibitively large number of levels in the vertical.

However, these benefits do not come without penalties. While *all* numerical ocean models experience difficulties in handling sharp topographic changes from one grid point to the next, the sigma-coordinate models appear to suffer proportionately more. The problem lies in the calculation of the pressure gradient terms in the momentum equations. In sigma coordinates, sharp topographic change from one grid point to the next means that the calculation of the pressure gradient involves taking the difference between two large terms [26] and therefore large roundoff errors. While this problem can be alleviated by increased horizontal resolution, it can also be mitigated by subtraction of horizontal averages of density from the density terms before computing the density-gradient induced pressure differences from one grid point to the next. However, the other problem associated with sharp topographic changes, namely the hydrostatic inconsistency, can be reduced in severity only by smoothing the horizontal gradients of topography. It is generally wise to process the bottom topography with a filter that caps the ratio of bottom depths of adjacent grid points before using it in the model. However care must be exercised to ensure that the topography is not severely corrupted by this processing, especially over the shallow coastal regions.

As mentioned earlier, the upper and bottom mixed layers constitute a significant fraction of the water column for coastal oceans and therefore play a very important role in the dynamics of the region. It is therefore essential to parameterize the vertical mixing as accurately as possible. (For a detailed discussion of solving for turbulence quantities in the geophysical context, see Mellor and Yamada [43] and Kantha and Clayson [34]). Second moment closure of turbulence, which involves solving the governing equations for Reynolds turbulence stresses (the second moments of the velocity field), provides one means of doing this. The model to be discussed incorporates this feature. The evolution of the upper mixed layer and the benthic boundary layer are therefore somewhat more realistic under both wind stirring and surface heat fluxes.

Finally, processes such as tides and storm surges are quite important aspects of shallow water circulation and to simulate these effects, the rigid lid approximation has to be revoked and free surface dynamics included. Since this results in severe time step limitations due to constraints introduced by fast external surface gravity wave motions, generated at the air–sea interface, it becomes necessary to invoke mode splitting as a solution strategy. Mode splitting consists of splitting the solution into two parts, the barotropic (external mode) part governed by the two-dimensional vertically integrated form of the governing equations and the baroclinic (internal mode) part governed by the full equations, as demonstrated in section 5.5. The baroclinic mode is solved less frequently relative to the barotropic mode, consistent with the slower propagation speed of the internal mode disturbances *vis-a-vis* the external mode. Considerable savings accrue as a result. However care must be taken to ensure that conservation properties are not violated by mode-splitting.

5.1 Tides and Tidal Forcing

One of the worked examples of this case study is a model for barotropic tides, which are introduced at this point and will be discussed in more detail later on. The tidal model is simply the barotropic part of the sigma-coordinate 3-D model. Fortran 77 codes for scalar (Unix workstation), vector (Cray YMP) and massively parallel (Connection Machine) machines and a series of exercises are provided. It is therefore appropriate to discuss tides and tidal forcing before dealing with details of the sigma-coordinate model.

Gravitational attraction of the sun and the moon are responsible for the tidal motions on the globe, in all three media, the atmosphere, the oceans and the solid Earth. We will not go into great detail regarding this topic and the interested readers are referred to excellent books on the topic (for example Chapter 13 of Pond and Pickard [54], Chapter 11 of Dietrich et al. [11]). However, we will give enough information here so that the student can appreciate the nature of tidal processes around the globe.

The rhythmic rise and fall of sea level along the world's coastlines are the most apparent manifestation of tides in the global oceans. In some coastal locations, tides are noticeable but not spectacular, but in other places like the West coast of Korea and the Bay of Fundy, the tides are spectacularly large. In some places, the sea level rises and falls with a period of about half a day (these are called semi-diurnal tides), whereas in other places the period is more like a day (called diurnal tides). Yet again, in some locations the tides are mixed. And there are periods during the year, when the sun and moon line up with the Earth when the tides are unusually large.

While the rhythmic modulation of sea level and its association with the motion of the sun and the moon must have been noticed since pre-historic times, a better understanding had to wait until Sir Isaac Newton applied his theory of gravitation to explain the underlying physical mechanism. He was able to construct an equilibrium theory of tides, that explained the semi-diurnal nature of tides in most parts of the world. If there were infinite time allowed for adjustment of the ocean to the astronomical forces, it is the equilibrium tides that would be the result. This is however not the case since the tidal forcing varies quite rapidly with time. Resonances in the oceanic response push tides in certain localities to be above the values predicted by the equilibrium theory. While the equilibrium theory predicts two bulges to form, one underneath the moon and the other on the opposite side of the globe, in reality the high water may significantly precede or lag the transit of the moon.

These differences are due to the dynamical response of the oceans to tidal forcing. It was Laplace who, a century later, laid the theoretical and mathematical foundations for a modern dynamical theory of ocean tides by considering oceanic tides to be the response of the fluid medium to the astronomical forcing by the sun and moon's gravitational attractions. His equations are similar to equations (83) to (85), but linear and in spherical coordinates. In this approach, the tides result from dynamical balances principally between the tractive forces due to gravitation and the retarding forces due to friction in the water column.

While the rise and fall of sea level due to tides is the most apparent aspect of tides, it is the tidal currents that are the direct manifestation of tides, and the sea level rise or fall is due to resulting convergences and divergences. The sun and the moon are the only important celestial bodies in producing terrestrial tides. While the moon is much smaller than the sun, it is nevertheless more important for tidal processes, because of its proximity to the Earth. It is the small imbalance between the centrifugal force and gravitational attraction of the moon on the water column that give rise to horizontal tractive forces, causing water motions that tend to cause two bulges in the sea surface, one immediately underneath and the other on the other side of the globe. These bulges tend to rotate around the globe along with the moon resulting in semi-diurnal tides with a period of half a lunar day (12.4 hours), even though the Earth's rotation is diurnal (period of 24 hours). To model tidal motions then, it is necessary to prescribe the astronomical forcing. The tidal potential term in the equations of motion can be expressed as a Fourier series, with each term representing a tidal constituent. While there are tens of such constituents in a general expansion, usually in the deep ocean, only 11 so-called primary components are important. Of these, four are semi-diurnal, M2, N2, S2 and K2; four are diurnal, K1, O1, P1 and Q1; and the rest, Mf, Mm and Ss are long-term.

Table 1 gives the period and relative size of each of these constituents. While in some isolated situations, where other constituents become important, it is seldom essential to include many more to obtain accurate tidal predictions. In shallow water, the so-called compound tides generated by nonlinear interaction of primary constituents become important. For example, M4, generated by nonlinear self interaction of the M2 constituent has half the period of M2.

A general approach to tidal predictions in the oceans is to gather observations over a period of roughly a year and use the time series to extract the various constituents by harmonic analysis. This method works only for places where observations are available, such as coastal stations and a few "island" stations in the middle of the basins. However, for the majority of the interior of the ocean basins, there exist no observations and it is necessary to resort to numerical models. It is possible to solve for the tidal response with equations such as equations (83) to (85) but with tidal potential terms on the right hand side. However for marginal seas open to primary ocean basins, and coastal oceans, it is necessary to prescribe the tidal forcing on the boundaries open to the ocean basin. In many cases, it is this forcing that is more important than the astronomical forcing. The Persian Gulf is such an example. The tides there co-oscillate with the tides entering the Gulf from the Arabian Sea through the Straits of Hormuz. The direct astronomical forcing is negligible. On the other hand, the

Table 1: Primary Tidal Components

Tidal Component	Period (solar hours)	Description	Nature
M2	12.42	Principal lunar	semi-diurnal
S2	12.00	Principal solar	semi-diurnal
N2	12.66	Larger lunar elliptic	semi-diurnal
K2	11.97	Luni-solar	semi-diurnal
K1	23.93	Luni-solar diurnal	diurnal
O1	25.82	Principal lunar diurnal	diurnal
P1	24.07	Principal solar diurnal	diurnal
Q1	26.87	Larger lunar elliptic	diurnal
MF	327.90	Lunar fortnightly	Long term
MM	661.30	Lunar monthly	Long term
SSA	4383.00	solar semi annual	Long term
M4	6.21		Compound
MS4	6.10		Compound

tides in the Red Sea are primarily due to the direct astronomical forcing due to the highly constricted Straits of Bab-al-Mandeb that connects it to the Arabian Sea. For simplicity, we will present only a model of the Persian Gulf, which does not need the tidal potential terms in the governing equations of motion.

The most important parameters in a tidal model are the bottom depth and the bottom friction. Usually neither of them can be well-represented usually in a tidal model to sufficient resolution and therefore it is essential to fine-tune the model to yield good agreement with observations. It is a classical inverse-modeling problem although it is usually accomplished by trial and error. Another approach to obtain faithful tidal results is to include observations through the process of data assimilation. Both approaches can be experimented with in this model and we will come back to this in section 6.

5.2 Governing Equations

The model uses orthogonal curvilinear coordinates in the horizontal and the sigma coordinate system in the vertical. Let x_1, x_2 be the horizontal coordinates and z the vertical coordinate of a right handed orthogonal curvilinear coordinate system. We will write down the equations in the z system before transforming to the σ coordinate system in the vertical. Let u_1 and u_2 be the velocities in the x_1 and x_2 directions and w the velocity in the vertical direction. (Note that for curvilinear formulation this notation is more convenient and logical than U and V. Just remember $u_1 \equiv U, u_2 \equiv V, x_1 \equiv x, x_2 \equiv y$).

The continuity equation is

$$\frac{\partial}{\partial x_1}(h_2 u_1) + \frac{\partial}{\partial x_2}(h_1 u_2) + h_1 h_2 \frac{\partial w}{\partial z} = 0, \tag{30}$$

where h_1, h_2 are the metric coefficients satisfying the identity

$$ds^2 = h_1^2\, dx_1^2 + h_2^2\, dx_2^2 + dz^2, \tag{31}$$

where ds is the length of a segment in x_1, x_2, z space.

The governing equations are simplified by assuming that the fluid is incompressible and essentially of constant density. Thus variations in density are ignored except when the density is multiplied by gravitational acceleration, thus retaining the important stratification (i.e. buoyancy) effects. This is the so-called Boussinesq approximation. All terms except the gravitational and pressure gradient terms are ignored in the momentum equation in the vertical, equivalent to a hydrostatic balance, even though the fluid is in motion.

The momentum equations under Boussinesq and hydrostatic approximations can be written as

$$\begin{aligned}\frac{\partial u_1}{\partial t} &+ \frac{1}{h_1 h_2}\left[\frac{\partial}{\partial x_1}(h_2 u_1^2) + \frac{\partial}{\partial x_2}(h_1 u_1 u_2)\right] + \frac{\partial}{\partial z}(w u_1) + \frac{u_1 u_2}{h_1 h_2}\frac{\partial h_1}{\partial x_2} - \frac{u_2^2}{h_1 h_2}\frac{\partial h_2}{\partial x_1} - f u_2 \\ &= -\frac{1}{\rho_0 h_1}\frac{\partial p}{\partial x_1} + \frac{1}{h_1 h_2}\left[\frac{\partial}{\partial x_1}(h_2 \tau_{11}) + \frac{\partial}{\partial x_2}(h_1 \tau_{21}) + \tau_{21}\frac{\partial h_1}{\partial x_2} - \tau_{22}\frac{\partial h_2}{\partial x_1}\right] + \frac{\partial}{\partial z}(K_{\mathrm{M}}\frac{\partial u_1}{\partial z})\end{aligned}$$

(32)

$$\begin{aligned}\frac{\partial u_2}{\partial t} &+ \frac{1}{h_1 h_2}\left[\frac{\partial}{\partial x_1}(h_2 u_1 u_2) + \frac{\partial}{\partial x_2}(h_1 u_2^2)\right] + \frac{\partial}{\partial z}(w u_2) + \frac{u_1 u_2}{h_1 h_2}\frac{\partial h_2}{\partial x_1} - \frac{u_1^2}{h_1 h_2}\frac{\partial h_1}{\partial x_2} - f u_1 \\ &= -\frac{1}{\rho_0 h_2}\frac{\partial p}{\partial x_2} + \frac{1}{h_1 h_2}\left[\frac{\partial}{\partial x_1}(h_2 \tau_{12}) + \frac{\partial}{\partial x_2}(h_1 \tau_{22}) + \tau_{12}\frac{\partial h_2}{\partial x_1} - \tau_{11}\frac{\partial h_1}{\partial x_2}\right] + \frac{\partial}{\partial z}(K_{\mathrm{M}}\frac{\partial u_2}{\partial z})\end{aligned} \tag{33}$$

and

$$\frac{\rho}{\rho_0} g = -\frac{1}{\rho_0}\frac{\partial p}{\partial z}, \tag{34}$$

where τ_{11}, τ_{12} and τ_{22} are the components of the symmetric Reynolds stress tensor in the horizontal plane and can be written as

$$\begin{aligned}\tau_{11} &= 2A_{\mathrm{M}}\left[\frac{1}{h_1}\frac{\partial u_1}{\partial x_1} + \frac{u_2}{h_1 h_2}\frac{\partial h_1}{\partial x_2}\right] \\ \tau_{12} &= A_{\mathrm{M}}\left[\frac{h_1}{h_2}\frac{\partial}{\partial x_2}\left(\frac{u_1}{h_1}\right) + \frac{h_2}{h_1}\frac{\partial}{\partial x_1}\left(\frac{u_2}{h_2}\right)\right] = \tau_{21} \\ \tau_{22} &= 2A_{\mathrm{M}}\left[\frac{1}{h_2}\frac{\partial u_2}{\partial x_2} + \frac{u_1}{h_1 h_2}\frac{\partial h_2}{\partial x_1}\right]\end{aligned} \tag{35}$$

The quantity A_{M} is the horizontal diffusivity, while K_{M} denotes vertical diffusivity. Both are quantities determined by turbulent mixing in the fluid column. Also ρ is the fluid density, ρ_0 the reference density, g the gravitational acceleration, p the pressure and f the Coriolis parameter. Note that $f = 2\Omega \sin \phi$, where Ω is the angular rotation of the Earth in radians/sec and ϕ is the latitude. Only the vertical component of Coriolis force has been retained in the momentum equations.

Note that equation (34) incorporates hydrostatic approximation, and can be readily integrated in the vertical to provide the pressure p at any depth z:

$$p = p_{\mathrm{a}} + \rho_0 g \eta + g \int_z^0 \rho(\xi)\, d\xi, \tag{36}$$

where p_{a} is the atmospheric pressure and η is the free surface height. Although p_{a} is usually neglected, it is essential for simulation of the atmospheric loading effects on the ocean, which are important for example in hurricane-induced storm surge processes.

Note also that the form of the Coriolis terms is general in the sense that no approximations such as the f-plane or β-plane have been invoked. The former approximation ignores the latitudinal variations of f, while the latter makes a linear approximation $f = f_0 + \beta y$, where β is $\partial f/\partial y$ and y is the coordinate in the latitudinal direction equal to $R\phi$, where R is the radius of the Earth.

The density variations in the ocean are of fundamental importance in determining the ocean circulation. Density ρ is a complicated function of the temperature T, salinity S and the pressure (or equivalently depth z). It is common to take into account the pressure effects by considering ρ to be potential density, which is a function of only the potential temperature Θ and salinity S. The potential temperature Θ is usually referred to the atmospheric pressure, meaning that it is the temperature attained by a fluid parcel of *in-situ* temperature T and salinity S brought adiabatically from depth z to the surface. The baroclinic pressure gradient terms in the momentum equations and the vertical stability of the fluid column can be evaluated accurately using the horizontal and vertical gradients of potential density ρ, which can be regarded as a function of Θ and S only:

$$\rho = \rho(\Theta, S). \tag{37}$$

This equation of state is usually expressed as a power series expansion in Θ and S, but can be easily evaluated numerically. The most popular equations of state in general use in ocean models are those due to Fofonoff [15] and more recently from UNESCO [22]. The model has provisions to use either one.

The potential temperature Θ and salinity S are governed by conservation relations of the form:

$$\frac{\partial \Theta}{\partial t} + \frac{1}{h_1 h_2}\left[\frac{\partial}{\partial x_1}(h_2 u_1 \Theta) + \frac{\partial}{\partial x_2}(h_1 u_2 \Theta)\right] + \frac{\partial}{\partial z}(w\Theta) = \tag{38}$$

$$\frac{1}{h_1 h_2}\left[\frac{\partial}{\partial x_1}\left(A_{\mathrm{H}}\frac{h_2}{h_1}\frac{\partial \Theta}{\partial x_1}\right) + \frac{\partial}{\partial x_2}\left(A_{\mathrm{H}}\frac{h_1}{h_2}\frac{\partial \Theta}{\partial x_2}\right)\right] + \frac{\partial}{\partial z}\left(K_{\mathrm{H}}\frac{\partial \Theta}{\partial z}\right) + \frac{\partial Q_{\mathrm{S}}}{\partial z},$$

and

$$\frac{\partial S}{\partial t} + \frac{1}{h_1 h_2}\left[\frac{\partial}{\partial x_1}(h_2 u_1 S) + \frac{\partial}{\partial x_2}(h_1 u_2 S)\right] + \frac{\partial}{\partial z}(wS) = \tag{39}$$

$$\frac{1}{h_1 h_2}\left[\frac{\partial}{\partial x_1}\left(A_{\mathrm{H}}\frac{h_2}{h_1}\frac{\partial S}{\partial x_1}\right) + \frac{\partial}{\partial x_2}\left(A_{\mathrm{H}}\frac{h_1}{h_2}\frac{\partial S}{\partial x_2}\right)\right] + \frac{\partial}{\partial z}\left(K_{\mathrm{H}}\frac{\partial S}{\partial z}\right),$$

where K_{H} is the vertical and A_{H} the horizontal eddy diffusivities due to turbulent mixing of heat and salt in the water column. The last term in equation (38) accounts for the heating due to penetrative shortwave solar radiation. While the values of horizontal eddy diffusivities A_{M} and A_{H} are also influenced by numerical considerations arising from the need to damp subgrid scale computational noise, the vertical diffusivities K_{M} and K_{H} are principally determined from small scale turbulent mixing in the water column. Nevertheless, proper parameterization of A_{M}, A_{H}, K_{M} and K_{H} is the most important unresolved issue in ocean modeling since the model results are sensitive in varying degrees to the values of these coefficients and the theoretical underpinnings needed to confidently prescribe them are for the most part quite shaky.

It is not unusual to use zeroth order closure models for these diffusivities and regard them as constants throughout. This is rather counter-intuitive, since these values are functions of the prevailing turbulence field in the fluid and strictly speaking should be derived from properties of turbulent mixing occurring in the fluid. However, away from the fully turbulent mixed layers near the surface and the bottom of the ocean, very little is known about intermittent mixing processes that occur in the interior of the ocean. Traditionally, K_{M}, K_{H}, A_{M} and A_{H} are prescribed *a priori* as constant values and these values are "tuned" to obtain the desired results. However because of the sensitivity of the model output to these values, this *ad-hoc* procedure has become increasingly untenable and better prescriptions often using higher order closures have become the norm. For example, this model uses first-order closure for A_{M} and A_{H}, thus relating them to mean deformation rates in the fluid, while K_{M} and K_{H} are obtained from second order closure (also called second moment closure) for small-scale turbulent mixing that principally determines the vertical diffusivities in the upper and benthic mixed layers. In the interior of the ocean, K_{M} and K_{H} are still often assumed to be constant, even though there is ample evidence [20] to suggest that both K_{M} and K_{H} should be functions of vertical stratification of the water column and that K_{H} for heat should be different from that for salt. The model includes an option to prescribe K_{M} and K_{H} in the interior as

$$K_{\mathrm{M}} = K_{\mathrm{M}_0} N^{-1}, \quad K_{\mathrm{H}} = \alpha K_{\mathrm{M}}, \tag{40}$$

where N is the Brunt–Vaisala frequency indicative of the stability of the fluid column and α is a constant. N is given by

$$N^2 = -\frac{1}{\rho_0} g \frac{\partial \rho}{\partial z} + \frac{g^2}{c^2}, \tag{41}$$

where c is the sound speed defined as

$$c^2 = \left(\frac{\partial p}{\partial \rho} \right)_{\Theta,S}. \tag{42}$$

Vertical mixing coefficients K_{M} and K_{H} in the fully turbulent mixed layers at the surface and the bottom are obtained by second order closure model of turbulence based on the work of Mellor and Yamada [43, 44] ;see also the work of Galperin, Kantha, Hassid and Rosati [18]. The turbulence in this so-called level 2.25 model is characterized by two quantities, the turbulence kinetic energy $q^2/2$ and the turbulence macroscale l. This two-equation model of turbulence is governed by the following equations:

$$\begin{aligned} &\frac{\partial}{\partial t}(q^2) + \frac{1}{h_1 h_2}\left[\frac{\partial}{\partial x_1}(h_2 u_1 q^2) \frac{\partial}{\partial x_2}(h_1 u_2 q^2)\right] + \frac{\partial}{\partial z}(w q^2) = \\ &2K_{\mathrm{M}}\left[\left(\frac{\partial u_1}{\partial z}\right)^2 + \left(\frac{\partial u_2}{\partial z}\right)^2\right] + 2K_{\mathrm{H}}\frac{g}{\rho_0}\frac{\partial \rho}{\partial z} - \frac{2q^3}{B_1 l} \\ &+\frac{1}{h_1 h_2}\left[\frac{\partial}{\partial x_1}\left(A_{\mathrm{H}}\frac{h_2}{h_1}\frac{\partial q^2}{\partial x_1}\right) + \frac{\partial}{\partial x_2}\left(A_{\mathrm{H}}\frac{h_1}{h_2}\frac{\partial q^2}{\partial x_2}\right)\right] + \frac{\partial}{\partial z}\left(K_q \frac{\partial q^2}{\partial z}\right), \end{aligned} \tag{43}$$

and

$$\frac{\partial}{\partial t}(q^2l)+\frac{1}{h_1h_2}\left[\frac{\partial}{\partial x_1}(h_2u_1q^2l)\frac{\partial}{\partial x_2}(h_1u_2q^2l)\right]+\frac{\partial}{\partial z}(wq^2l)=$$

$$K_{\mathrm{M}}E_1l\left[\left(\frac{\partial u_1}{\partial z}\right)^2+\left(\frac{\partial u_2}{\partial z}\right)^2\right]+K_{\mathrm{H}}E_3l\frac{g}{\rho_0}\frac{\partial\rho}{\partial z}-\frac{q^3}{B_1}\left[1+E_2\left(\frac{l}{\kappa L}\right)^2\right] \tag{44}$$

$$+\frac{1}{h_1h_2}\left[\frac{\partial}{\partial x_1}\left(A_{\mathrm{H}}\frac{h_2}{h_1}\frac{\partial}{\partial x_1}(q^2l)\right)+\frac{\partial}{\partial x_2}\left(A_{\mathrm{H}}\frac{h_1}{h_2}\frac{\partial}{\partial x_2}(q^2l)\right)\right]+\frac{\partial}{\partial z}\left[K_q\frac{\partial}{\partial z}\left(q^2l\right)\right].$$

Second order closure (see [18]) relates the vertical mixing coefficients K_{M}, K_{H} and K_q to the turbulence scales q and l:

$$K_{\mathrm{M}}=lqS_{\mathrm{M}},\quad K_{\mathrm{H}}=lqS_{\mathrm{H}},\quad \text{and}\quad K_{\mathrm{q}}=lqS_{\mathrm{q}}, \tag{45}$$

where S_{M}, S_{H} and S_q are stability functions determined from algebraic relations derived analytically from simplifications made to the full second moment closure model:

$$S_{\mathrm{M}}=A_1\left[\frac{\left(1-\dfrac{6A_1}{B_1}-3C_1\right)+9(2A_1+A_2)S_{\mathrm{H}}G_{\mathrm{H}}}{(1-9A_1A_2G_{\mathrm{H}})}\right], \tag{46}$$

$$S_{\mathrm{H}}=A_2\left[\frac{1-\dfrac{6A_1}{B_1}}{1-3A_2G_{\mathrm{H}}(6A_1+B_2)}\right], \tag{47}$$

and

$$S_q=0.2, \tag{48}$$

where

$$G_{\mathrm{H}}=\frac{l^2}{q^2}\frac{g}{\rho_0}\frac{\partial\rho}{\partial z}. \tag{49}$$

A_1, A_2, B_1, and B_2 are constants that determine the ratios of various turbulence length scales to the turbulence macroscale l. The turbulence closure assumes that all turbulence length scales are proportional to one another.

Note that S_{M} and S_{H} are functions of G_{H}, which is in turn a function of the buoyancy gradient. The term multiplying q^3/B_1 in equation (44) is a wall proximity function inserted empirically to assure log-law behavior near solid boundaries and L is given by

$$L^{-1}=z^{-1}+(D+z)^{-1}, \tag{50}$$

where D is the depth of the fluid column.

Terms C_1, E_1, E_2 and E_3 are empirical constants determined by appealing to well-known laboratory experiments on turbulence, as are constants A_1, A_2, B_1 and B_2:

$$(A_1, A_2, B_1, B_2, C_1, E_1, E_2, E_3) = (0.92, 0.74, 16.6, 10.1, 0.08, 1.8, 1.8, 1.33). \tag{51}$$

κ is the well-known von Karman constant (=0.4) that occurs in the log-law governing the velocity profile adjacent to a boundary in a turbulent boundary layer.

See exercise 7.

5.3 Boundary Conditions

Free Surface

The flow must satisfy certain boundary conditions at the free surface $z = \eta(x_1, x_2)$. Since the free surface is a material surface, w must satisfy

$$w = \frac{\partial \eta}{\partial t} + u_1 \frac{\partial \eta}{\partial x_1} + u_2 \frac{\partial \eta}{\partial x_2}. \tag{52}$$

In addition, momentum and buoyancy fluxes (comprised of heat and salt fluxes) at the free surface are the driving mechanisms for the ocean and must satisfy

$$\begin{aligned} K_{\mathrm{M}} \left(\frac{\partial u_1}{\partial z}, \frac{\partial u_2}{\partial z} \right) &= \frac{1}{\rho_0} (\tau_{01}, \tau_{02}) \\ K_{\mathrm{M}} \left(\frac{\partial \Theta}{\partial z}, \frac{\partial S}{\partial z} \right) &= \frac{1}{\rho_0} (\overline{Q_{\mathrm{H}}}, \overline{Q_{\mathrm{S}}}), \end{aligned} \tag{53}$$

where τ_{01} and τ_{02} are the wind stress components, and $\overline{Q_{\mathrm{H}}}$ and $\overline{Q_{\mathrm{S}}}$ are the heat and salt fluxes at the surface. $\overline{Q_{\mathrm{H}}}$ is the result of energy balance at the ocean surface involving the impinging short and long wave solar radiation, the back radiation from the ocean, the sensible and latent heat fluxes from the ocean to the atmosphere:

$$\overline{Q_{\mathrm{H}}} = \overline{\beta}(1 - \overline{\alpha}) S_{\mathrm{W}} + L_{\mathrm{W}} - \varepsilon \overline{\sigma} T_{\mathrm{S}}^4 - H_{\mathrm{S}} - H_{\mathrm{L}}. \tag{54}$$

S_{W} is the short-wave solar radiative flux, L_{W} is the long wave radiative flux, $\overline{\alpha}$ is the albedo, ε the emissivity of the ocean surface, $\overline{\sigma}$ is the Stefan–Boltzmann constant, T_{s} is the sea surface temperature, and H_{S} and H_{L} are the the sensible and latent heat fluxes. $\overline{\beta}$ is the fraction of the short wave flux absorbed at the surface. If $\overline{\beta}$ is put equal to unity, then Q_{S} in equation (38) must be put to zero, implying that all the incident shortwave radiation is absorbed at the surface and there is no penetrative heating of the ocean. A more realistic scenario involves absorption of near infrared components close to the surface while the longer components are absorbed in the body of the fluid, the extent of penetration depending on the optical clarity of the upper layers. This more general prescription is crucial from the point of view of the biological productivity of the upper ocean. Here $\overline{\beta} = 0$ and

$$\overline{Q_S} = \sum_{i=1}^{N} \overline{\beta}_i (1 - \overline{\alpha}) S_W \exp(z/L_i) \qquad \text{where} \quad \sum_{i=1}^{N} \overline{\beta}_i = 1, \tag{55}$$

L_i denotes the extinction length scale of the ith short-wave component, which accounts for fraction $\overline{\beta}_i$ of the incident shortwave flux. Note that the longwave component L_W is all absorbed within a millimeter of the ocean surface. Normally about 5–6 spectral bands are adequate for ocean modeling purposes, although a much higher value of N is needed for modeling the optical characteristics and biological productivity of the upper ocean [57]. In many cases, a two-component decomposition of shortwave flux, where one component is absorbed close to the surface (small extinction scale) and the other is allowed to penetrate deeper (extinction scale of the order of tens of meters) appears adequate [10]. Needless to say, the extinction length scales are a strong function of the optical clarity of the water. Sediment-laden water near the coast and waters with high biological productivity have shorter extinction scales, compared to the clear water in the biological deserts of the mid-ocean gyres [32].

The salt flux $\overline{Q_S}$ at the ocean surface is

$$\overline{Q_S} = S_S(\dot{E} - \dot{P}), \tag{56}$$

where $\dot{E}$ is the evaporation and $\dot{P}$ the precipitation rates at the surface and S_s is the sea surface salinity. $\dot{E}$ is of course related to the latent heat flux H_L.

An alternative to equations (55) and (56) is to prescribe the sea surface temperature and salinity, if known:

$$(\Theta, S) = (T_S, S_S). \tag{57}$$

Yet another alternative is to damp the surface values of Θ and S to the sea surface values with a time lag t_l

$$\frac{\partial}{\partial t}(\Theta, S) = -\frac{1}{t_l}[(\Theta - T_S), (S - S_S)]. \tag{58}$$

Conditions (57) and (58) are most often used in climatological simulations, while equation (55) and (56) are useful for driving the ocean with synoptic momentum and buoyancy fluxes.

The conditions on q^2 and l at the free surface are

$$q^2 = B_1^{2/3} u_{*0}^2 \quad \text{and} \quad l = 0, \tag{59}$$

where u_{*0} is the friction velocity at the surface $= [(\tau_{01}^2 + \tau_{02}^2)/\rho_0^2]^{1/4}$.

Equation (59) assumes that surface waves do not contribute to the turbulence near the free surface. This is only a convenient approximation useful for most situations. However, when the upper mixed layer is shallow and winds are light, the surface wave contribution cannot be ignored, and can be included by parameterizing the kinetic energy flux due to waves and prescribing that instead at the free surface. Similarly l can be prescribed as a function of the significant wave height. Nevertheless, wave-induced turbulence dies off quite rapidly with depth and is seldom important at depths of more than a few meters.

5.3.1 Ocean Bottom

At the ocean bottom, $z = -H$, there can be no flux of heat or salt:

$$\left(\frac{\partial\Theta}{\partial z}, \frac{\partial S}{\partial z}\right)_{\mathrm{b}} = (0, 0). \tag{60}$$

There can also be no mass flux through the bottom leading to

$$w = -u_{1\mathrm{b}}\frac{\partial H}{\partial x_1} - u_{2\mathrm{b}}\frac{\partial H}{\partial x_2}, \tag{61}$$

where subscript b denotes the lower boundary.

The remaining boundary conditions are

$$\begin{aligned} K_{\mathrm{M}}\left(\frac{\partial u_1}{\partial z}, \frac{\partial u_2}{\partial z}\right) &= \frac{1}{\rho_0}(\tau_{\mathrm{b}1}, \tau_{\mathrm{b}2}) \\ q^2 &= B_1^{2/3}u_{*\mathrm{b}}^2 \qquad (62) \\ l &= 0 \end{aligned}$$

where $\tau_{\mathrm{b}1}$ and $\tau_{\mathrm{b}2}$ are the shear stress components at the bottom and $u_{*\mathrm{b}} = [(\tau_{\mathrm{b}1}^2 + \tau_{\mathrm{b}2}^2)/\rho_0^2]^{1/4}$ is the friction velocity at the bottom. The bottom stresses are determined by matching the velocities $u_{1\mathrm{b}}$, $u_{2\mathrm{b}}$ at the bottommost grid point z_{b} to a logarithmic law of the wall:

$$(\tau_{\mathrm{b}1}, \tau_{\mathrm{b}2}) = \rho_0 C_{\mathrm{D}}[u_{1\mathrm{b}}^2 + u_{2\mathrm{b}}^2]^{1/2}(u_{1\mathrm{b}}, (u_{2\mathrm{b}}), \tag{63}$$

where the drag coefficient C_{D} is determined from log-law:

$$C_{\mathrm{D}} = \left[\frac{1}{\kappa}\ln\left(\frac{H + z_{\mathrm{b}}}{z_0}\right)\right]^{-2}, \tag{64}$$

z_0 is the roughness scale, of the order of a centimeter or so for moderately rough bottom. Prescription (63) and (64) assumes that the bottommost grid point is in the log layer. If the model vertical resolution is not adequate to satisfy this condition, the drag coefficient is set to a value of 0.0025, so that a conventional quadratic drag law results. The model algorithm chooses the larger of this value and the value given by equation (64), to satisfy this prescription.

5.3.2 Lateral Boundaries

For a closed basin, the lateral boundary conditions are quite straightforward. The conditions of zero mass, momentum, heat, salt and turbulence fluxes must be satisfied at a solid lateral boundary. However, at open boundaries, the influence of the region exterior to the model domain must be specified in one form or another. Open lateral boundary conditions are therefore the hardest to prescribe, since the external conditions are usually unknown. If sufficient observational data exist at the open boundary or conditions there are known from another model containing the exterior region, it would not be a problem to prescribe the lateral boundary conditions. But these conditions are seldom satisfied and various approximations, some more close to reality than others, need to be made. In general, the model results are usually only as good as the prescribed lateral boundary conditions and sufficient care must be exercised to assure that the prescription leads to meaningful results.

Nevertheless, it is possible to lay down some general rules. As far as scalars Θ, S, q^2 and l are concerned, whether there is inflow or outflow determines the form of the lateral boundary conditions. When there is inflow, Θ and S need to be prescribed, while for outflow, Θ and S need to be advected out:

$$\frac{\partial}{\partial t}(\Theta, S) + u_n \frac{\partial}{\partial n}(\Theta, S) = 0, \tag{65}$$

where n denotes the coordinate normal to the lateral boundary. As far as q^2 and l are concerned, it is fairly accurate to ignore any advection at the lateral boundaries.

Prescription of mass and momentum conditions at an open boundary is more difficult, since this is really a function of the interaction with the exterior domain, which is *a priori* unknown when modeling a limited region. Nevertheless, inflow and outflow must be specified somehow as a function of time. The most important requirement is to satisfy the mass balance. Thus open boundary conditions must be specified such that there is no net mass increase over a specified period of time. For tidal (or barotropic) calculations, the free surface elevation $\eta(t)$ may be prescribed on the boundary. Often a Sommerfeld radiation condition of the form

$$\frac{\partial \phi}{\partial t} + c\frac{\partial \phi}{\partial n} = 0, \tag{66}$$

is used, where ϕ is any quantity such as η, u_1, ... and c is the phase speed of a disturbance approaching the boundary from the interior of the domain. Equation (66) is designed to not bottle up transient disturbances generated inside. However its application is often not unambiguous, especially since the phase speed of the disturbance is not known *a priori* and also it is difficult to decide which disturbances should be propagated out. One strategy to alleviate the former is to compute the phase speed in the interior immediately adjacent to the open boundary from the interior solutions and use it in equation (66). This is the so-called Orlonski approach [52]. Its application requires considerable care since it can lead to very noisy values for c, which in turn can affect the interior solutions [33].

It is important to remember that conditions such as equation (66) are no substitutes for knowing how the exterior region is effecting the open lateral boundary conditions.

5.4 Transformation to Sigma Coordinates

A topographically conformal vertical coordinate system has, as discussed earlier, many advantages in dealing with an ocean basin with wide disparities in bottom depth, although this does not come without some disadvantages. We will now transform the governing equations from z coordinate to σ-coordinate, where

$$\sigma = \frac{z-\eta}{H+\eta}. \tag{67}$$

Formally, we transform the equations from a (x_1, x_2, z, t) coordinate system to the $(\bar{x}_1, \bar{x}_2, \sigma, \bar{t})$ system, where $x_1 = \bar{x}_1$, $x_2 = \bar{x}_2$, and $t = \bar{t}$. Let f be a dependent variable that denotes any quantity representative of an ocean property. Then the derivatives of this quantity are related in the two coordinate systems thus:

$$\begin{aligned}
\frac{\partial \phi}{\partial x_1} &= \frac{\partial \phi}{\partial \bar{x}_1} - \frac{\partial \phi}{\partial \sigma}\left(\frac{\sigma}{D}\frac{\partial D}{\partial \bar{x}_1} + \frac{1}{D}\frac{\partial \eta}{\partial \bar{x}_1}\right) \\
\frac{\partial \phi}{\partial x_2} &= \frac{\partial \phi}{\partial \bar{x}_2} - \frac{\partial \phi}{\partial \sigma}\left(\frac{\sigma}{D}\frac{\partial D}{\partial \bar{x}_2} + \frac{1}{D}\frac{\partial \eta}{\partial \bar{x}_2}\right) \\
\frac{\partial \phi}{\partial z} &= \frac{1}{D}\frac{\partial \phi}{\partial \sigma} \\
\frac{\partial \phi}{\partial t} &= \frac{\partial \phi}{\partial \bar{t}} - \frac{\partial \phi}{\partial \sigma}\left(\frac{\sigma}{D}\frac{\partial D}{\partial \bar{t}} + \frac{1}{D}\frac{\partial \eta}{\partial \bar{t}}\right)
\end{aligned} \tag{68}$$

where $D = H + \eta$, the total depth of the water column. Note that σ as defined in equation (67), goes from 0 at the free surface $z = \eta$ to -1 at the bottom $z = -H$. (It is also possible to define σ such that it goes from $+1$ to -1). Using equations (68) and dropping overbars for greater clarity, continuity equation (52), the momentum equations (54) to (56), conservation equations (60) and (61) and the turbulence equations (65) and (66) can be written as:

$$\frac{\partial \eta}{\partial t} + \frac{1}{h_1 h_2}\left[\frac{\partial}{\partial x_1}(h_2 u_1 D) + \frac{\partial}{\partial x_2}(h_1 u_2 D)\right] + \frac{\partial w}{\partial \sigma} = 0, \tag{69}$$

$$\begin{aligned}
\frac{\partial}{\partial t}(u_1 D) \quad &+ \quad \frac{1}{h_1 h_2}\left[\frac{\partial}{\partial x_1}(h_2 u_1^2 D) + \frac{\partial}{\partial x_2}(h_1 u_1 u_2 D)\right] + \frac{\partial}{\partial \sigma}(w u_1) + \frac{u_1 u_2 D}{h_1 h_2}\frac{\partial h_1}{\partial x_2} \\
&- \quad \frac{u_2^2 D}{h_1 h_2}\frac{\partial h_2}{\partial x_1} - f u_2 D = -D P_1 + \frac{\partial}{\partial \sigma}\left(\frac{K_{\mathrm{M}}}{D}\frac{\partial u_1}{\partial \sigma}\right) + D F_1,
\end{aligned} \tag{70}$$

$$\begin{aligned}
\frac{\partial}{\partial t}(u_2 D) \quad &+ \quad \frac{1}{h_1 h_2}\left[\frac{\partial}{\partial x_1}(h_2 u_1 u_2 D)\frac{\partial}{\partial x_2}(h_1 u_2^2 D)\right] + \frac{\partial}{\partial \sigma}(w u_2) + \frac{u_1 u_2 D}{h_1 h_2}\frac{\partial h_2}{\partial x_1} \\
&- \quad \frac{u_1^2 D}{h_1 h_2}\frac{\partial h_1}{\partial x_2} - f u_1 D = -D P_2 + \frac{\partial}{\partial \sigma}\left(\frac{K_{\mathrm{M}}}{D}\frac{\partial u_2}{\partial \sigma}\right) + D F_2,
\end{aligned} \tag{71}$$

$$\begin{aligned}\frac{\partial}{\partial t}(\Theta D)+\frac{1}{h_1h_2}\left[\frac{\partial}{\partial x_1}(h_2u_1\Theta D)\right. &+ \left.\frac{\partial}{\partial x_2}(h_1u_2\Theta D)\right]+\frac{\partial}{\partial\sigma}(w\Theta)\\ &= \frac{\partial}{\partial\sigma}\left(\frac{K_{\mathrm{H}}}{D}\frac{\partial\Theta}{\partial\sigma}\right)+DF_{\Theta},\end{aligned} \tag{72}$$

$$\begin{aligned}\frac{\partial}{\partial t}(SD)+\frac{1}{h_1h_2}\left[\frac{\partial}{\partial x_1}(h_2u_1SD)\right. &+ \left.\frac{\partial}{\partial x_2}(h_1u_2SD)\right]+\frac{\partial}{\partial\sigma}(wS)\\ &= \frac{\partial}{\partial\sigma}\left(\frac{K_{\mathrm{H}}}{D}\frac{\partial S}{\partial\sigma}\right)+DF_{S},\end{aligned} \tag{73}$$

$$\begin{aligned}&\frac{\partial}{\partial t}(q^2D)+\frac{1}{h_1h_2}\left[\frac{\partial}{\partial x_1}(h_2u_1q^2D)+\frac{\partial}{\partial x_2}(h_1u_2q^2D)\right]+\frac{\partial}{\partial\sigma}(wq^2)\\ =\;&\frac{\partial}{\partial\sigma}\left(\frac{K_{\mathrm{q}}}{D}\frac{\partial q^2}{\partial\sigma}\right)+\frac{2K_{\mathrm{M}}}{D}\left[\left(\frac{\partial u_1}{\partial\sigma}\right)^2+\left(\frac{\partial u_2}{\partial\sigma}\right)^2\right]+2K_{\mathrm{H}}\frac{g}{\rho}\frac{\partial\rho}{\partial\sigma}\\ -\;&\frac{2q^3D}{B_1l}+DF_q,\end{aligned} \tag{74}$$

and

$$\begin{aligned}&\frac{\partial}{\partial t}(q^2lD)+\frac{1}{h_1h_2}\left[\frac{\partial}{\partial x_1}(h_2u_1q^2lD)+\frac{\partial}{\partial x_2}(h_1u_2q^2lD)\right]+\frac{\partial}{\partial\sigma}(wq^2l)\\ =\;&\frac{\partial}{\partial\sigma}\left[\frac{K_{\mathrm{q}}}{D}\frac{\partial}{\partial\sigma}(q^2l)\right]+K_{\mathrm{M}}E_1\frac{l}{D}\left[\left(\frac{\partial u_1}{\partial\sigma}\right)^2+\left(\frac{\partial u_2}{\partial\sigma}\right)^2\right]+K_{\mathrm{H}}E_3l\frac{g}{\rho}\frac{\partial\rho}{\partial\sigma}\\ -\;&\frac{q^3D}{B_1}[1+E_2\left(\frac{l}{kL}\right)^2]+DF_l,\end{aligned} \tag{75}$$

where F_1, F_2, F_Θ, F_q and F_l denote horizontal diffusion terms for momentum and scalars θ, q^2 and q^2l respectively, and P_1 and P_2 denote the horizontal gradients of pressure. Notice that the overbar has been dropped from the $\overline{w}$ in equations (69)–(75); which is a pseudo-vertical velocity in the new coordinate system given by

$$\overline{w}=w-u_1\sigma\frac{\partial D}{\partial\bar{x}_1}+\frac{\partial\eta}{\partial\bar{x}_1}-u_2\sigma\frac{\partial D}{\partial\bar{x}_2}+\frac{\partial\eta}{\partial\bar{x}_2}-\left(\sigma\frac{\partial D}{\partial\bar{t}}+\frac{\partial\eta}{\partial\bar{t}}\right). \tag{76}$$

This relationship simplifies both the governing equations above and the boundary conditions that need to be satisfied at the free surface and the ocean bottom (see section 5.3):

$$\overline{w}=0 \quad \text{at} \quad \sigma=0 \quad \text{and} \quad \sigma=-1. \tag{77}$$

The pressure gradient terms DP_1 and DP_2 can be derived from equation (36):

$$\begin{aligned}
DP_1 &= \frac{D}{\rho_0}\frac{\partial p_{\rm a}}{\partial x_1} + gD\frac{\partial \eta}{\partial x_1} + \frac{gD^2}{\rho_0}\left[\frac{\partial}{\partial x_1}\int_\sigma^0 \rho\, d\sigma' - \rho\left(\frac{\sigma}{D}\frac{\partial D}{\partial x_1} + \frac{1}{D}\frac{\partial \eta}{\partial x_1}\right)\right] \\
&- \frac{gD}{\rho_0}\frac{\partial D}{\partial x_1}\int_\sigma^0 \sigma'\frac{\partial \rho}{\partial \sigma'}\, d\sigma' \qquad (78)
\end{aligned}$$

$$\begin{aligned}
DP_2 &= \frac{D}{\rho_0}\frac{\partial p_{\rm a}}{\partial x_2} + gD\frac{\partial \eta}{\partial x_2} + \frac{gD^2}{\rho_0}\left[\frac{\partial}{\partial x_2}\int_\sigma^0 \rho\, d\sigma' - \rho\left(\frac{\sigma}{D}\frac{\partial D}{\partial x_2} + \frac{1}{D}\frac{\partial \eta}{\partial x_2}\right)\right] \\
&- \frac{gD}{\rho_0}\frac{\partial D}{\partial x_2}\int_\sigma^0 \sigma'\frac{\partial \rho}{\partial \sigma'}\, d\sigma' \qquad (79)
\end{aligned}$$

The horizontal viscosity terms F_1 and F_2 are given by:

$$\begin{aligned}
DF_1 &= \frac{1}{h_1 h_2}\left\{\frac{\partial}{\partial x_1}(h_2\tau_{11}) - h_2\frac{\partial}{\partial \sigma}\left[\left(\frac{\sigma}{D}\frac{\partial D}{\partial x_1} + \frac{1}{D}\frac{\partial \eta}{\partial x_1}\right)\tau_{11}\right]\right\} \\
&+ \frac{\partial}{\partial x_2}\left\{(h_1\tau_{21}) - h_1\frac{\partial}{\partial \sigma}\left[\left(\frac{\sigma}{D}\frac{\partial D}{\partial x_2} + \frac{1}{D}\frac{\partial \eta}{\partial x_2}\right)\tau_{21}\right]\right. \\
&+ \left.\tau_{21}\frac{\partial h_1}{\partial x_2} - \tau_{22}\frac{\partial h_2}{\partial x_1}\right\}, \qquad (80)
\end{aligned}$$

$$\begin{aligned}
DF_2 &= \frac{1}{h_1 h_2}\left\{\frac{\partial}{\partial x_1}(h_2\tau_{12}) - h_2\frac{\partial}{\partial \sigma}\left[\left(\frac{\sigma}{D}\frac{\partial D}{\partial x_1} + \frac{1}{D}\frac{\partial \eta}{\partial x_1}\right)\tau_{12}\right]\right\} \\
&+ \frac{\partial}{\partial x_2}\left\{(h_1\tau_{22}) - h_1\frac{\partial}{\partial \sigma}\left[\left(\frac{\sigma}{D}\frac{\partial D}{\partial x_2} + \frac{1}{D}\frac{\partial \eta}{\partial x_2}\right)\tau_{22}\right]\right. \\
&+ \left.\tau_{12}\frac{\partial h_2}{\partial x_1} - \tau_{11}\frac{\partial h_1}{\partial x_2}\right\} \qquad (81)
\end{aligned}$$

where

$$\begin{aligned}
\tau_{11} &= 2A_{\rm M}\left\{\frac{1}{h_1}\left[\frac{\partial}{\partial x_1}(u_1 D) - \frac{\partial}{\partial \sigma}\left[u_1\left(\sigma\frac{\partial D}{\partial x_1} + \frac{\partial \eta}{\partial x_1}\right)\right]\right] + \frac{u_2 D}{h_1 h_2}\frac{\partial h_1}{\partial x_2}\right\} \\
\tau_{12} &= 2A_{\rm M}\left\{\frac{h_1}{h_2}\left[\frac{\partial}{\partial x_2}\left(\frac{u_1 D}{h_1}\right) - \frac{1}{h_1}\frac{\partial}{\partial \sigma}\left[\left(\sigma\frac{\partial D}{\partial x_2} + \frac{\partial \eta}{\partial x_2}\right)u_1\right]\right]\right. \\
&\qquad \left. + \frac{h_2}{h_1}\left[\frac{\partial}{\partial x_1}\left(\frac{u_2 D}{h_2}\right) - \frac{1}{h_2}\frac{\partial}{\partial \sigma}\left[\left(\sigma\frac{\partial D}{\partial x_1} + \frac{\partial \eta}{\partial x_1}\right)u_2\right]\right]\right\} \qquad (82) \\
\tau_{22} &= 2A_{\rm M}\left\{\frac{1}{h_2}\left[\frac{\partial}{\partial x_2}(u_2 D) - \frac{\partial}{\partial \sigma}\left(u_2\left(\sigma\frac{\partial D}{\partial x_2} + \frac{\partial \eta}{\partial x_2}\right)\right)\right]\frac{u_1 D}{h_1 h_2}\frac{\partial h_2}{\partial x_1}\right\}
\end{aligned}$$

The horizontal diffusion term F_θ is given by:

$$\begin{aligned} DF_\Theta &= \frac{1}{h_1 h_2}\left\{\frac{\partial}{\partial x_1}(h_2 q_1) - h_2\frac{\partial}{\partial\sigma}\left[\left(\frac{\sigma}{D}\frac{\partial D}{\partial x_1} + \frac{1}{D}\frac{\partial\eta}{\partial x_1}\right) q_1\right]\right. \\ &+ \left.\frac{\partial}{\partial x_2}(h_1 q_2) - h_1\frac{\partial}{\partial\sigma}\left[\left(\frac{\sigma}{D}\frac{\partial D}{\partial x_2} + \frac{1}{D}\frac{\partial\eta}{\partial x_2}\right) q_2\right]\right\} \end{aligned} \tag{83}$$

where

$$q_1 = A_\mathrm{H}\frac{1}{h_1}\left\{\frac{\partial}{\partial x_1}(\Theta D) - \frac{\partial}{\partial\sigma}\left[\left(\sigma\frac{\partial D}{\partial x_1} + \frac{\partial\eta}{\partial x_1}\right)\Theta\right]\right\}, \tag{84}$$

and

$$q_2 = A_\mathrm{H}\frac{1}{h_2}\left\{\frac{\partial}{\partial x_2}(\Theta D) - \frac{\partial}{\partial\sigma}\left[\left(\sigma\frac{\partial D}{\partial x_2} + \frac{\partial\eta}{\partial x_2}\right)\Theta\right]\right\}, \tag{85}$$

The horizontal diffusion terms F_s, F_q, F_l in equations (73) to (75) are given by expressions similar to equations (83) to (85) except that Θ is replaced by S, q^2 and $q^2 l$ respectively.

The above expressions for horizontal diffusion quantities are general expressions. It is possible to simplify these expressions by ignoring $\frac{\partial\eta}{\partial x_1}$ and $\frac{\partial\eta}{\partial x_2}$ terms, since as a rule $\frac{\partial\eta}{\partial x_1} \ll \frac{\partial D}{\partial x_1}$ and $\frac{\partial\eta}{\partial x_2} \ll \frac{\partial D}{\partial x_2}$ except in very shallow coastal waters, and further we can put $D \cong H$, the bottom depth.

It is readily apparent that even then, the most general form of the expressions for horizontal diffusion terms are complicated and rather expensive to compute. There is therefore a need for simplification. Besides, there is still a great deal of uncertainty associated with the choice of horizontal mixings coefficients A_M and A_H. More often than not, horizontal diffusion is regarded as merely a numerical necessity to control subgrid scale energy pileup in a numerical calculation and the values of A_M and A_H are prescribed in an *ad-hoc* manner, governed more by numerical than physical consideration. Our understanding of horizontal mixing, especially as they relate to subgrid scale processes is rather primitive (especially as compared to the much better understanding of vertical mixing processes due to small scale turbulence) and we are therefore justified in simplifying the expressions for F_1, F_2, F_θ, F_s, F_q and F_l.

With this in mind, we simplify the expression for F_θ to

$$DF_\Theta = \frac{1}{h_1 h_2}\left[\frac{\partial}{\partial x_1}(h_2 q_1) + \frac{\partial}{\partial x_2}(h_1 q_2)\right] \tag{86}$$

where

$$\begin{aligned} q_1 &= A_\mathrm{H}\frac{1}{h_1}\left[H\frac{\partial\Theta}{\partial x_1} - \left(\frac{\partial H}{\partial x_1}\cdot\sigma\frac{\partial\Theta}{\partial\sigma}\right)\right] \\ q_2 &= A_\mathrm{H}\frac{1}{h_2}\left[H\frac{\partial\Theta}{\partial x_2} - \left(\frac{\partial H}{\partial x_2}\cdot\sigma\frac{\partial\Theta}{\partial\sigma}\right)\right]. \end{aligned} \tag{87}$$

In equations (86) and (87) care must be taken to avoid artificial (purely numerical) diffusion of Θ along sigma surfaces, even when there are no horizontal gradients of Θ [3].

The expression for F_s is similar to equation (85) except that S replaces Θ in equations (86) and (87). The expressions for F_q and F_l are also similar except that in addition, we can safely ignore the second term in square brackets of equations (86) and (87) since along isopycnal diffusion of q^2 and $q^2 l$ is quite small in the deep ocean, because of the very small magnitudes of q^2 and $q^2 l$. Therefore, unlike Θ and S, there is not a threat of significant drift in water mass properties for long term integrations.

The expressions for horizontal viscosities F_1 and F_2 can also be simplified to considerable computational advantage and negligible loss in accuracy [41]:

$$\begin{aligned}
DF_1 &= \frac{1}{h_1}\frac{\partial}{\partial x_1}\left[2A_{\mathrm{M}}D\frac{1}{h_1}\frac{\partial u_1}{\partial x_1}\right] + \frac{1}{h_2}\frac{\partial}{\partial x_2}\left[A_{\mathrm{M}}D\left(\frac{1}{h_2}\frac{\partial u_1}{\partial x_2} + \frac{1}{h_1}\frac{\partial u_2}{\partial x_1}\right)\right] \\
DF_2 &= \frac{1}{h_2}\frac{\partial}{\partial x_2}\left[2A_{\mathrm{M}}D\frac{1}{h_2}\frac{\partial u_2}{\partial x_2}\right] + \frac{1}{h_1}\frac{\partial}{\partial x_1}\left[A_{\mathrm{M}}D\left(\frac{1}{h_2}\frac{\partial u_1}{\partial x_2} + \frac{1}{h_1}\frac{\partial u_2}{\partial x_1}\right)\right]
\end{aligned} \tag{88}$$

5.5 Mode Splitting

Because the free surface dynamics are included in the above equations and the rigid lid approximation is not invoked to filter out the external surface gravity waves, the solutions will involve adjustment due to both internal and external gravity waves. It is therefore necessary to solve these equations at a time step dictated by the Courant–Friedrichs–Levy (CFL) condition for the fast external gravity waves to avoid numerical instabilities. It is generally unnecessary to obtain solutions at such a high temporal resolution, and it is also prohibitively expensive. It is therefore desirable to eliminate external mode calculations as far as possible. This is achieved by a technique called mode-splitting [60], which involves separating out the external and internal mode equations and solving each of them separately at the appropriate time steps dictated by the respective gravity wave speeds, making sure that the two calculations are consistent and synchronous with each other. The principal advantage of this method is significant savings in computing time, because the vertically integrated, barotropic equations governing external modes are fewer and much simpler to solve. The baroclinic (or vertical structure) equations, on the other hand, are more expensive to solve and are solved at much larger time steps dictated by the slow speed of internal gravity waves, under this scheme. The barotropic equations still need to be solved at smaller time steps determined by the fast external gravity waves, but these calculations are only a small fraction of the total.

The external mode equations are obtained from integrating the continuity and momentum equations (61) to (63), vertically over the water column. Denoting vertically integrated quantities by an overbar, for example,

$$\overline{\phi} = \int_{-1}^{0} \phi \, d\sigma, \tag{89}$$

the continuity and momentum equations become

$$\frac{\partial \eta}{\partial t} + \frac{1}{h_1 h_2}\left[\frac{\partial}{\partial x_1}(h_2 \bar{u}_1 D) + \frac{\partial}{\partial x_2}(h_1 \bar{u}_2 D)\right] = 0, \tag{90}$$

$$\begin{aligned}
& \frac{\partial}{\partial t}(\bar{u}_1 D) + \frac{1}{h_1 h_2}\left[\frac{\partial}{\partial x_1}(h_2 \bar{u}_1^2 D) + \frac{\partial}{\partial x_2}(h_1 \bar{u}_1 \bar{u}_2 D)\right] - f \bar{u}_2 D \\
+ \;& \frac{\bar{u}_1 \bar{u}_2 D}{h_1 h_2}\frac{\partial h_1}{\partial x_2} - \frac{\bar{u}_2^2 D}{h_1 h_2}\frac{\partial h_2}{\partial x_1} = -\frac{D}{\rho_0}\frac{\partial p_{\mathrm{a}}}{\partial x_1} - gD\frac{\partial \eta}{\partial x_1} \\
+ \;& (\tau_{01} - \tau_{\mathrm{b}1}) + \frac{gD^2}{\rho_0}\left[\frac{\partial}{\partial x_1}\int_{-1}^{0} d\sigma \int_{\sigma}^{0} \rho \, d\sigma' - \left(\frac{\sigma}{D}\frac{\partial D}{\partial x_1} + \frac{1}{D}\frac{\partial \eta}{\partial x_1}\right)\int_{-1}^{0} \rho \, d\sigma'\right] \\
+ \;& \frac{gD}{\rho_0}\frac{\partial D}{\partial x_1}\int_{-1}^{0} d\sigma \int_{\sigma}^{0} \sigma' \frac{\partial \rho}{\partial \sigma'} d\sigma' + D\overline{F}_1
\end{aligned} \tag{91}$$

$$\begin{aligned}
& \frac{\partial}{\partial t}(\bar{u}_2 D) + \frac{1}{h_1 h_2}\left[\frac{\partial}{\partial x_1}(h_2 \bar{u}_1 \bar{u}_2 D) + \frac{\partial}{\partial x_2}(h_1 \bar{u}_2^2 D)\right] + f \bar{u}_1 D \\
+ \;& \frac{\bar{u}_1 \bar{u}_2 D}{h_1 h_2}\frac{\partial h_2}{\partial x_1} - \frac{\bar{u}_1^2 D}{h_1 h_2}\frac{\partial h_1}{\partial x_2} = -\frac{D}{\rho_0}\frac{\partial p_{\mathrm{a}}}{\partial x_2} - gD\frac{\partial \eta}{\partial x_2} \\
+ \;& (\tau_{02} - \tau_{\mathrm{b}2}) + \frac{gD^2}{\rho_0}\left[\frac{\partial}{\partial x_2}\int_{-1}^{0} d\sigma \int_{\sigma}^{0} \rho \, d\sigma' - \left(\frac{\sigma}{D}\frac{\partial D}{\partial x_2} + \frac{1}{D}\frac{\partial \eta}{\partial x_2}\right)\int_{-1}^{0} \rho \, d\sigma'\right] \\
+ \;& \frac{gD}{\rho_0}\frac{\partial D}{\partial x_2}\int_{-1}^{0} d\sigma \int_{\sigma}^{0} \sigma' \frac{\partial \rho}{\partial \sigma'} d\sigma' + D\overline{F}_2
\end{aligned} \tag{92}$$

where the last term in each momentum equation contains the vertically integrated horizontal diffusion terms as well as the so-called dispersion terms:

$$\begin{aligned}
D\overline{F}_1 \;=\; & \frac{1}{h_1 h_2}\left[\frac{\partial}{\partial x_1}(h_2 \bar{\tau}_{11}) + \frac{\partial}{\partial x_2}(h_1 \bar{\tau}_{21}) + \bar{\tau}_{21}\frac{\partial h_1}{\partial x_2} - \bar{\tau}_{22}\frac{\partial h_2}{\partial x_1}\right] \\
- \;& \frac{1}{h_1^2 h_2}\left\{\frac{\partial}{\partial x_1}\left[h_1 h_2 D \int_{-1}^{0} (u_1 - \bar{u}_1)^2 \, d\sigma\right] + \frac{\partial}{\partial x_2}\left[h_1^2 D \int_{-1}^{0} (u_1 - \bar{u}_1)(u_2 - \bar{u}_2) \, d\sigma\right]\right\} \\
+ \;& \left\{\frac{1}{h_1^2}\frac{\partial h_1}{\partial x_1}\int_{-1}^{0} (u_1 - \bar{u}_1)^2 \, d\sigma + \frac{1}{h_1 h_2}\frac{\partial h_2}{\partial x_1}\int_{-1}^{0} (u_2 - \bar{u}_2)^2 \, d\sigma\right\},
\end{aligned} \tag{93}$$

and

$$\begin{aligned} D\overline{F}_2 &= \frac{1}{h_1 h_2}\left[\frac{\partial}{\partial x_1}(h_2\bar{\tau}_{12}) + \frac{\partial}{\partial x_2}(h_1\bar{\tau}_{22}) + \bar{\tau}_{12}\frac{\partial h_2}{\partial x_1} - \bar{\tau}_{11}\frac{\partial h_1}{\partial x_2}\right] \\ &- \frac{1}{h_1 h_2^2}\left\{\frac{\partial}{\partial x_1}\left[h_2^2 D\int_{-1}^{0}(u_1-\bar{u}_1)(u_2-\bar{u}_2)\,d\sigma\right] + \frac{\partial}{\partial x_2}\left[h_1 h_2 D\int_{-1}^{0}(u_2-\bar{u}_2)^2\,d\sigma\right]\right\} \\ &+ \left\{\frac{1}{h_1 h_2}\frac{\partial h_1}{\partial x_2}\int_{-1}^{0}(u_1-\bar{u}_1)^2\,d\sigma + \frac{1}{h_2^2}\frac{\partial h_2}{\partial x_2}\int_{-1}^{0}(u_2-\bar{u}_2)^2\,d\sigma\right\}, \end{aligned} \tag{94}$$

where

$$\begin{aligned} \bar{\tau}_{11} &= 2A_{\mathrm{M}}\left[\frac{h_2}{h_1}\frac{\partial}{\partial x_1}(\bar{u}_1 D) + \frac{\bar{u}_2 D}{h_1 h_2}\frac{\partial h_1}{\partial x_2}\right] \\ \bar{\tau}_{12} &= A_{\mathrm{M}}\left[\frac{h_1}{h_2}\frac{\partial}{\partial x_2}\left(\frac{\bar{u}_1 D}{h_1}\right) + \frac{h_2}{h_1}\frac{\partial}{\partial x_1}\left(\frac{\bar{u}_2 D}{h_2}\right)\right] = \bar{\tau}_{21} \\ \bar{\tau}_{22} &= 2A_{\mathrm{M}}\left[\frac{h_1}{h_2}\frac{\partial}{\partial x_2}(\bar{u}_2 D) + \frac{\bar{u}_1 D}{h_1 h_2}\frac{\partial h_2}{\partial x_1}\right] \end{aligned} \tag{95}$$

The terms in curly brackets are dispersion terms arising due to baroclinicity, or equivalently the vertical velocity structure.

5.6 Discretization

Numerical solutions require the domain to be discretized and the governing equations reduced to their finite difference equivalents. Figure 19 shows the numerical grid employed for spatial discretization. The grid is the so-called Arakawa C grid, which belongs to a class of staggered grids. In a C grid, quantities such as η and H are defined at the center of the grid, while the east–west component of velocity $\bar{u}_1$ is displaced half a grid to the west of the center and the north–south component $\bar{u}_2$ displaced half a grid to the south of the center. Contrast this to the B grid used in Bryan–Cox–Semtner type ocean models where $\bar{u}_1$, $\bar{u}_2$ are at the same location but displaced by half a grid from H and η. Which scheme is preferable depends very much on the size of the numerical grid relative to the Rossby radius. For a coarse grid, such as in ocean models used for climate modeling and global ocean modeling purposes, the B grid was once preferable, because of the favorable wave propagation characteristics of such a grid. However, as available computational power has increased dramatically in recent years, it has now become possible to model even the global oceans at a fine resolution. Under these circumstances the C grid appears to be a much better choice for discretization. Besides, for application to shallow coastal waters around ocean basins, high spatial resolution is rather imperative so that the shorter spatial scales typical of the processes in such regions be can resolved. Once again a staggered C grid is better suited to this application.

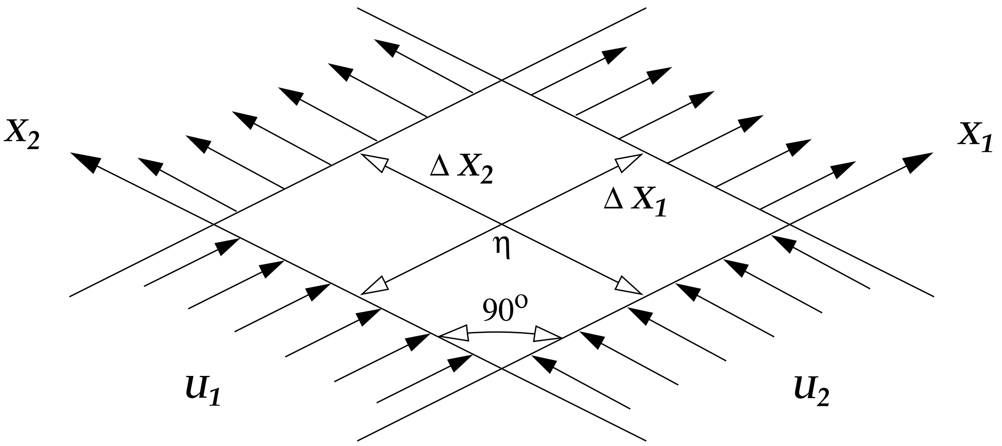

Figure 19: The physical interpretation of equation (98) which describes the mass balance in the control volume shown.

The numerical model solves for prognostic variables η, u_1, u_2, Θ, S, q^2 and l as a function of time, starting from a specified set of initial conditions, and forced by the wind stress and buoyancy flux at the ocean surface and prescribed transports at open lateral boundaries. These prognostic variables are staggered not only in the horizontal but also in the vertical direction. While q, l, w, K_{M}, K_{H} are located at σ levels, variables u_1, u_2, Θ, S, and ρ are staggered in the vertical and therefore located between two corresponding σ levels (see Figure 19). Note that w, q, l, Θ, S, ρ, K_{M}, K_{H} are located at the center of the grid, while u_1, u_2 are staggered in the horizontal as described earlier (see also Figure 19). While shear stresses τ_1 and τ_2 are staggered in the horizontal in the same way as u_1 and u_2 respectively, they are however located at σ levels.

Note that the governing differential equations are in flux-conservative form so that mass and energy are conserved when the equations are discretized. Finite difference approximations can now be derived by appealing to a control volume approach. To do this, it is necessary to recognize that

$$h_1 \delta x_1 = \Delta x_1 \quad \text{and} \quad h_2 \delta x_2 = \Delta x_2, \tag{96}$$

where Δx_1 and Δx_2 are the grid sizes in the x_1 and x_2 directions. We therefore multiply all the governing equations, both for the internal mode, equations (69) to (75), and external, equations (90) to (92), by $h_1\,\delta x_1 \cdot h_2\,\delta x_2$ before finite differencing. Thus the continuity equation (69) becomes

$$\begin{gathered}(h_1\delta x_1)(h_2\delta x_2)\frac{\partial\eta}{\partial t}+\frac{\partial}{\partial x_1}(h_2\delta x_2\cdot u_1D)\delta x_1+\frac{\partial}{\partial x_2}(h_1\delta x_1\cdot u_2D)\delta x_2\\+(h_1\delta x_1)(h_2\delta x_2)\frac{\partial w}{\partial\sigma}=0\end{gathered}\tag{97}$$

By virtue of equation (96), the finite difference equivalent of the continuity equation becomes

$$\Delta x_1\cdot\Delta x_2\delta_t\eta+\Delta_{x_1}(\Delta x_2\cdot u_1D)+\Delta_{x_2}(\Delta x_1\cdot u_2D)+\Delta x_1\cdot\Delta x_2\delta_\sigma w=0\tag{98}$$

where δ_t, Δ_{x1}, Δ_{x2}, δ_σ denote finite difference operators. Thus for any quantity $\phi(x_1,x_2,\sigma,t)$:

$$\begin{aligned}\delta_t\phi&=\frac{1}{2\Delta t}[\phi(x_1,x_2,\sigma,t+\Delta t)-\phi(x_1,x_2,\sigma,t-\Delta t)]\\\delta_\sigma\phi&=\frac{1}{\Delta\sigma}[\phi(x_1,x_2,\sigma+\frac{\Delta\sigma}{2},t)-\phi(x_1,x_2,\sigma-\frac{\Delta\sigma}{2},t)]\\\Delta_{x_1}\phi&=[\phi(x_1+\frac{\Delta x_1}{2},x_2,\sigma,t)-\phi(x_1-\frac{\Delta x_1}{2},x_2,\sigma,t)]\\\Delta_{x_2}\phi&=[\phi(x_1,x_2+\frac{\Delta x_2}{2},\sigma,t)-\phi(x_1,x_2-\frac{\Delta x_2}{2},\sigma,t)]\end{aligned}$$

$$\delta_{x_1}\phi=\frac{1}{\Delta x_1}\cdot\Delta_{x_1}\phi,\quad\delta_{x_2}\phi=\frac{1}{\Delta x_2}\cdot\Delta_{x_2}\phi\tag{99}$$

Figure 19 makes the physical interpretation of equation (98), which describes the mass balance in the control volume shown.

Scalar conservation equations (such as for turbulence K.E.) can also be reduced to finite difference form in a similar manner:

$$\begin{gathered}(h_1\delta x_1)(h_2\delta x_2)\frac{\partial}{\partial t}(q^2D)+\frac{\partial}{\partial x_1}(h_2\delta x_2\cdot u_1q^2D)\delta x_1+\frac{\partial}{\partial x_2}(h_1\delta x_1\cdot u_2q^2D)\delta x_2\\+(h_1\delta x_1)(h_2\delta x_2)\frac{\partial}{\partial\sigma}(wq^2)=\frac{\partial}{\partial x_1}\left(h_2\delta x_2\cdot A_{\rm H}D\frac{1}{h_1}\frac{\partial q^2}{\partial x_1}\right)\delta x_1\\+\frac{\partial}{\partial x_2}\left(h_1\delta x_1\cdot A_{\rm H}D\frac{1}{h_2}\frac{\partial q^2}{\partial x_2}\right)\delta x_2+\frac{1}{D}(h_1\delta x_1)(h_2\delta x_2)\frac{\partial}{\partial\sigma}\left(K_{\rm H}\frac{\partial q^2}{\partial\sigma}\right)\end{gathered}\tag{100}$$

which leads to

$$\begin{aligned}&\Delta x_1\cdot\Delta x_2\delta_t(q^2D)+\Delta_{x_1}(u_1q^2D\cdot\Delta x_2)+\Delta_{x_2}(u_2q^2D\cdot\Delta x_1)\\&+\Delta x_1\cdot\Delta x_2\delta_\sigma(wq^2)=\Delta_{x_1}[\Delta x_2\cdot A_{\rm H}D\cdot\delta_{x_1}(q^2)]\\&+\Delta_{x_2}[\Delta x_1\cdot A_{\rm H}D\cdot\delta_{x_2}(q^2)]+\frac{\Delta x_1\cdot\Delta x_2}{D}\cdot\delta_\sigma[K_{\rm H}\delta_\sigma(q^2)]\end{aligned}\tag{101}$$

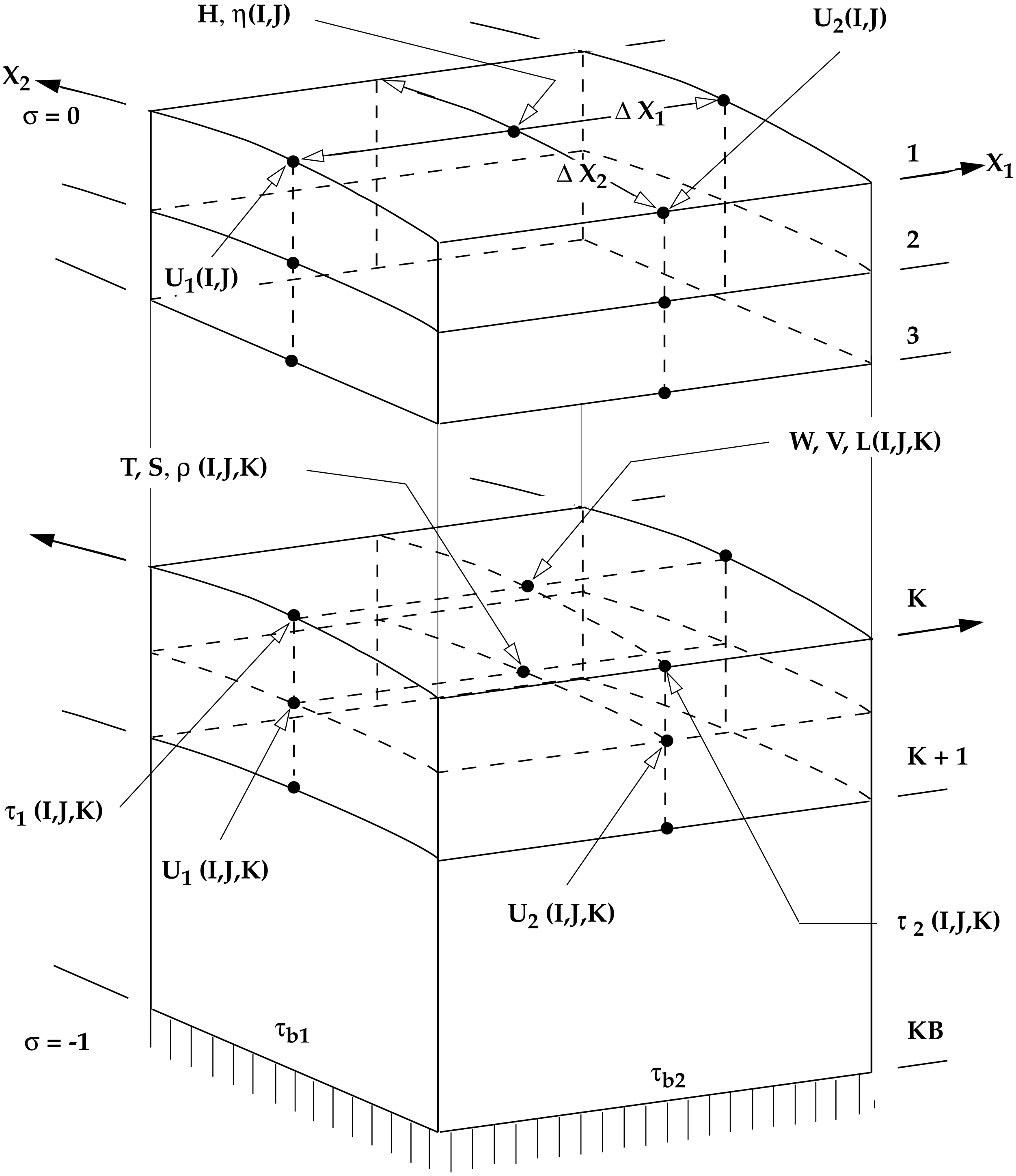

Figure 20: The staggered numerical model grid with the location of model variables indicated.

Similar equations can be written down for Θ, S and q^2l. The u_1 momentum equation (70) can be written as:

$$\begin{aligned}
&(h_1\delta x_1)(h_2\delta x_2)\frac{\partial}{\partial t}(u_1D)+\frac{\partial}{\partial x_1}(u_1^2D\cdot h_2\delta x_2)\delta x_1+\frac{\partial}{\partial x_2}(u_1u_2D\cdot h_1\delta x_1)\delta x_2\\
&+u_1u_2D\frac{\partial}{\partial x_2}(h_1\delta x_1)\cdot\delta x_2-u_2^2D\cdot\frac{\partial}{\partial x_1}(h_2\delta x_2)\cdot\delta x_1-(h_1\delta x_1)(h_2\delta x_2)fu_2D\\
&+(h_1\delta x_1)(h_2\delta x_2)\frac{\partial}{\partial\sigma}(wu_1)=\ldots \qquad (102)
\end{aligned}$$

Therefore the finite difference form of the u_1 momentum equation is

$$\begin{aligned}
&\Delta x_1\cdot\Delta x_2\delta_t(u_1D)+\Delta_{x_1}(u_1^2D\cdot\Delta x_2)+\Delta_{x_2}(u_1u_2D\cdot\Delta x_1)\\
&-\Delta x_1\cdot\Delta x_2\{f+\frac{1}{\Delta x_1\cdot\Delta x_2}[u_2\Delta_{x_1}(\Delta x_2)-u_1\Delta_{x_2}(\Delta x_1)]\}u_2D\\
&+\Delta x_1\cdot\Delta x_2\cdot\delta_\sigma(wu_1)=\ldots \qquad (103)
\end{aligned}$$

Notice that a pseudo-Coriolis parameter $\tilde{f}$ can be defined in an orthogonal curvilinear coordinate system:

$$\tilde{f}=f+\frac{1}{\Delta x_1\cdot\Delta x_2}[u_2\Delta_{x_1}(\Delta x_2)-u_1\Delta_{x_2}(\Delta x_1)], \qquad (104)$$

$\tilde{f}$ accounts for the acceleration terms arising out of the changes in grid size from grid point to grid point. The finite difference form of the u_2 momentum equation (71) is

$$\begin{aligned}
&\Delta x_1\cdot\Delta x_2\cdot\delta_t(u_2D)+\Delta_{x_1}(u_1u_2D\Delta x_2)+\Delta_{x_2}(u_2^2D\Delta x_1)\\
+\ &\Delta x_1\cdot\Delta x_2\cdot\tilde{f}u_1D+\Delta x_1\cdot\Delta x_2\cdot\delta_\sigma(wu_2)=\ldots. \qquad (105)
\end{aligned}$$

Note that for convenience and algebraic clarity we have avoided writing down the terms on the R.H.S. of equations (103) and (105).

The external mode (barotropic) equations (90) to (92) are also cast in similar finite difference forms, which, for brevity, we are not going to write down. The resulting external and internal mode finite difference equations are solved in a split-mode method, as discussed earlier, to obtain solutions for the prognostic quantities as a function of time. The external mode is solved using explicit differencing techniques, while the internal mode equations are solved implicitly in the vertical direction, but explicitly in the horizontal. The finite difference equations for the internal mode are cast in a tri-diagonal matrix form, which are then solved using well-known techniques such as the Thomas tri-diagonal algorithm (see chapter 6.2.2 volume 1 of [14]). Close synchronization between the two modes, external and internal, is assured by passing onto the external mode, from the internal mode, the bottom friction and the component of the pressure gradient that is due to the density field. In turn, the external mode supplies the internal mode with the sea surface elevation and vertically averaged currents that it needs. This interaction takes place at each internal time step. The procedure then is to start with one external mode (barotropic) calculation and then pass

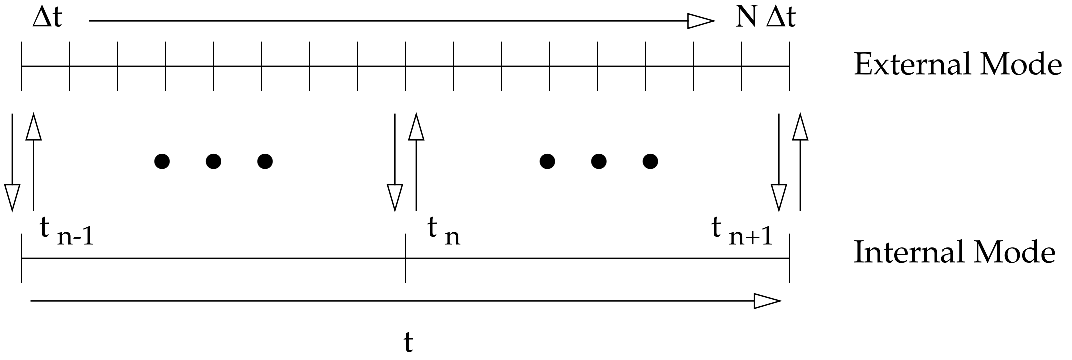

Figure 21: External Mode and Internal Mode representation of the full 3-D Sigma Coordinate Model

on the needed information to the internal (baroclinic) mode and take one time step with it. The internal mode then passes on the needed information to the external mode and the whole process is repeated until the end of the calculation is reached.

As mentioned in earlier sections, the data to initialize these models come from historical archives, such as the National Oceanographic Data Center (NODC), and forcing data for the model can be from historical archives at National Oceanic and Atmospheric Administration (NOAA) or Numerical Weather Prediction (NWP) Centers around the world, such as the National Meteorological Center (NMC) in the U.S. or European Center for Medium range Weather Forecasting (ECMWF) in Europe. Excellent bathymetric data for the world, including the oceans, at about 9 km resolution, called ETOP05, is available from the National Center for Atmospheric Research (NCAR). From these archives, it is possible to derive the bottom topography, as well as the initial 3-D temperature and salinity fields at all model grid points. This involves considerable processing of the data bases to remove data errors and other uncertainties and obtain meaningful fields to initialize the model. The same applies to deriving the momentum and buoyancy flux fields at the ocean surface from NWP or NOAA products to drive the model. For the sake of brevity and clarity, we will not detail these procedures. Suffice it to say that data preparation (and analyses of the model output) is a very significant fraction of any ocean modeling effort.

It is important to realize that we have described only the dynamical oceanographic component of the model. In many practical applications such as investigating the fate of man-made carbon dioxide, a large fraction of which is absorbed and sequestered in the global oceans, we need to consider and solve equations for the chemical and biological variables also. Once again, this involves writing down the governing partial differential equations (PDEs) very much similar to the governing equations for Θ and S (equations (38) and (39)) for the quantities of interest, casting them in finite difference form as described above, and solving them numerically. For example, for investigating the inorganic carbon cycle in the ocean, where the carbon dioxide is absorbed at the sub-polar/polar latitudes (and expelled in warmer tropics) and converted to the carbonate, bicarbonate and dissolved gas forms, it is necessary to solve for the total carbon and the pH of the water parcel. The governing equations for these are similar to the one for salinity, except that the right hand side now involves source and sink terms. Also an equation involving chemical reaction rates that results in an appropriate balance between the three forms of dissolved carbon needs to be solved. Nevertheless, the same methodology can be used to explore how the oceans absorb the excess carbon mankind is introducing into the atmosphere by fossil-fuel burning. This problem is of obvious importance to the future climate our children will live in, as a result of our massive uncontrolled tinkering with our global environment by profligate use of fossil carbon that took nature millions of years to create.

The carbon cycle in the oceans involves another component, the organic cycle. Phytoplankton (microscopic plants) in the upper layers of the ocean take up the dissolved carbon dioxide within the photic zone (the upper layers where there is sufficient light for photosynthesis), and are in turn consumed by zooplanktonic organisms, whose carbonate shells rain down onto the ocean floor upon their death and remain undissolved and hence sequestered from the atmosphere for thousands of years. Thus the amount of carbon sequestered by the ocean and thus not contributing to an immediate global warming, is a strong function of the biological productivity of the upper layers of the ocean. However, planktonic organisms need for growth nutrients such as nitrates and phosphates, which have to come from the deeper ocean. Thus both light and nutrients are needed for biological productivity, and it is only a fraction of the oceanic upper layers (a few per cent) around the globe that are responsible for more than 90% of the biological productivity and the food chain so crucial to the growing population on the globe. These are the so-called upwelling regions, mostly around coasts where the winds blow such that the ocean waters are expelled from the coast and deeper, nutrient-rich waters come up to replace them. If conditions are right, as for example the spring–summer time, biological productivity literally explodes.

To account for the organic cycle, it is necessary to solve for the chemical and biological variables involved, such as the nutrient concentrations, and the phytoplankton and zooplankton densities in the water column, in addition to solving for the circulation. Once again it is a matter of solving the appropriate PDEs cast in finite difference form as above. The only difference, of course is that these equations involve complex source/sink terms on the right hand side that need to be appropriately parameterized, in view of our knowledge of how the planktonic organisms behave. Thus while in theory at least, it is rather straightforward to solve for the physical, chemical and biological state of our oceans, practically speaking, the solution becomes extremely complex, time-consuming and computationally very expensive. It is not unusual for a relatively high resolution (50 km grid size) physical global ocean model itself to take several hundred hours on a modern computer such as the CRAY YMP, just to do a year's worth of model simulation. It is easy to imagine therefore a full physical–chemical–biological model of the global oceans requiring the next generation of computers, the massively parallel ones of the CM-5 type. In fact, understanding and predicting the state of the global oceans is one of the "grand challenge" problems that require the power of the Teraflop massively parallel computers that are expected to become available early in the next century.

See exercise 8.

---

6 Tidal Model Exercise

To illustrate how it is all done, we will rewrite governing equations and the finite difference equivalents in a simplified form here appropriate to a rectilinear coordinate system (as opposed to the curvilinear system in equations (90) to (92)), omitting for simplicity the density terms, atmospheric pressure terms, astronomical forcing terms and the horizontal diffusion terms. We will also put $x_1 \equiv x$, $x_2 \equiv y$, $\bar{u}_1 \equiv U$, and $\bar{u}_2 \equiv V$).

$$\frac{\partial \eta}{\partial t} + \frac{\partial}{\partial x}(UD) + \frac{\partial}{\partial y}(VD) = 0, \tag{106}$$

$$\frac{\partial}{\partial t}(UD) + \frac{\partial}{\partial x}(U^2 D) + \frac{\partial}{\partial y}(UVD) - fVD = -gD\frac{\partial \eta}{\partial x} + (\tau_{0x} - \tau_{\mathrm{b}x}), \tag{107}$$

$$\frac{\partial}{\partial t}(VD) + \frac{\partial}{\partial x}(UVD) + \frac{\partial}{\partial y}(V^2 D) - fUD = -gD\frac{\partial \eta}{\partial y} + (\tau_{0y} - \tau_{\mathrm{b}y}), \tag{108}$$

are now the simplified set of governing equations. Their finite difference equivalents are

$$\Delta x \cdot \Delta y \delta_t \eta + \Delta_x(\Delta y \cdot UD) + \Delta_y(\Delta x \cdot VD) = 0, \tag{109}$$

$$\begin{aligned} & \Delta x \cdot \Delta y \delta_t(UD) + \Delta_x(\Delta y \cdot U^2 D) + \Delta_y(\Delta x \cdot UVD) - \Delta x \cdot \Delta y\, fVD \\ = \; & -gD \cdot \Delta x \cdot \Delta y \Delta_x(\eta) + \tau_{0x} - \tau_{\mathrm{b}x}, \end{aligned} \tag{110}$$

$$\begin{aligned} & \Delta x \cdot \Delta y \delta_t(VD) + \Delta_x(\Delta y \cdot UVD) + \Delta_y(\Delta x \cdot V^2 D) - \Delta x \cdot \Delta y\, fUD \\ = \; & -gD \cdot \Delta x \cdot \Delta y \Delta_y(\eta) + \tau_{0y} - \tau_{\mathrm{b}y}, \end{aligned} \tag{111}$$

where

$$\begin{aligned} \delta_t \eta &= (\eta^{n+1}_{i,j} - \eta^{n-1}_{i,j})/(\Delta t) \\ \Delta_x \eta &= (\eta^{n}_{i,j} - \eta^{n}_{i-1,j})/(\Delta x) \\ \Delta_y \eta &= (\eta^{n}_{i,j} - \eta^{n}_{i,j-1})/(\Delta y), \end{aligned} \tag{112}$$

simplified relationships for the other δ_t, Δ_x and Δ_y terms in equations (109) to (111). Note Δx and Δy are the grid spacings in the x and y directions and Δt is the time step. Δx and

Δy are of course under modeler's control, subject only to physical and computer-resource considerations. Once Δx, Δy are chosen, because the differencing scheme is explicit, Δt must be chosen so that it is

$$\Delta t \leq \text{Min}\left[\left(\frac{1}{\Delta x^2}+\frac{1}{\Delta y^2}\right)^{-1/2}(gH)^{-1/2}\right]. \tag{113}$$

This is the CFL condition for numerical stability of the scheme, which can only be avoided by employing an implicit scheme.

For the Persian Gulf model, $\Delta x = \Delta y = 18$ km. Maximum H is about 100m, so that Δt must be less than 128 sec. We have put DTE=120 sec in the file *pegtdu10*. Try running it with a larger value, say 240 sec, and watch the model blow up rather quickly (of course DTE can be made lower but it only wastes computer time!).

In the data assimilation runs, at time step dictated by DTT in *pegtdu10*, the model generated η is replaced (at gridpoints where observations are available) by a weighted combination of model η and observed η. In other words η_{model} is replaced by $\eta_{\text{model}}(1-a)+a\eta_{\text{obs}}$, where a is given by FRACTN in *pegtdu10*. By changing a and DTT we can control how strongly the model is forced towards observations. Strictly speaking, a should be a function of both the model and observational data error statistics. That is a fancy way of saying that we should look at how accurate the data are and how reliable the model is before deciding what a should be. There has been a tremendous amount of work done in the past 5 decades on how to do data assimilation in dynamical models. There are extremely sophisticated and highly resource-intensive methods (such as Kalman filters, adjoint methods) that do this properly. However, we prefer here to fix the a value *a priori*. The results will not be too different than when a more sophisticated approach is used.

6.1 Objective

The student should be able to run a tidal model on a workstation (such as the Sparc 2, a Cray YMP, or a CM5), obtain results, and plot those for different trials. Also, the student should manipulate data input to the program, and this will provide an introductory experience in ocean modeling. The practical application in this exercise is a tidal prediction model for the Persian Gulf.

6.2 Discussion

Presenting and illustrating the full 3-D model would require considerable computing resources in order to obtain meaningful calculations. These resources include extensive input and forcing data derived as mentioned in the previous section. Instead, we will present a *sub-component* of the sigma model, namely the *barotropic model* (the next release will deal with the 3-D model itself, as applied to a small oceanic region such as the Sea of Japan). This model is quite simple to learn, and it should run even on a modest workstation. Yet, it is quite useful and is used extensively for practical applications such as the prediction of hurricane-induced storm surge effects (such as flooding of coastal regions, devastation and loss of life), and prediction of tidal sea surface heights in the global oceans. It is the latter application that we will describe with a real-life application: predicting the tidally-induced sea level heights in the *Persian Gulf.* This model (as well as the full 3-D version) proved very useful to our naval forces during Desert Storm.

Tidal sea level can be modeled by solving equations (90) to (92). In general, the right hand sides of equations (91) and (92) need to be modified to include the tide-generating gravitational potential terms due to the sun and the moon. However, for some semi-enclosed seas, such as the Persian Gulf, and most coastal oceans these terms can be neglected. Then the tides are the so-called *co-oscillating* tides excited by the tides generated in the adjoining primary ocean basins. It is relatively easy to prescribe these at the openings to the primary basin, in this case the Straits of Hormuz, where the tidal variations are well known. Thus the governing equations are solved with prescribed sea level conditions at the open boundary, to derive the resulting sea level fluctuations inside.

There are several components of tides that are important (see section 5.1): the *semi-diurnal tides* (i.e., M2, S2, N2 and K2), with roughly two tidal cycles every day; *diurnal tides* (K1, O1, P1 and Q1), with roughly one tidal cycle per day and the *long term tides* (such as the MF, MM and SSA), which are fortnightly, monthly and semi-annual in nature. In addition, in shallow water the so-called *compound tides* generated by non-linear interaction of semi-diurnal and diurnal tides due to shallow water depths can often be important. In this exercise, we will confine ourselves to solving for the semi-diurnal and diurnal tides in the Persian Gulf, even though the model is capable of solving for the full spectrum of tides.

6.3 Computer Model

Hardware: This model can be run on any Unix-based machine. The program has been tested successfully on a Sparc 2, RS 6000, Silicon Graphics IRIX, Cray YMP, Cray C-90 and CM-5. The model itself should run on any Unix-based computer using Fortran 77.

Software: The Fortran compiler f77 as well as the GMT package for the animation and graphics are needed.

Files: This is a list of the files you should have in your directory in order to run this exercise: (Note: You may either retrieve them separately or in one archived file.)

Archives of the model (code, input, output and misc files), and of the instructions and files used in the animation of results, as well as the CM5 code, are available at the anonymous ftp site on compsci.cas.vanderbilt.edu in the subdirectory : CSEP/ebook_codes .

Model code: *main.f*, *tides.f*, *xmode.f*, *bcond.f*, *wrtprg.f* and *rest.f* routines

Include files: *Ogcm1.h*, *Ogcm2.h*, *Ogcm3.h*, *Ogcmt.h* and *Ogcmmd.h*, only the first of which needs to be changed when going to another region.

Input file: *pegtdu10*—Parameter input data

Input file: *pegtdu40*—Ocean Model input data

Input file: *pegtdstn*—File containing observed data at tidal coastal stations.

Input file: *pegtdt*—File containing the time series of observed and model tidal heights at selected stations where tide gauge data are available for comparison

Restart file: *pegtdu70*—Ocean Model input data file for a restart. This file is written to periodically by the model so that a crash recovery can take place.

Restart file: *pegfldtd*—Ocean Model intermediate data file for a restart.

Restart file: *pegsertd*—Intermediate 2-D surface fields saved periodically in the event for a restart.

Output file: *pegmovtd*—File used to create a movie for the animation of tides.

Output file: *pegtdc*—File containing the co-amplitude and co-phase, the maximum tidal sea surface height, at each grid point and the corresponding time at which it occurs.

Monitoring file: *mon*—Monitor file to check the operation of the program.

6.4 Procedure

1. Use the Unix command `make`. This will create the executable file called Pegtd.
2. Edit the file *pegtdu10.* This file has the following format:

```
$VALUES RSTART=0,DAYS=10.0,DTE=120.0,RAMPUP=5.0,
  SAVEF=1.0,SAVES=25.0,SAVEM=0.05,SWITCH=9.0,
  HORCON=0.02,AAA=20.0,ISPLIT=30,PRTD1=5.0,PRTD2=0.5,
  DATE=0.0,YEAR=1991,ITDASM=0,DTT=240.0,CD=0.0020,
  FRACTN=0.9,IALL=1,
  TIDE=1.,0.,0.,0.,
  0.,0.,0.,0.,
  0.,0.,0.,
  0.,0.
$END
```

The procedure is to edit the *pegtdu10* file to run the desired components. The 13 numbers assigned to TIDE in this NAMELIST file allow you to do this. Putting a number here to 1 turns the corresponding component on and a zero value turns it off. The numbers correspond to M2, S2, N2, K2, K1, O1, P1, Q1, MF, MM, SSA, M4 and MS4 in that order (See Table 1). The last two are compound tides and should not be run. The long term components should also not be run, as they require a long run time. Running the rest of the components takes approximately 2 minutes on a Cray YMP using only one processor and about 40 minutes on a Sparc2. As an exercise the students may verify these values.

The model can be started from scratch by putting RSTART=0. Then the model is slowly ramped up over 5 days and then run for a total of 10 days. It is also possible to continue further from a previously made run by putting RSTART=1. In that case, a restart file has to be supplied as *pegtdu70.* The model routinely writes a restart file and over-writes the previous one every day so that at the end of say a 10-day run, you will have one restart file called *pegfldtd* that contains the fields needed to make a run starting from the 10th day. All that is needed is to copy *pegfldtd* into *pegtdu70* and put RSTART=1.

See exercise 9.

6.5 Results

The code generates a *pegsertd* file, which is a printed output useful only if something goes wrong and you need to debug, but as this code has been tested extensively, debugging should not become necessary. In addition, it produces a *pegtdc* and a *pegtdt* file that contain information on the tidal sea level field everywhere in the model domain, and time series information at selected coastal stations respectively. It also produces a *pegmovtd* file that can be used to animate tides. The file *pegtdc* contains co-amplitude (the maximum tidal sea surface height at each grid point) and co-phase (and the corresponding time at which maximum tidal sea surface height occurs, referred to Greenwich standard time, in degrees) fields. File *pegtdt* contains time series of observed and model tidal heights at selected stations where tide gauge data are available for comparison. It gives a graphic description of how well the model does.

The input on bottom depths etc. needed by the model is contained in *pegtdu40*. The model needs only the bottom depths to be derived from national archives. It does not need any forcing data, winds or buoyancy fluxes. File *pegtdstn* contains observed data from tidal coastal stations for comparison with model output and for assimilation into the model, as we will discuss shortly.

6.6 Displaying the Results and Using GMT

6.6.1 GMT

The plotting program plots the co-amplitude and co-phase fields using the public domain software called GMT, which is developed by the University of Hawaii and the University of San Diego, and is distributed by CSEP. The most recent version is available by anonymous ftp at 128.171.151.16. README.PLT explains how the package is used for this exercise.

Sample color plots of the co-amplitudes and co-phases produced by the model for M2, with and without data assimilation are available as data files and can be viewed. README.CPT tells you how to *select a color scale* for color-fill plots that you will find useful when running and plotting other tidal constituents. Experiment with these to gain expertise in the use of this visualization tool. The resulting PostScript files can be printed on any standard PostScript color printer, or displayed on the screen using ghostview.

6.6.2 Animation

The animation package takes the movie file *pegmovtd* generated by the model. This is explained in README.PLT. We highly recommend you view this model with the animation package. The results are fascinating to watch. The tides going in and out of the Straits of Hormuz and rotating roughly once per day in some places and roughly twice/day in others, depending on which components dominate the tides, diurnal or semi-diurnal, are fun to watch as well as educational. The movie plots contain color maps of Sea Surface Height (SSH), red indicating large upward and blue large downward deflections of the sea surface. Superimposed on these are velocity vectors that indicate which way the average tidal currents in the water column are going and their magnitude. The plots show the behavior of SSH and currents nearly every hour during the last day of each simulation. You can learn a lot about tides just by watching this movie. A sample is included.

6.6.3 Data Assimilation

So far, the dynamics-based model has been executed without any modifications and results were viewed and animated. In this section, we will include observational data into the model and look at the difference they make in model performance.

As we said earlier, ITDASM turns data assimilation on or off. Getting accurate results from a tidal model (or any model for that matter) involves an iterative procedure, where parameters such as the bottom depth, bottom friction coefficient (CD in *pegtdu10*) and open boundary conditions are "tuned" to arrive at the best possible result. Even then, the results are limited by how much we know and what the model limitations are. For example, we need to know the tidal distribution at the Straits of Hormuz accurately and we need to have the correct value of friction and bottom depth at each grid point, and a model resolution approaching one or two km, to do the tides well in the Persian Gulf. The model resolution in this example is only 18 km and this will influence the result, because the bottom depths can not be represented accurately at this coarse resolution. Also it is difficult to prescribe bottom friction accurately in a barotropic model. For these reasons, a model run will never agree "perfectly" with observations (see the time series comparison produced using *pegtdt*). The solution to this problem is data assimilation, bringing observed tidal data to bear upon the model results.

Data assimilation is an inescapable part of all prediction modeling in geophysics involving real nonlinear systems, due to the ubiquitous nature of chaos [23]. Because inevitable errors in initial conditions, no matter how small you make them, eventually cause the model to depart radically from reality, occasional or continuous updating of the model with observational data is essential to keep models faithful to nature. Data assimilation is routinely used in weather forecast. Every 12 hours, the forecast model is reinitialized with observations from around the globe and the model rerun by the NWP centers to make forecasts for the next two days. In the oceans, a better method may be to inject observed data into the model as they become available and update the model continuously. This continuous assimilation method is what is used in this tidal model.

The tidal elevation at any point in time is known from observations of tidal data from tide gauges at coastal stations around the world. The tidal components derived from these data can be obtained from an historical archive in Canada. As the model is running, the model produced SSH can be replaced by a weighted combination of the model SSH and what the SSH should be according to observations, at those grid points where data are available. Thus the model will be constrained to follow nature at those points where we have observations. The hope is that, in the rest of the domain, the model will do better as a result. This is what is done in the TIDASM routine in *tides.f*. The relevant observational data comes from *pegtdstn*. Data assimilation can be turned on by putting ITDASM=1. The frequency of assimilation can be controlled by prescribing DTT. This should be a multiple of DTE, the external time step. We urge you to make runs with and without data assimilation to see the power of assimilation, without which most of our endeavors in the field of geophysical prediction would be worthless.

See exercises 10, 11, 12, 13, and 14.

6.7 Conclusion

We have tried to give you an up-to-date but concise idea of how ocean models work. It is our hope that some of you will be motivated by this chapter to pursue *Ocean Modeling* as a career. Given the grave environmental challenges such as global warming, protein shortages, and environmental pollution facing mankind in the coming century, and because oceans play such a very important role in governing the degree of global warming, fisheries yield, and degree of pollution along our beaches, your study of the oceans through a variety of means (remote sensing, ship surveys, etc.) including numerical modeling can not but lead to a better understanding of how the oceans work. The hope is that as a result, we will leave behind as our legacy to our children, a world that is both livable as well as enjoyable in all its majesty.

7 Exercises

Exercise 1 *An estimation of the size of the database necessary to store a representative grid of the Earth.*

Determine the distance corresponding to a 5 min interval, then a) calculate the size of the database, considering the area of the Earth's surface, b) observe what happens if the interval is increased or decreased.

Exercise 2 *An illustration of the use of the stored topography of the world's oceans.*

a) Extract data from the database for the Sea of Japan using the input file (5 values);

b) Plot the data, using GMT and explain the topographic variations. Do you see the sharp dropoff in depth as you go even a few kilometers from shore? Compare your plot with that of Figure 9.

Exercise 3 *An illustration of one of the input parameters for the ocean model that can be obtained from experimental readings.*

a) Look at the winds database for a period of a year—4 seasons— and quantify the magnitude of winds. Also look at another sea, extract a region of the ocean, scale the color map to that region of the ocean.

b) Using the program provided, extract the wind stress acting over the Sea of Japan for each month of the year. Animate and describe. Do you see the strong winds from Siberia during winter? Compare your wind plots to Figures 10-13.

Exercise 4 *An illustration of another input parameter for an ocean model.*

Use the supplied program to extract the T and S fields for the Sea of Japan during the four seasons. Using sea surface temperature and salinity as guides, describe the evolution over the seasons of surface water mass properties. Do you see drastic cooling in the north during winter and a large inflow of fresh water through the Tsushima Straits from the Yellow Sea rivers during the summer?

Exercise 5 *Students should think about where this code is easily vectorized or parallelized.*

Exercise 6 *Evaluation of the ocean model.*

a) Run the code on one or more platforms.
b) Obtain profiles on various architectures.
c) Deduce where the code vectorizes.
d) Discuss on which platform the code executes most efficiently.
e) Create a table of the profile data for the different architectures. Note: Use the Cray code as appropriate, because due to the peculiarity of this machine to be averse to powers of 2, it uses an odd numbered grid size, just as the Connection Machines prefer powers of 2.

Exercise 7 *Determine the equations for a simple rectilinear coordinate system from governing equations for mass and momentum.*

a) Look at the governing equations for mass, momentum, T, s, q^2, $q^2 l$ and write down the versions for a simple rectilinear coordinate system (hint: $h_1\,\partial x \equiv \partial x, h_2\,\partial y \equiv \partial y, \frac{\partial h_2}{\partial x_1} = 0, \frac{\partial h_1}{\partial x_2} = 0$; put $u_1 \equiv u$, $v_1 \equiv v$).
b) Then repeat this for a spherical coordinate system (hint: $h_1 \equiv R\cos\phi, h_2 \equiv R, h_1\,\partial x_1 \equiv R\cos\phi, h_2\,\partial x_2 \equiv R\,\partial\phi$, where R is the radius of the Earth, ϕ is the latitude and λ is the longitude.

Exercise 8 *Determine by inspection the z-level and the σ-coordinate versions of the governing equations.*

Write down by inspection both the z-level and σ-coordinate versions of governing equations for a photochemical compound (carbonyl sulphide). Assume its creation rate is proportional to local solar insolation (hint: look at the equation for T) and its destruction rate is proportional to its concentration, but with a coefficient that is a function of temperature T.

Exercise 9 *An evaluation of the Persian Gulf Tidal Model for various platforms and with slight changes of the input parameters.*

a) Determine the time that it takes to execute the Persian Gulf Tidal Model on the Sparc workstation, the CRAY YMP, and CM5.

b) Try your hand at running different tidal components or all of them, from scratch, by changing the TIDE variable in *pegtdu10* appropriately. Make sure ITDASM=0. Make sure you save the resulting *pegfldtd* files, if you plan to continue the runs further in time.

Exercise 10 *Persian Gulf Tidal Model for M2 and K1 constituents.*

Run the model for semi-diurnal constituent M2 and diurnal constituent K1 with and without data assimilation and compare the results at tidal station locations.

Exercise 11 *Tidal Model for with semi-diurnal constituents and data assimilation.*

Run the model for all semi-diurnal constituents with data assimilation. Animate the tidal sea level and currents from the *pegmovtd* file using the animation package. Comment on how semi-diurnal currents vary in space and time through the day.

Exercise 12 *Tidal Model with diurnal constituents and data assimilation.*

Run the model for all diurnal constituents with data assimilation. Animate as before and describe how tidal currents vary in time and space during the day.

Exercise 13 *Tidal Model with semi-diurnal and diurnal constituents and data assimilation.*

Run the model for all semi-diurnal and diurnal constituents with data assimilation. Animate as before and describe how the tidal currents and SSH vary in space and time during the day.

Exercise 14 *Tidal Model with semi-diurnal and diurnal constituents but no data assimilation.*

Repeat the previous exercise without data assimilation and comment on the results.

References

[1] Backhaus, J.O. and Maier-Reimer, E., *On Seasonal Circulation in the North Sea*, in "North Sea Dynamics", p. 63, 1983 [`see Sundermann`].

[2] Bleck, R. and Boudra, D.B., *Wind-driven spin-up in eddy-resolving ocean models formulated in isopycnic and isobaric coordinates*, J. Geophys. Res. 91, p. 7611, 1986. [`This type of model is best for deep basic physics`]

[3] Blumberg, A. F. and Mellor, G.L., *A description of a three-dimensional coastal ocean circulation model.* In Three-Dimensional Coastal Ocean Models. ed. N. Heaps, American Geophysical Union, pp. 1–16, 1987. [`This type of model is best for shallow coastal waters`]

[4] Bryan, K., *A Numerical Method for the Study of the Circulation of the World Ocean*, J. Comp. Phys. 4, p. 347, 1969. [`The most popular and the oldest ocean model`]

[5] Cartwright, D.E., *Detection of tides from artificial satellites (review)*, in Tidal Hydrodynamics, ed. by B.B. Parker, John Wiley & Sons, pp. 547–568, 1991.

[6] Creegan, A., *A numerical investigation of the circulation in the Norwegian Sea*, Tellus 28, p. 451, 1976.

[7] Davis, R.E., DeSzoeke, R. and Niiler, P.P., *Variability in the upper ocean during MILE, Part 2: Modeling the mixed-layer response*, Deep-Sea Res. 28, p. 1453, 1981.

[8] Davies, A.M., *Application of a Three-Dimensional Shelf Model to the Calculation of North Sea Currents*, in "North Sea Dynamics", p. 44, 1983 [`see Sundermann`].

[9] Davies, A.M. and James, I.D., *Three-Dimensional Galerkin-Spectral Sea Models of the North Sea and German Bight*, in "North Sea Dynamics", p. 85, 1983 [`see Sundermann`].

[10] Dickey, T.D. and Simpson, J.J., *The relationship between downward irradiance and upper ocean structure*, J. Phys. Ocean. 11, 309–323, 1981.

[11] Dietrich, G., Kalle, K., Krauss, W. and Siedler, G., *General Oceanography. An Introduction.* 2nd Ed., pp. 626, 1980. [`Good text on oceanography`]

[12] Durance, J.A. and Hughes, D.G., *Experiments with Two- and Three-Dimensional Numerical Models of the North-East Coast of England*, in "North Sea Dynamics", p. 120, 1983 [`see Sundermann`].

[13] Flather, R.A. and Proctor, R., *Prediction of North Sea Storm Surges Using Numerical Models: Recent Developments in the U.K.*, in "North Sea Dynamics", p. 299, 1983 [`see Sundermann`]

[14] Fletcher, C.A.J., *Computational Techniques for Fluid Dynamics*, Vol. 1 and 2, Springer–Verlag, 1987. [`Excellent reference on numerical solutions of fluid flow equations`]

[15] Fofonoff,N.P., *Physical properties of sea water*, in "The Sea", Vol. 1, ed. N.M. Hill, Interscience Publications, pp. 3–30, 1962.

[16] Foreman, M.G.G., Henry, R.F., Walters, R.A. and Ballantyne, V.A., *A finite element model for tides and resonance along the north coast of British Columbia.* J. Geophys. Res. 98, pp. 2509–2531, 1993.

[17] Furnes, G.K., *Wind Effects in the North Sea*, J. Phys. Ocean. 10, p. 978, 1980.

[18] Galperin, B., Kantha, L.H., Hassid, S. and Rosati, A., *A quasi-equilibrium turbulent energy model for geophysical flows*, J. Atmos. Sci. 45, pp. 55–62, 1988.

[19] Galperin, B., Rosati, A., Kantha, L.H. and Mellor,G.L., *Modeling rotating stratified turbulent flows with application to oceanic mixed layers*. J. Phys. Ocean. 19, pp. 901–916, 1989.

[20] Gargett, A.E. and Holloway, G., *Sensitivity of the GFDL ocean model to different diffusivities for heat and salt*, J. Phys. Ocean. 22, pp. 1158–1177, 1992.

[21] Garwood, R.W., *An oceanic mixed-layer model capable of simulating cyclic states*, J. Phys. Ocean. 7, p. 455, 1977.

[22] Gill, A.E., *Atmosphere–Ocean Dynamics*, Academic Press, pp. 662, 1982. [`Excellent text on ocean and atmospheric dynamics`]

[23] Gleick, J., *Chaos: making of a new science*, Viking Press, 1987. [`Fascinating account of the evolution of the subject of chaos in nonlinear systems`]

[24] Grammeltvedt, A., *A Survey of Finite-Difference Schemes for the Primitive Equations for a Barotropic Fluid*, Mon. Wea. Rev. 97, p. 384, 1969.

[25] Haidvogel, D.B., Wilkin, J.L. and Young, R., *A Semi-spectral Primitive Equation Model Using Vertical Sigma and Orthogonal Curvilinear Horizontal Coordinates*, J. Comp. Phys. 94, p. 151, 1991.

[26] Haney, R.L., *On the pressure gradient force over steep topography in sigma-coordinate ocean models*, J. Phys. Ocean. 21, 610–619, 1991.

[27] Heaps, N.S., ed., *Three-dimensional coastal Ocean Models*, AGU Press, 1987. [`A monograph on 3-D coastal models. Advanced material for serious coastal ocean modelers. Collection of technical papers.`]

[28] Heathershaw, A.D., and Codd, J.M., *The accuracy of mixed layer model predictions: a preliminary analysis of the effects of errors in the oceanographic and meteorological inputs*, Admiralty Research Establishment Technical Memorandum 86125, 1986.

[29] Hellerman, S. and Rosenstein, M., *Normal monthly wind stress over the world ocean with error estimates*, J. Phys. Ocean. 13, pp. 1093–1104, 1983.

[30] Holland, W.R. and Lin, l.B., *On the generation of mesoscale eddies and their contribution to the oceanic general circulation*, J. Phys. Ocean. 5, p. 642, 1975.

[31] Hurlburt, H.E. and Thompson, J.D., *A Numerical Study of Loop Current Intrusions and Eddy Shedding*, J. Phys. Ocean. 10, p. 1611, 1980.

[32] Jerlov, N. G., *Marine Optics*, Elsevier, 1976. [`Standard reference on optical properties of sea water`]

[33] Kantha, L.H., Blumberg, A.F. and Mellor, G.L, *Computing phase speeds at an open boundary*, J. Hydraulic Engineering 116, pp. 592–597, 1990.

[34] Kantha, L.H. and Clayson, C.A., *An improved mixed layer model for geophysical applications*, submitted to J. Geophys. Res., 1993. [`A good review of mixed layer models`]

[35] Kantha, L.H. and Mellor, G.L., *A two-dimensional coupled ocean–ice model of the Bering Sea marginal ice zone*, J. Geophys. Res. 94, pp. 10921–10936, 1989.

[36] Killworth, P.D., Stainforth, D., Webb, D.J. and Patterson, S.M., *The Development of a Free-Surface Bryan–Cox–Semtner Ocean Model*, J. Phys. Ocean. 21, p. 1333, 1991.

[37] Levitus, S., *Annual cycle of temperature and heat storage in the world ocean*, J. Phys. Ocean. 14, pp. 727–746, 1984.

[38] Liu, W.T., Katsaros, K.B. and Businger, J.A., *Bulk parametrization of air–sea exchanges of heat and water vapor including the molecular constraints at the interface*, J. Atmos. Sci. 39, p. 1722, 1979.

[39] Madala, R.V. and Piacsek, S.A., *A Model for Baroclinic Oceans*, J. Comp. Phys., p. 167, 1977.

[40] Martin, P.J., *Simulation of the Mixed Layer at OWS November and Papa With Several Models*, J. Geophys. Res. 90, p. 903, 1985.

[41] Mellor., G.L. and Blumberg, A.F., *Modeling vertical and horizontal diffusivities with the sigma coordinate system*, Mon. Wea. Rev., 113, pp. 1380–1388, 1985.

[42] Mellor, G.L. and Kantha, L.H., *An ice–ocean coupled model*, J. Geophys. Res. 94, pp. 10937–10954, 1989.

[43] Mellor, G. and Yamada, T., *Development of a Turbulence Closure Model for Geophysical Fluid Problems*, Rev. Geophy. Space Phys. 20, no. 4, p. 851, 1982.

[44] Mellor, G. and Yamada, T., *A hierarchy of turbulence closure models for planetary boundary layers*, J. Atm. Sci. 31, p. 1791, (1974).

[45] Mesinger, F. and Arakawa, A., *Numerical methods used in atmospheric models*, Vol. 1, Global Atmospheric Research Program Publication 17, pp. 64, 1976.

[46] Nihoul, J.C.J. and Jamart,B.M., 1987. *Three-Dimensional Models of Marine & Estuarine Dynamics.* Elsevier. [`A monograph on 3-D ocean models. Advanced material for serious ocean modelers. Collection of technical papers.`]

[47] Niiler, P.P., *Deepening of the wind-mixed layer*, J. Mar. Res. 33, p. 405, (1975).

[48] Nowlin, W.D., *A steady, wind-driven, frictional model of two moving layers in a rectangular ocean basin*, Deep-Sea Res. 14, p. 89 (1967).

[49] Oberhuber, J.M., *Simulation of the Atlantic Circulation with a coupled Sea Ice–Mixed Layer–Isopycnal general circulation model.* Part I. Model description, J. Phys. Oceanogr. 23, 808–829, 1993.

[50] O'Brien, J.J., *The non-linear response of a two-layer, baroclinic ocean to a stationary, axially-symmetric hurricane*, Tech. Report 65-34T, Texas A&M Univ., pp. 99, 1965.

[51] O'Brien, J.J., *Advanced Physical Oceanographic Numerical Modeling*, D. Reidel Publ. Co., 1985. [A collection of talks at the NATO Advanced Study Institute held in early 80's on the topic of ocean modeling. Excellent survey of the field at that point in time. Contains material on numerical methods for solving different PDEs as well as survey articles on different ocean models, how they were constructed and how they are applied. A must for an ocean modeler.]

[52] Orlonski, I., *A simple boundary condition for unbounded hyperbolic flows.* J. Comp. Phys., 21, 251–269, 1976.

[53] Pickard, G.L. and Emery, W.J., *Descriptive Physical Oceanography*, Pergamon Press, 1990. [A good introduction to the physical properties of global oceans, the water masses and circulation. A must for any beginner to oceanography. Along with its companion book Pond and Pickard, it gives one an excellent introduction as to how our oceans work.]

[54] Pond, S. and Pickard, G. L., *Introductory Dynamical Oceanography*, Second Edition, Pergamon Press, pp. 329, 1989. [An easy-to-follow introduction to the dynamics of oceans. Much easier to follow than textbooks such as Pedlosky's Geophysical Fluid Dynamics. Gives a beginner an excellent knowledge on ocean dynamics to build upon. Along with its companion book Pickard and Emery, it forms a good introduction to oceanography. A must for ocean modelers.]

[55] Preller, R. and Hurlburt, H.E., in Hydrodynamics of Semi-enclosed Seas, ed. J.C.J. Nihoul, p. 75–89, Elsevier Publ., 1982.

[56] Roache, P.J., *Computational Fluid Dynamics*, Hermosa Publishers, Albuquerque, N.M. 1972.

[57] Sathyendranath, S. and Platt, T., *The spectral irradiance field at the surface and in the interior of the ocean: A model for applications in oceanography and remote sensing*, J. Geophys. Res. 93, 9270–9280, 1988.

[58] Semtner, A.J., Jr. and Chervin, R.M., *Ocean general circulation from a global eddy-resolving model*, J. Geophys. Res. 97, 5493–5550, 1992.

[59] Schwiderski, E.W., *On charting global ocean tides*, Rev. Geophy. Space Phys. 18, 243–268, 1980.

[60] Simons, T.J., *Verification of numerical models of Lake Ontario*, Part 1. Circulation in spring and early summer, J. Phys. Ocean. 4, 507–523, 1974.

[61] Smith, W.O., Jr., ed., *Polar Oceanography*, Part A, Academic Press, 1990. [Excellent introduction to how polar oceans work. There is a chapter also on sea-ice modeling and its coupling to polar oceans.]

[62] Soetje, K.C. and Brockmann, C., *An Operational Numerical Model of the North Sea and the German Bight*, in "North Sea Dynamics", p. 95, 1983 [see Sundermann].

[63] Sundermann, J. and Lenz, W., editors, *North Sea Dynamics*, Springer–Verlag, 1983.

[64] Trenberth, K.E., *Climate System Modeling*, Cambridge University Press, 1992. [An excellent introduction to all aspects of climate and climate modeling. Each chapter written by an expert on the topic. A must for the serious climate modeler.]

[65] Warn-Varnas, A., French, J., Piacsek, S., Martin, P., and Harding, J., *Real-Time Shear Predictions*, NORDA Tech. Note 307, Jan (1986), pp. 57.

[66] Warn-Varnas, A. and Piacsek, S., *An Investigation of the Importance of Third-Order Correlations and Choice of Length Scale in Mixed Layer Modeling*, Geophys. and Astrophys. Fluid Dyn. 13, p. 225, 1979.

[67] Warren, B.A. and Wunsch, C., *Evolution of Physical Oceanography*, M.I.T. Press, 1981. [A collection of surveys on various topics on oceanography. Each chapter written by an expert on the subject. Excellent follow-on to the above introductory books. A required reading for a serious student of oceanography and ocean modeling.]

[68] Washington, W.M. and Parkinson, C.L., *An Introduction to Three-Dimensional Climate Modeling*, Oxford University Press, 1986. [A monograph on climate modeling. A good introduction to how climate results and how to model it.]

[69] Wessel, P. and Smith, W.H.F., *Free software helps map and display data*, EOS Transactions 72, 441–446, 1991.

[70] Wu, J., *Wind-Stress Coefficients Over Sea Surface from Breeze to Hurricane*, J. Geophys. Res. 87, p. 9704, 1982.